# NACA

# RESEARCH MEMORANDUM

TRANSONIC CHARACTERISTICS OF OUTBOARD AILERONS ON

A 4-PERCENT-THICK 30° SWEPTBACK WING, INCLUDING

SOME EFFECTS OF AILERON TRAILING-EDGE

THICKNESS AND AERODYNAMIC BALANCE

By Charles F. Whitcomb and Chris C. Critzos

Langley Aeronautical Laboratory
Langley Field, Va.

# NATIONAL ADVISORY COMMITTEE
# FOR AERONAUTICS
## WASHINGTON

July 9, 1958
Declassified January 12, 1961

NATIONAL ADVISORY COMMITTEE FOR AERONAUTICS

RESEARCH MEMORANDUM

TRANSONIC CHARACTERISTICS OF OUTBOARD AILERONS ON

A 4-PERCENT-THICK 30° SWEPTBACK WING, INCLUDING

SOME EFFECTS OF AILERON TRAILING-EDGE

THICKNESS AND AERODYNAMIC BALANCE

By Charles F. Whitcomb and Chris C. Critzos

SUMMARY


An investigation has been conducted in the Langley 16-foot transonic tunnel to determine the roll effectiveness, hinge-moment characteristics, and aileron center-of-load locations for an outboard 40-percent-semispan flap-type aileron installed on a 30° sweptback wing having an aspect ratio of 3.0, a taper ratio of 0.2, and NACA 65A004 airfoil sections. Aileron loads as well as forces and moments on the complete model were obtained for angles of attack from 0° to 21° and for Mach numbers between 0.80 and 1.03. Data were also obtained for the aileron with a blunt trailing edge and for a 65-percent-overhang nose-balanced aileron. The nose of the aerodynamic balance was constructed to unport immediately upon positive deflection of the aileron.

The results of the investigation indicated that the rolling-moment effectiveness of the tested aileron configurations was considerably influenced by flow separation which originated over the outboard portions of the wing. An increase in the control trailing-edge thickness increased its roll effectiveness for low angles of attack by as much as 50 percent. Curves showing the variation of hinge-moment coefficient with control deflection for all three ailerons were generally nonlinear. This was particularly true for the balanced slab-sided aileron at angles of attack of 0° and 4° at Mach numbers of 0.80 and 0.90 where reversals in the slope of the curves occur. Increasing the control trailing-edge thickness increased the negative slopes of these curves at low angles of attack. The addition of the overhang balance considerably decreased the negative slopes of the curves at low angles of attack. Generally, only slight aileron center-of-load movements (for the most part rearward and inboard) were noted for the three ailerons with increasing angle of attack, deflection angle, or Mach number in the ranges where there was significant loading on the controls.

## INTRODUCTION

An experimental research program is being conducted in the Langley 16-foot transonic tunnel to determine the effectiveness and loading characteristics of flap-type ailerons on a series of thin wings at transonic speeds. Portions of this program, which include effectiveness information for an outboard aileron on an unswept wing and for ailerons at three spanwise positions on a $45^\circ$ swept wing have been published in references 1 and 2, respectively. In addition, aileron force and hinge-moment characteristics are available in reference 1 for the unswept case and in reference 3 for the $45^\circ$ swept case. The present paper includes effectiveness, aileron hinge-moment, and aileron center-of-load data for an outboard aileron on a $30^\circ$ sweptback wing.

Some effects of aileron trailing-edge thickness and aerodynamic balance have also been investigated on this configuration and are presented herein. The balanced aileron of the present investigation was designed to provide complete unporting of the overhang nose immediately upon positive deflection of the control. The basic aileron, the thickened trailing-edge aileron, and the balanced aileron were made to have equal areas back of the control hinge line.

Hinge-moment, center-of-load, and effectiveness characteristics for the three control configurations are reported for angles of attack from $0^\circ$ to approximately $21^\circ$ at control deflections up to $15^\circ$ over a Mach number range from 0.80 to 1.03. The Reynolds number varied from about $6.8 \times 10^6$ at a Mach number of 0.80 to $8.2 \times 10^6$ at a Mach number of 1.03.

## SYMBOLS

The complete configuration forces are referenced to the wind axis and the moments are referenced to the body axis.

$b$         wing span

$b_a$        aileron span

$c$         local wing chord

$c'$        mean aerodynamic chord of wing

$c_a'$       mean aerodynamic chord of aileron rearward of hinge line

$C_D$    drag coefficient, $\dfrac{\text{Drag}}{qS}$

$C_h$    aileron hinge-moment coefficient, $\dfrac{H}{2qM_1}$

$C_L$    lift coefficient, $\dfrac{\text{Lift}}{qS}$

$C_m$    pitching-moment coefficient, $\dfrac{\text{Pitching-moment about } 0.25c'}{qSc'}$

$C_n$    yawing-moment coefficient, $\dfrac{\text{Yawing moment}}{qSb}$

$C_Y$    lateral-force coefficient, $\dfrac{\text{Lateral force}}{qS}$

$C_l$    rolling-moment coefficient, $\dfrac{\text{Rolling moment}}{qSb}$

$\Delta C_l$    incremental rolling-moment coefficient due to aileron deflection

D       body diameter

H       aileron hinge moment measured about hinge line

M       free-stream Mach number

$M_1$    area moment about hinge line of aileron area rearward of hinge line

q       free-stream dynamic pressure

S       wing area

t       ratio of aileron trailing-edge thickness to aileron thickness at hinge line

x       longitudinal distance along aileron mean aerodynamic chord line parallel to plane of symmetry, positive downstream of hinge line

y            lateral distance along aileron span, positive outboard of inboard
             end of aileron

$\alpha$     angle of attack of model

$\alpha_{av}$   averaged angle of attack of model for three configurations

$\delta$     aileron deflection angle in plane normal to aileron hinge line,
             positive when trailing edge is down

$\delta_N$   nominal aileron deflection (not corrected for deflection due to
             load)

$\Delta\delta$   deviation of actual control angle of deflection from nominal
             settings as a result of deflection due to load

$$C_{l_\delta} = \left(\frac{\partial C_l}{\partial \delta}\right)_\alpha$$

$$C_{h_\delta} = \left(\frac{\partial C_h}{\partial \delta}\right)_\alpha$$

$$C_{h_\alpha} = \left(\frac{\partial C_h}{\partial \alpha}\right)_\delta$$

## MODEL, APPARATUS, AND TESTS

### Model

The steel wing had $30°$ sweep of the quarter-chord line, an aspect
ratio of 3.0, a taper ratio of 0.20, and NACA 65A004 airfoil sections
parallel to the plane of symmetry. The fuselage had a fineness ratio
of 11, an ogive nose, a cylindrical center section, and a boattail after-
body. The wing was mounted to the fuselage in the midwing position and
was designed to have no geometric twist, incidence, or dihedral. The
general arrangement of the model with pertinent dimensional details is
shown in figure 1.

Dimensional details of the three aileron configurations are also
shown in figure 1. The ailerons spanned the outboard 40 percent of the
wing semispan and their hinge line was along the 81.5-percent chord line.
The three aileron configurations consisted of an unbalanced aileron with

normal wing-section ordinates, an unbalanced slab-sided aileron ($0^O$ trailing-edge angle), and a balanced slab-sided aileron with a sharp-nosed overhang which extended forward of the hinge line 65 percent of the aileron chord back of the hinge line. The nose of the balance overhang was located to provide complete unporting from the upper surface immediately upon positive deflection of the aileron. The lower wing surface extended to approximately the control hinge-line location (see aileron cross-sectional details, fig. 1); thus, the negative control deflection is limited to about $6^O$. The ailerons were mounted on the right wing by two strain-gage support beams (rectangular cross section) spaced near the inboard and outboard ends of the control. A constant-width chordwise unsealed gap of 0.030 inch was maintained between the aileron and the wing. Photographs of the model with controls installed are presented in figure 2. The multiple holes apparent in the photographs of the ailerons were made to reduce the weight of the ailerons and were filled with plastic and recontoured to the original surfaces of the controls.

## Apparatus

The tests were conducted in the Langley 16-foot transonic tunnel, the air flow and power characteristics for which are presented in reference 4. The model was sting supported and the complete configuration forces and moments were measured by a six-component internal strain-gage balance. The angle of attack was measured by means of a pendulum-type strain-gage attitude transmitter. The aileron normal forces, hinge moments, and moments about the aileron inboard end were measured by strain gages attached to the aileron support beams. The nominal angles of control deflection were obtained by selective use of various couplings between the support beams and the controls.

## Tests

Tests of the model with the three aileron configurations were made at Mach numbers from 0.80 to 1.03. The angle of attack ranged from $0^O$ to approximately $21^O$ at the lower loading conditions and from $0^O$ to approximately $12.5^O$ at the highest loading condition.

The unbalanced faired aileron was tested at nominal control-deflection angles of $0^O$, $8^O$, and $15^O$ with the model upright and $-0^O$, $-8^O$, and $-15^O$ with the model inverted (thus, the aileron is located on the opposite or left wing). Tests were conducted for the unbalanced slab-sided aileron at nominal control deflections of $-6^O$, $0^O$, $4^O$, $8^O$, and $15^O$ and for the balanced slab-sided aileron at $-6^O$, $0^O$, $8^O$, and $15^O$.

The Reynolds number, based on wing mean aerodynamic chord, ranged from about $6.8 \times 10^6$ (M = 0.80) to $8.2 \times 10^6$ (M = 1.03).

## Corrections and Accuracy

The Mach numbers assigned to the data presented herein are believed to be accurate to within ±0.005 (see ref. 4) and the angles of attack presented are believed to be accurate to within ±0.1°.

Lift and drag data were adjusted to the condition of free-stream static pressure at the model base. Drag data were not corrected for sting effects since the results of reference 5 indicated that these would be small. Corrections for tunnel boundary-interference effects are generally negligible at Mach numbers up to 1.03 in this tunnel. (See ref. 6.)

The data were not adjusted for wing aeroelasticity. Reference 7 indicated the twist of the tip section of this wing to be only -0.4° with ailerons undeflected at a Mach number of 1.0 and an angle of attack of 20°. The aileron deflection angles presented herein have been corrected for the deflection due to aileron loading. This correction was determined from the static bench loading calibration and the measured aileron aerodynamic loads. The resulting values of corrected deflection $\delta$ are believed accurate to within ±0.15°.

The accuracy of the measured coefficients, based on balance accuracy and repeatability of data, is believed to be within the following limits:

$C_L$ . . . . . . . . . . . . . . . . . . . . . . . . . . . . . . . . . . . ±0.01
$C_D$ at low lift coefficients . . . . . . . . . . . . . . . . . . . . . ±0.001
$C_D$ at high lift coefficients . . . . . . . . . . . . . . . . . . . . ±0.003
$C_m$ . . . . . . . . . . . . . . . . . . . . . . . . . . . . . . . . . . . ±0.004
$C_l$ . . . . . . . . . . . . . . . . . . . . . . . . . . . . . . . . . . . ±0.001
$C_n$ . . . . . . . . . . . . . . . . . . . . . . . . . . . . . . . . . . . ±0.001
$C_Y$ . . . . . . . . . . . . . . . . . . . . . . . . . . . . . . . . . . . ±0.002
$C_h$ . . . . . . . . . . . . . . . . . . . . . . . . . . . . . . . . . . . ±0.02

## RESULTS AND DISCUSSION

The longitudinal and lateral aerodynamic characteristics, with the exception of the rolling-moment coefficients, of the three aileron configurations at nominal control deflections are presented in figures 3, 4, and 5. The rolling-moment coefficients for the three ailerons at

nominal deflection angles are presented in figure 6.  The negative
deflections for the faired unbalanced aileron were obtained by inverting
the model and thereby locating the aileron on the opposite or left wing.
Therefore the rolling-moment, yawing-moment, and side-force coefficients
for these negative deflections were arbitrarily reversed to simulate a
right-wing control deflection.  It is believed that the nominal control
deflections indicated in these figures for each of the three ailerons
tested correspond closely enough to the actual control deflections to
allow the figures to be utilized in a preliminary quantitative analysis
of the results.  Curves showing the deviation of the actual control
deflections from the nominal values are presented in figure 7.  They
indicate a maximum deviation of $1.7^O$ which occurs for the unbalanced
faired aileron at a Mach number of $0.98$, a nominal deflection of $15^O$,
and at an angle of attack of $21.2^O$.  Figure 8 presents the incremental
rolling-moment coefficients due to control deflection plotted against
control deflection for constant angles of attack at the various test
Mach numbers.  The aileron rolling-moment effectiveness parameter $C_{l_\delta}$

(obtained over a small deflection range of $-5^O$ to $5^O$) for the three con-
figurations, plotted against Mach number, is presented in figure 9.  The
variation of hinge moment with angle of attack and with control deflec-
tion for each configuration is presented in figures 10 and 11, respec-
tively.  Figure 12 presents the hinge-moment parameters $C_{h_\delta}$ and $C_{h_\alpha}$

plotted against Mach number.  The chordwise and spanwise locations of
the aileron center of load are shown in figures 13 and 14, respectively,
as functions of control deflection at constant angles of attack through-
out the range of Mach numbers.  The drag coefficients of the three
aileron configurations at $0^O$ deflection for lift coefficients of 0 and
$0.4$ plotted against Mach number are presented in figure 15.


## Aileron Characteristics

Rolling-moment effectiveness.- In many cases the curves of figure 6
show rather large variations of $C_l$ with $\alpha$ for each of the tested
aileron configurations.  In general, these variations were associated
with flow separation which occurred on the upper surface of the basic
wing.  As shown by the pressure distributions over the basic wing pre-
sented in reference 7, this flow separation occurred initially near the
outboard leading-edge portion of the wing at low Mach numbers and near
the outboard trailing-edge portion at the higher Mach numbers.  The
initial angle of attack of occurrence and the spreading rate with
increasing angle of attack also depended upon Mach number.  It would be
expected, therefore, that the ability of the ailerons to provide roll
control was considerably influenced by the flow-separation phenomena.
This is supported by the nonlinear variation of $\Delta C_l$ with deflection

(fig. 8) and the changes in the effectiveness parameter $C_{l_\delta}$ with
angle of attack (fig. 9) which occur for conditions of angle of attack
and Mach number for which the flow over the wing in the vicinity of the
aileron is known to have been separated. Additionally, of course, the
aileron deflection would be expected to have a definite influence on
the amount of flow separation.

At a Mach number of 0.94 and angles of attack near 12°, figures 6(a)
and 6(c) indicate large changes in $C_l$ for even a nominal control
deflection of 0°. Unpublished data show that these changes, which are
caused by differences in flow separation on the opposite wings, also
occurred for the basic model. Apparently, the flow was very sensitive
to boundary-layer changes in this angle-of-attack range at a Mach num-
ber of 0.94, as indicated by the abrupt changes in the lift curves of
figures 3(a) and 5(a). Further indications of this sensitivity are
shown in figures 4(a) and 6(b) where asymmetric flow separation and its
resultant effect on rolling moment did not occur for the unbalanced
slab-sided aileron at nominal deflection angles of 0° and 4°. The
effect of asymmetric flow separation on aileron effectiveness is shown
in figure 8 by severe nonlinearities in the variation of $C_l$ with
deflection and reversal in the curve slopes.

The nonlinear variation of $\Delta C_l$ with $\delta$ (fig. 8) for the three
ailerons in the low and intermediate range of Mach numbers limit the
usefulness of the curve slopes $C_{l_\delta}$ presented in figure 9 as a measure
of control effectiveness. The parameter $C_{l_\delta}$ in figure 9 is then
representative of the aileron characteristics only over a small range
of deflections of approximately ±5°. At the higher Mach numbers, how-
ever, the variations in $\Delta C_l$ with $\delta$ were, in general, more linear
since the supersonic flow field was well established over the wing and
control surfaces and flow-separation effects became delayed and less
pronounced. Even at these higher Mach number conditions, however, the
curves of the balanced control showed some loss in aileron effectiveness.

The variations of the rolling-moment effectiveness parameter $C_{l_\delta}$
with Mach number as presented in figure 9 were quite similar for each
of the three tested ailerons. The decrease in effectiveness at angles
of attack of 0° and 4° which occurred for all the ailerons between a
Mach number of 0.90 and 0.98 may be associated with the effects of a
shock wave which formed and moved toward the trailing edge in this Mach
number range. (See pressure distributions of ref. 7.) The unbalanced
slab-sided aileron was as much as 50 percent more effective than the
faired aileron at angles of attack of 0° and 4° and, to a lesser extent,
at 8°. At these angles, some improvement existed throughout the Mach

number range.  At the higher angles of 12° and 16°, a slight improvement of the effectiveness attributed to the slab-sided aileron is noted at the higher Mach numbers only.  The addition of the aerodynamic balance decreased the effectiveness of the slab-sided aileron slightly at angles of attack through 4°.

Hinge moment.- The hinge-moment coefficients for the three aileron configurations are shown in figure 10 to have a generally negative slope with increasing angle of attack.  Exceptions are noted for zero and positive control deflections at low angles of attack and Mach numbers up to 0.94 for which the slopes are positive.  Nonlinearities are indicated in the curves, particularly for low angles of attack, at Mach numbers as high as 0.94 and 0.96.  The values of the parameter $C_{h_\alpha}$ taken at $\alpha = 0°$ presented in figure 12(b) are, therefore, indicative of the hinge-moment characteristics over only a small range of angle of attack, particularly for the low and intermediate Mach number ranges.

The hinge-moment-coefficient variations with control deflection (fig. 11) are generally nonlinear for all three ailerons.  This is particularly true for the balanced slab-sided aileron at angles of attack of 0° and 4° and Mach numbers of 0.80 and 0.90 where reversals in the slope of the curve occur.  The hinge-moment parameter $C_{h_\delta}$ therefore is applicable over only a small deflection range.  For this reason, values of this parameter were obtained at control deflections of both 0° and 12° and are presented in figure 12(a).

At $\delta = 0°$, the values of $C_{h_\delta}$ (fig. 12) for each aileron configuration increased negatively with Mach number up to about 0.98 for angles of attack between 0° and 12° and indicated a rearward shift in the aileron center of load or an increase in aileron load.  Some rearward shifting of the aileron load center with increasing Mach number up to 0.98 is indicated in figure 13 for positive angles of deflection above the lowest values.  Values of $C_{h_\delta}$ at $\delta = 0°$ for the unbalanced slab-sided aileron were more negative than those for the faired aileron at angles of attack up to 8° and generally less negative for angles of attack between 12° and 20°, although the difference at the higher angles was much smaller.  Adding the aerodynamic balance to the slab-sided aileron decreased the hinge-moment slopes at $\delta = 0°$ for angles of attack up to 8°.  Above an angle of attack of 8°, however, no balancing effects were indicated.  In this angle-of-attack range, it is believed that the balance was submerged in the separated flow region over the upper surface outboard portions of the wing.

At $\delta = 12°$, the hinge-moment slopes for the unbalanced faired aileron were somewhat greater than those for either the unbalanced or

balanced slab-sided aileron throughout the test Mach number and angle-of-attack ranges. Some balancing was indicated for the aerodynamic balance at most angles of attack below 20° for Mach numbers of 0.90 and above.

As mentioned previously, the values of the parameter $C_{h_\alpha}$ presented in figure 12(b) for the three ailerons are applicable only over a small angle-of-attack range. Above a Mach number of approximately 0.90, the trends toward large negative increases in $C_{h_\alpha}$ were similar for the three ailerons with increasing Mach numbers. The values for the unbalanced slab-sided aileron were somewhat larger negatively than those for the other two ailerons in this Mach number range.

Center of load.- The longitudinal center-of-load locations shown in figure 13 were computed directly from the hinge-moment data of figure 11 and from the measured aileron normal forces (not presented herein). The discontinuities in the curves for the longitudinal and lateral centers-of-load locations shown in figures 13 and 14, respectively, occurred when the aileron normal forces approached zero. As can be determined from figures 11 and 13, the aileron normal forces at angles of attack above 4° were larger at positive aileron deflections than at the corresponding negative deflections.

At the positive control deflections the center of load generally moved slightly rearward with increasing angle of attack and Mach number to a maximum rearward location of approximately $0.5 \frac{x}{c_a'}$ for the unbalanced ailerons and $0.4 \frac{x}{c_a'}$ for the balanced aileron (fig. 13). At negative deflections greater than those for which discontinuities in the curves exist, similar rearward shifts occurred. At angles of deflection greater than those for which discontinuities occur, increasing the deflection angle generally caused a slight rearward shift in the center of load for the unbalanced ailerons. Generally, the load center of the balanced aileron was well forward of those for the unbalanced ailerons. Spanwise, there was a gradual inboard movement of the aileron center of load from approximately $0.5 \frac{y}{b_a}$ to $0.4 \frac{y}{b_a}$ with increasing angle of attack (fig. 14). The lateral location of the center of load was little affected by changes in Mach number or control deflection.

Other Aerodynamic Characteristics

Longitudinal characteristics.- The unbalanced and balanced slab-
sided ailerons indicated variations of lift coefficient with angle of
attack similar to those for the unbalanced faired aileron except for
some slight previously noted differences at a Mach number of 0.94
(parts (a) of figs. 3 to 5).  Drag at low lift coefficients increased
with control deflection.  Maximum increases occurred for the balanced
aileron at the largest tested deflection.  (See parts (b) of figs. 3
to 5.)  Figure 15 indicates that the thickened trailing edge of the two
slab-sided ailerons had little effect on the drag of the model for lift
coefficients near zero.

The magnitude of the unstable pitching-moment tendencies of the
model at moderate lifts for subsonic Mach numbers below 0.94 was ampli-
fied by control deflection in some cases.  (See parts (c) of figs. 3
to 5, particularly at M = 0.90.)  In addition, control deflection gen-
erally caused a shift in model trim lift coefficient.

Lateral characteristics.- The yawing-moment and side-force char-
acteristics of the three configurations showed little change due to
angle of attack or Mach number except at high angles of attack between
16° and about 21° for Mach numbers below 0.94.  (See parts (d) and (e)
of figs. 3 to 5.)  In this angle-of-attack range, for which the wing
flow separation became an increasingly important factor, a general
increase in the magnitude of both the yawing moment and side force was
indicated.  It is to be noted in figure 6 that at these same conditions
the rolling-moment coefficients were increasing negatively.  There are
no comparable trends in the lift or drag curves of parts (a) and (b) of
figures 3 to 5.  Positive yawing-moment-coefficient combined with nega-
tive rolling-moment-coefficient increments at low deflection angles seem
to indicate that the separated areas over the two wings differed greatly.
The reasoning is further strengthened by the fact that, at a Mach number
of 0.94 and below at low and medium angles of attack where sensitive
flow conditions caused large changes in rolling-moment coefficient, only
slight changes in yawing-moment and side-force coefficient occurred.

Figures 4(d) and 5(d) indicate that, in general, the adverse yawing
moment resulting from deflection of the balanced aileron was greater
than that for deflection of the unbalanced aileron.

CONCLUSIONS

A transonic investigation of the effectiveness and loads character-
istics of 40-percent-semispan outboard ailerons installed on a 4-percent-
thick, 30° sweptback wing including effects of aileron trailing-edge

thickness and aerodynamic balance led to the following conclusions:

1. The rolling-moment effectiveness of the tested aileron configurations was considerably influenced by flow separation which originated over the outboard portions of the wing. Decreasing the aileron trailing-edge angle to $0^{\circ}$ by slab siding the control increased the control rolling-moment effectiveness by as much as 50 percent for angles of attack up to $8^{\circ}$. The addition of an overhang nose balance to the slab-sided aileron slightly decreased the rolling-moment effectiveness at angles of attack up to $4^{\circ}$.

2. The variation of the hinge-moment coefficient with control deflection was generally nonlinear for all three aileron configurations. This was particularly true for the balanced slab-sided aileron at angles of attack of $0^{\circ}$ and $4^{\circ}$ at Mach numbers of 0.80 and 0.90 where reversals in the slope of the curves occur. The slab-sided aileron indicated more negative slope in the variation of the hinge-moment effectiveness with control deflection than that for the faired aileron for angles of attack to $8^{\circ}$. The addition of the overhang nose balance to the slab-sided aileron considerably decreased the negative slope of this parameter at low angles of attack.

3. Generally, only slight aileron center-of-load movements (for the most part, rearward and inboard) were noted for the three ailerons with increasing angle of attack, deflection angle, or Mach number in the ranges where there was significant loading on the controls.


Langley Aeronautical Laboratory,
        National Advisory Committee for Aeronautics,
                Langley Field, Va., April 14, 1958.

REFERENCES

1. Hieser, Gerald:  Transonic Investigation of the Effectiveness and
     Loading Characteristics of a Flap-Type Aileron With and Without
     Paddle Balances on an Unswept Wing-Fuselage Model.  NACA RM L56B02,
     1956.

2. Hieser, Gerald, and Whitcomb, Charles F.:  Effectiveness at Transonic
     Speeds of Flap-Type Ailerons for Several Spanwise Locations on a
     4-Percent-Thick Sweptback-Wing—Fuselage Model With and Without
     Tails.  NACA RM L56J04, 1957.

3. Runckel, Jack F., and Hieser, Gerald:  Normal-Force and Hinge-Moment
     Characteristics at Transonic Speeds of Flap-Type Ailerons at Three
     Spanwise Locations on a 4-Percent-Thick Sweptback-Wing—Body Model
     and Pressure Distribution Measurements on an Inboard Aileron.  NACA
     RM L57I23, 1957.

4. Ward, Vernon G., Whitcomb, Charles F., and Pearson, Merwin D.:  Air-
     Flow and Power Characteristics of the Langley 16-Foot Transonic
     Tunnel With Slotted Test Section.  NACA RM L52E01, 1952.

5. Cahn, Maurice S.:  An Experimental Investigation of Sting-Support
     Effects on Drag and a Comparison With Jet Effects at Transonic
     Speeds.  NACA RM L56F18a, 1956.

6. Whitcomb, Charles F., and Osborne, Robert S.:  An Experimental
     Investigation of Boundary Interference on Force and Moment Char-
     acteristics of Lifting Models in the Langley 16- and 8-Foot
     Transonic Tunnels.  NACA RM L52L29, 1953.

7. Arabian, Donald D.:  Investigation at Transonic Speeds of the Loading
     Over a 30° Sweptback Wing of Aspect Ratio 3, Taper Ratio 0.2, and
     NACA 65A004 Airfoil Section Mounted on a Body.  NACA RM L57G09a,
     1957.

| Wing Data | |
|---|---|
| Wing section | NACA 65A004 |
| Wing area | 8.165, sq ft |
| Aspect ratio | 3.00 |
| Taper ratio | 0.20 |
| Sweep angle, c/4 | 30° |
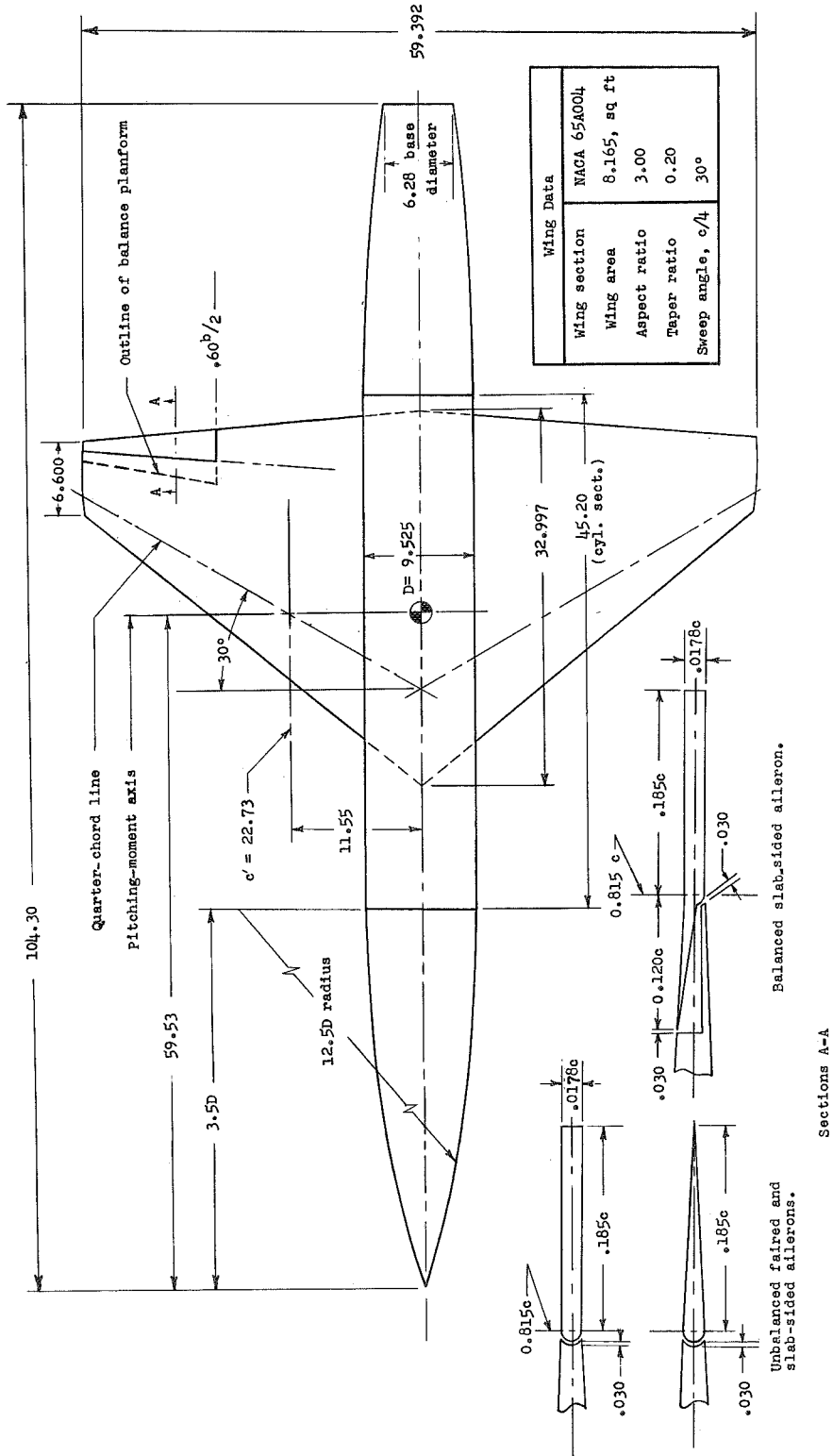
Figure 1.- Dimensional details of model.  All linear dimensions are in inches.
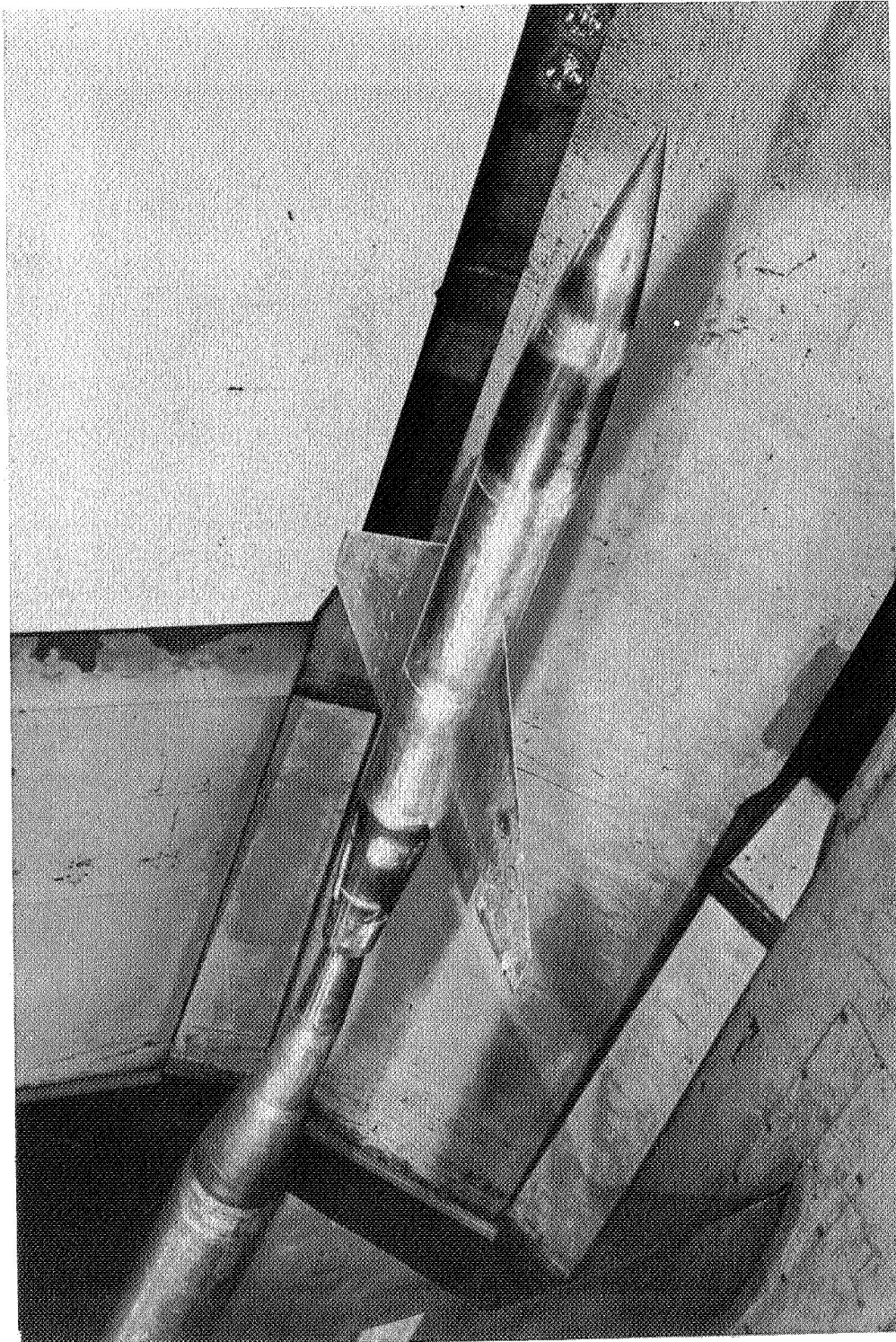
(a) Wing-body combination with faired aileron.      L-96059

Figure 2.- Photographs of model.
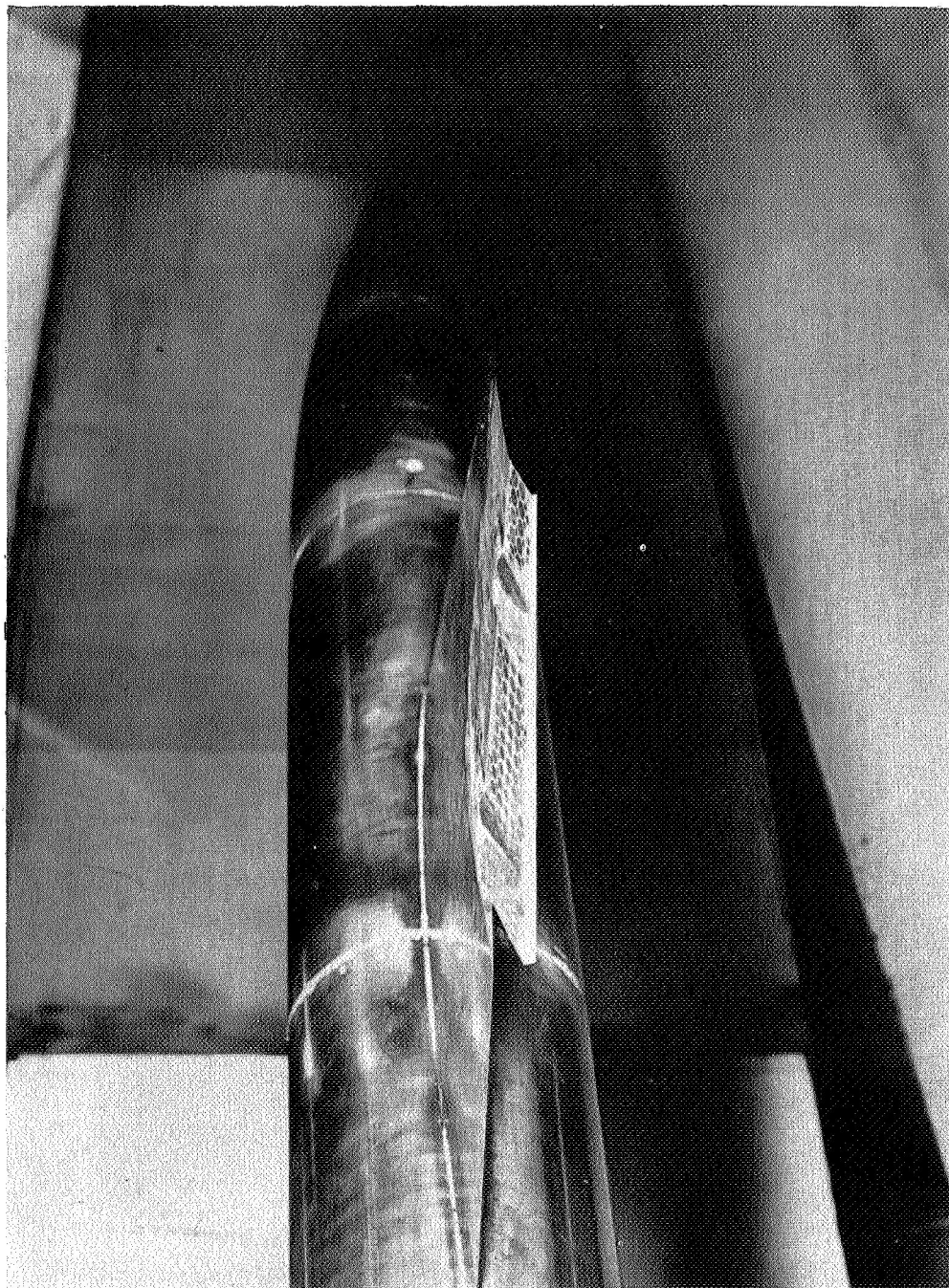
L-96060

(b) Unbalanced slab-sided aileron.

Figure 2.- Continued.
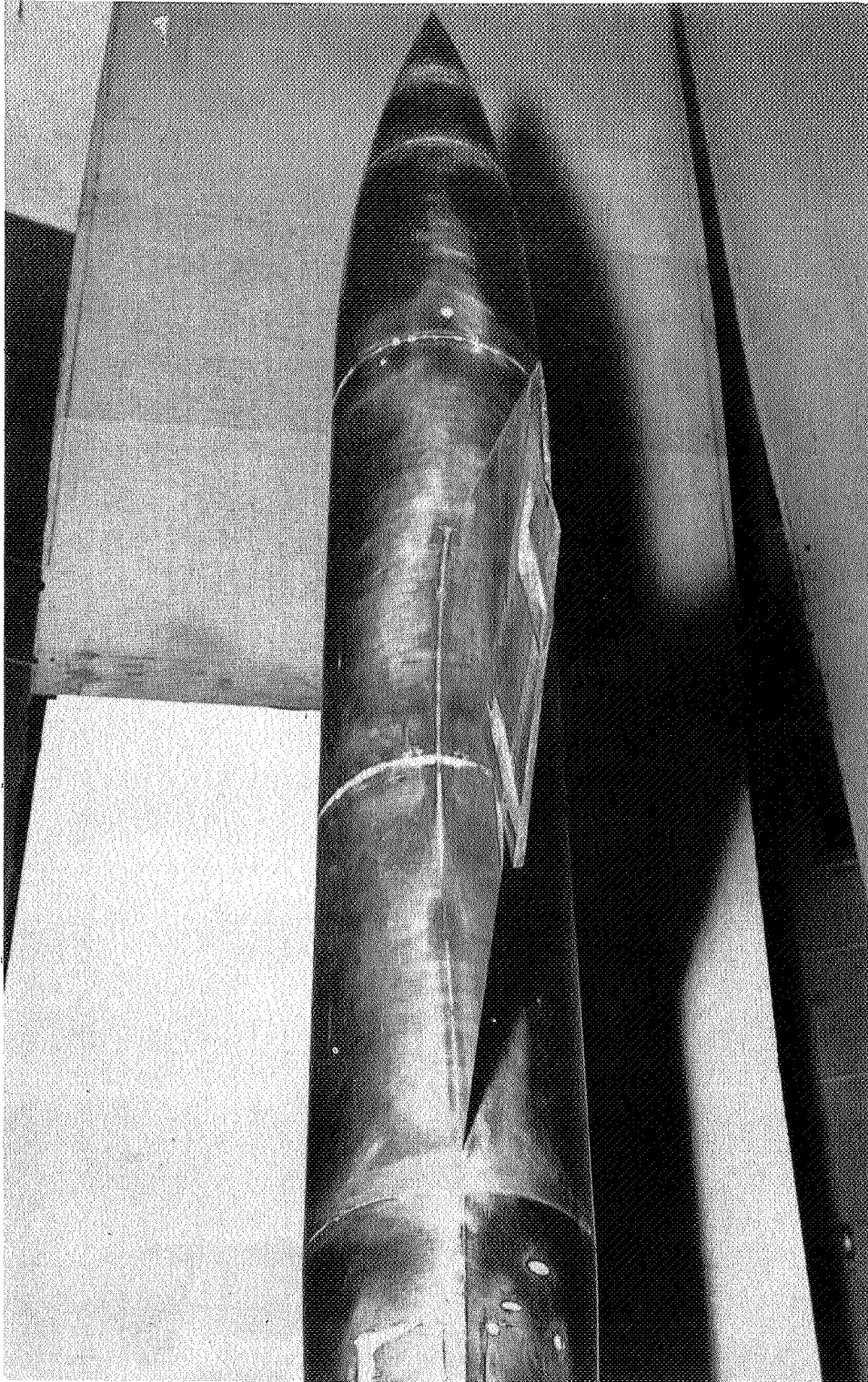
(c) Balanced slab-sided aileron.    L-96090

Figure 2.- Concluded.
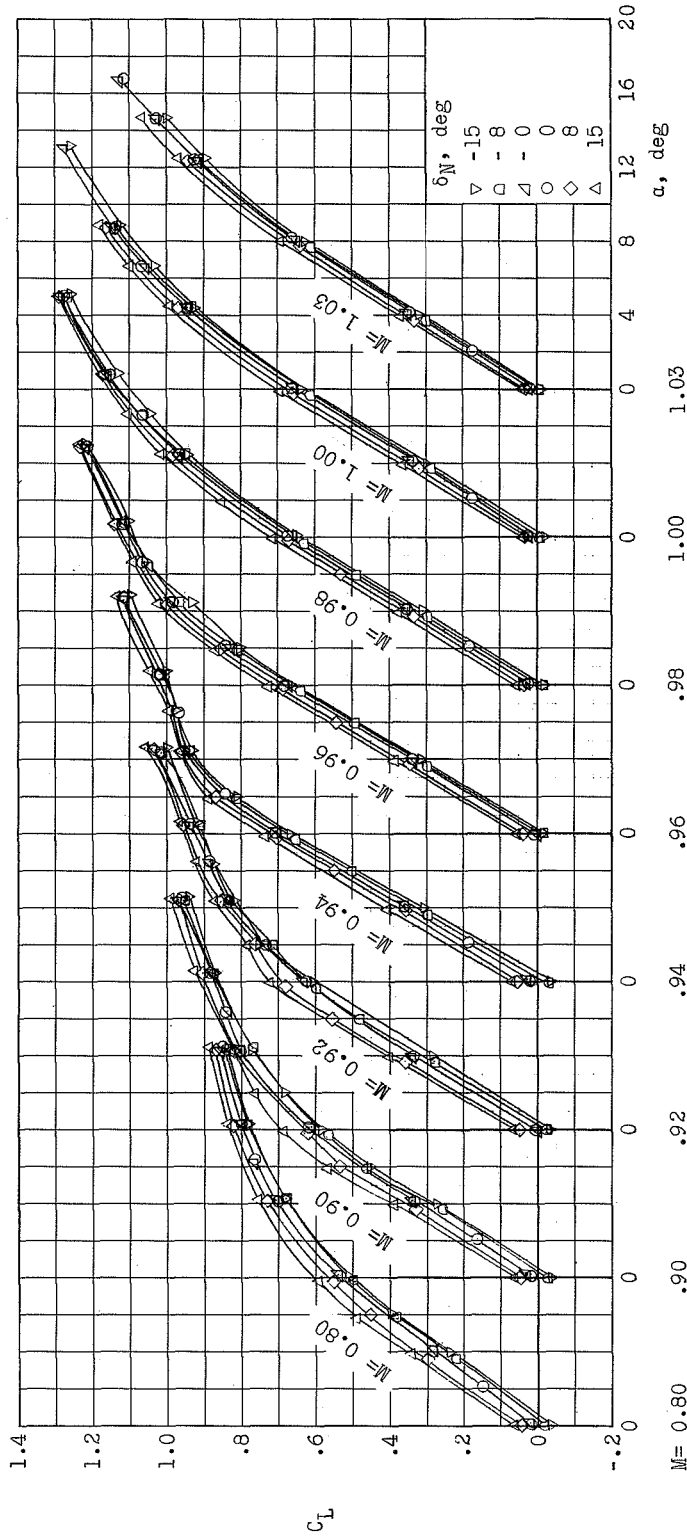
(a) $C_L$ against $\alpha$.

Figure 3.- Variation with angle of attack or lift coefficient of the force and moment character-
istics of the wing-body combination equipped with a faired umbalanced aileron at several
control-deflection angles for constant Mach numbers.
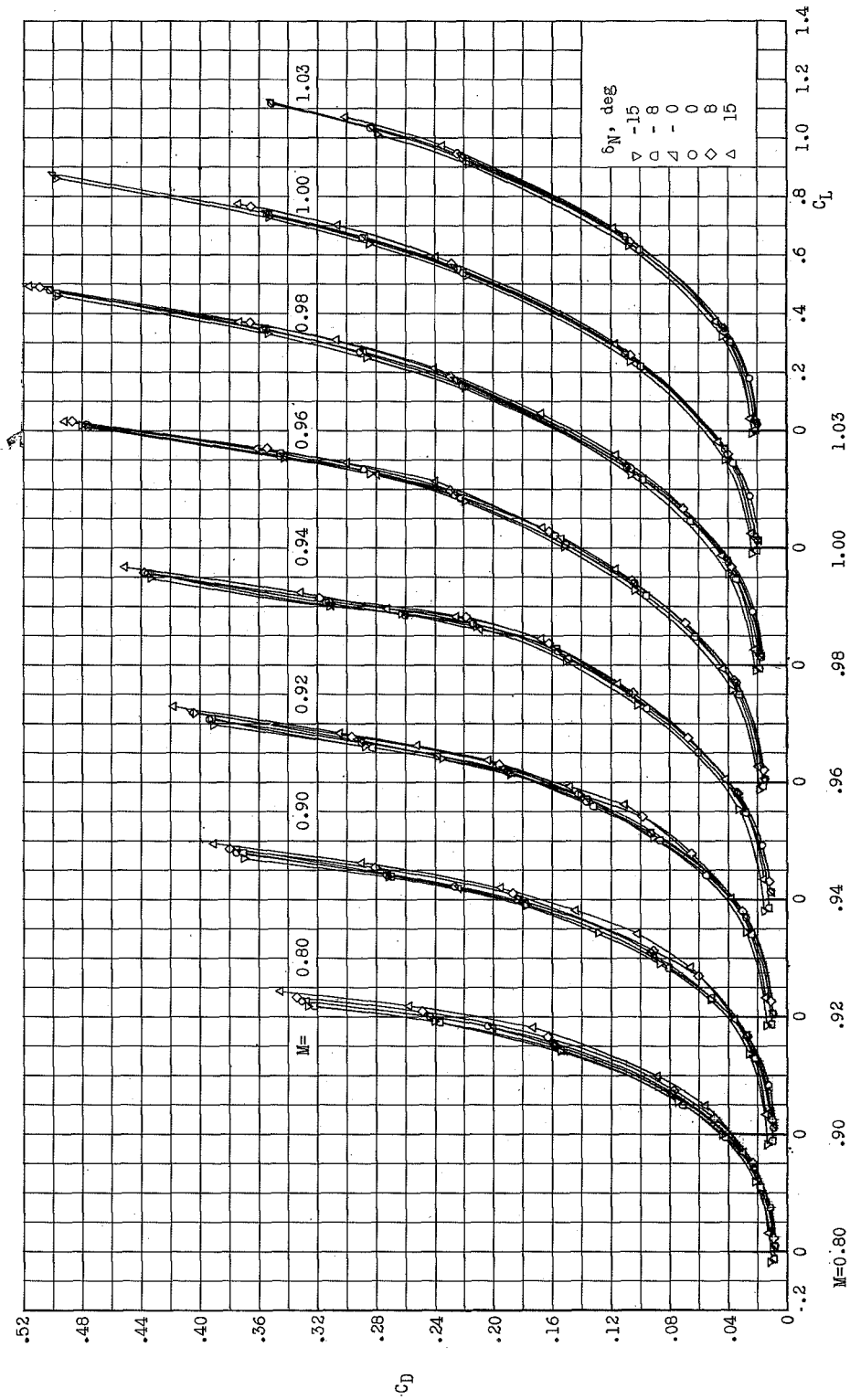
(b) $C_D$ against $C_L$.
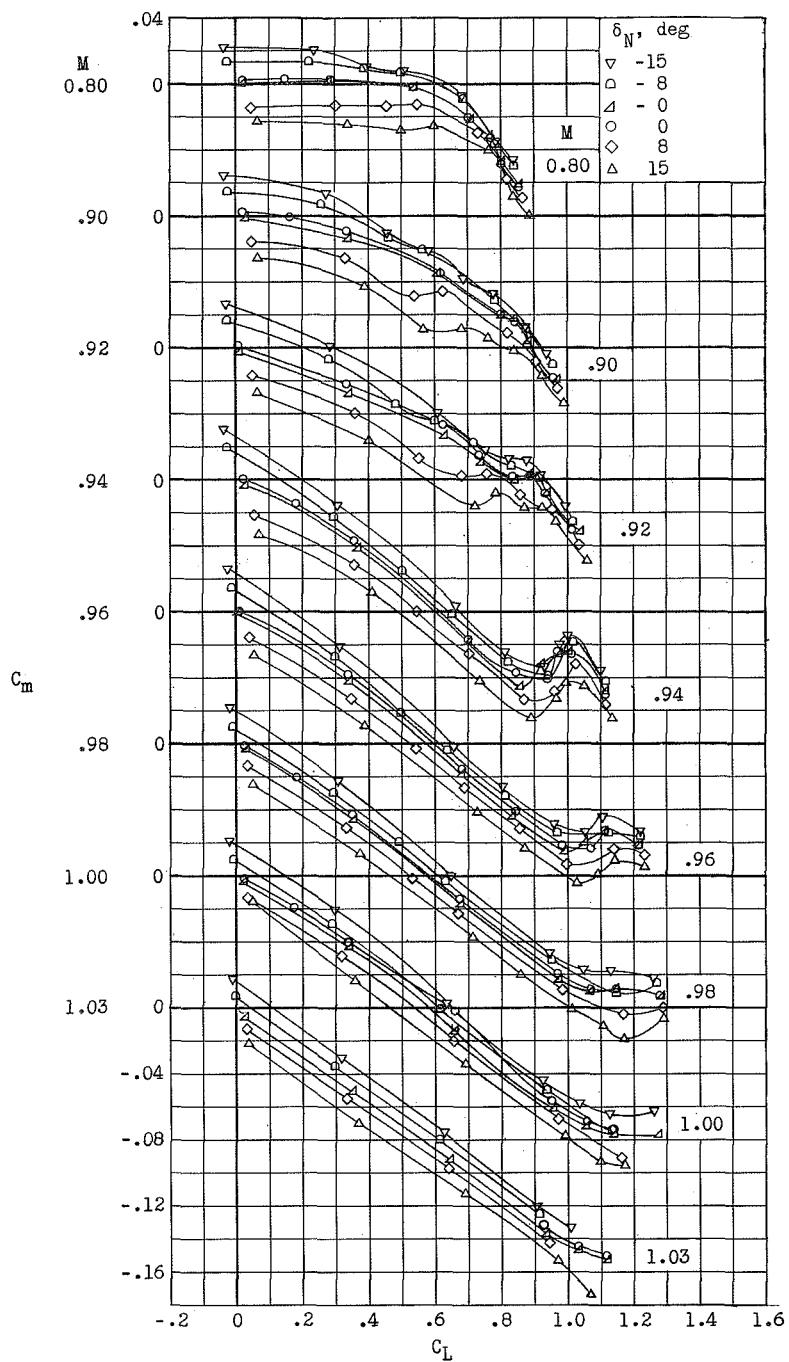
Figure 3.- Continued.

(c)  $C_m$  against  $C_L$.
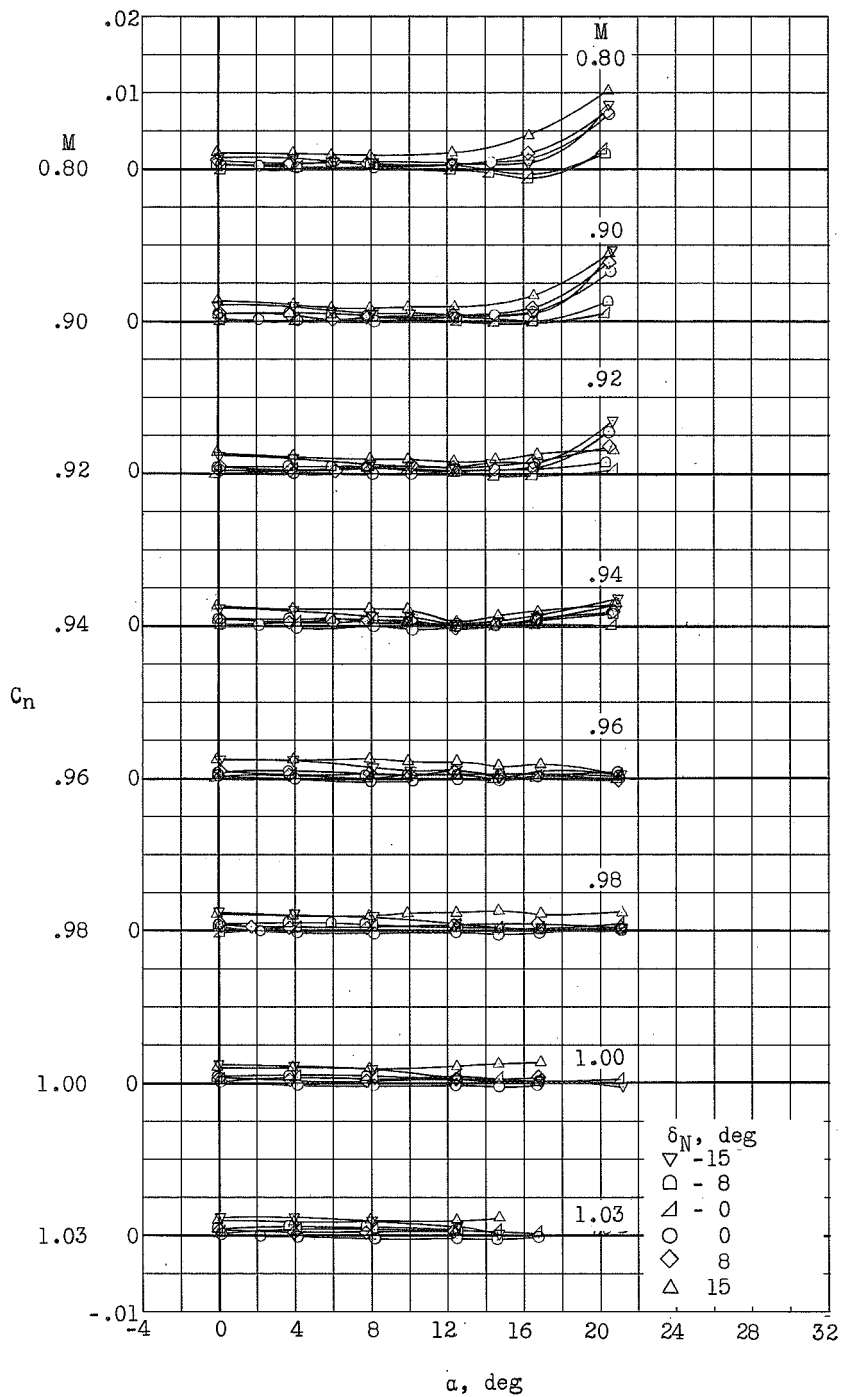
Figure 3.- Continued.

(d) $C_n$ against $\alpha$.

Figure 3.- Continued.
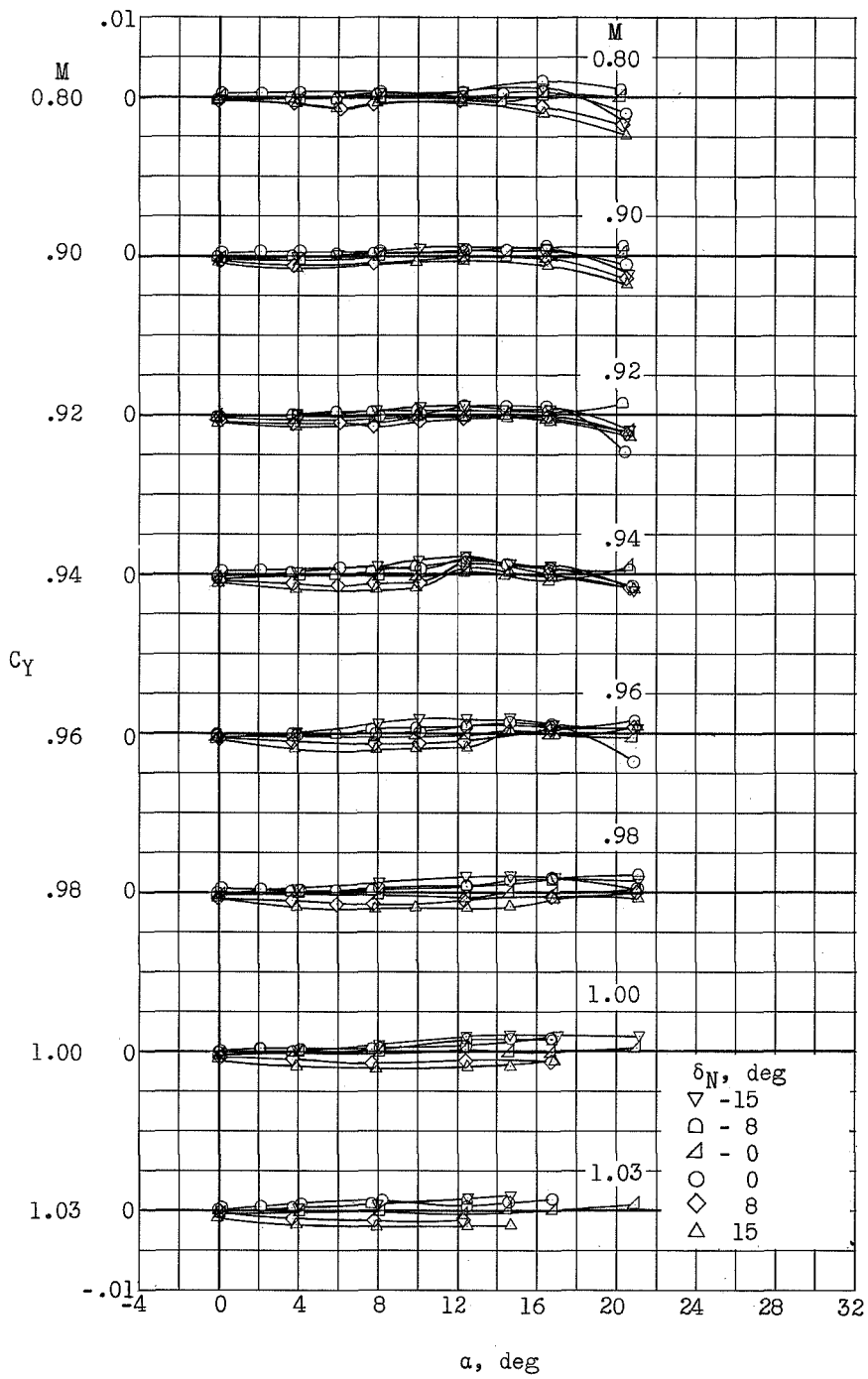
(e) $C_Y$ against $\alpha$.

Figure 3.- Concluded.
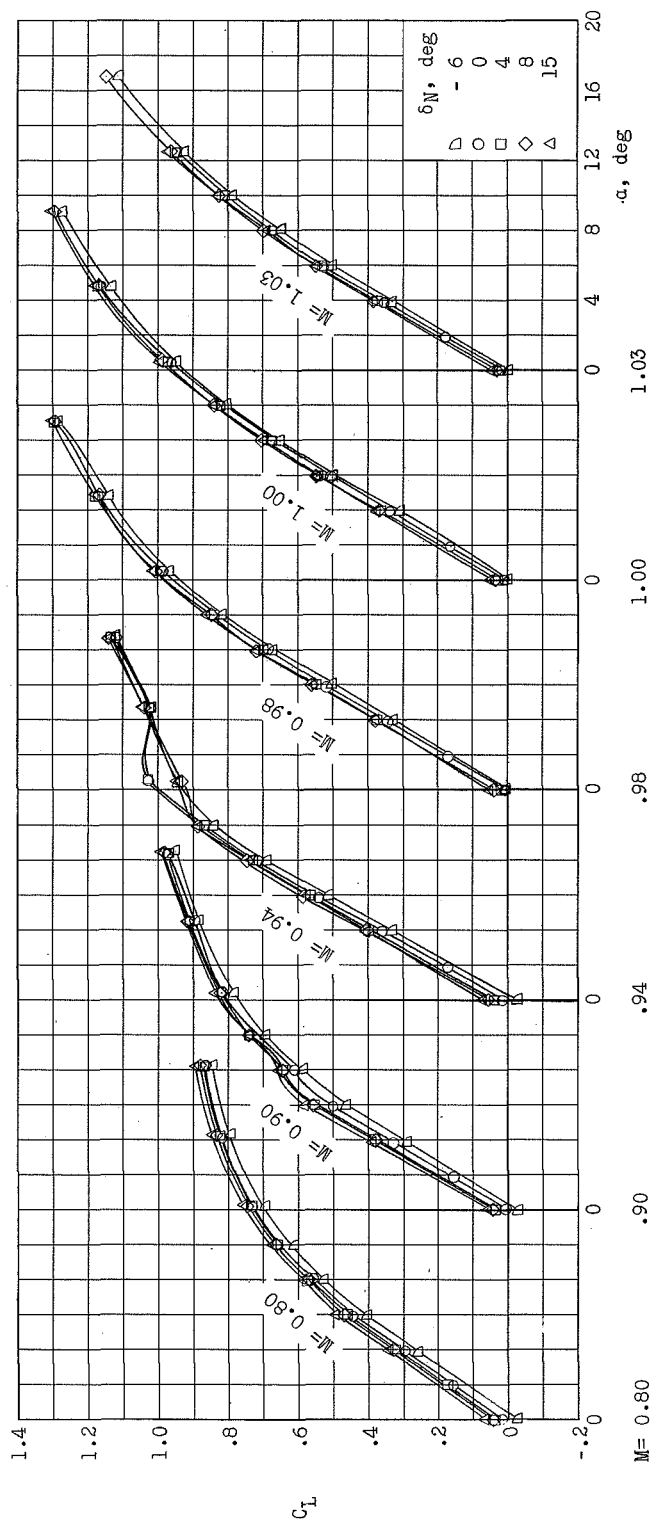
(a) $C_L$ against $\alpha$.

Figure 4.- Variation with angle of attack or lift coefficient of the force and moment character-
istics of the wing-body combination equipped with a slab-sided unbalanced aileron at several
control-deflection angles for constant Mach numbers.
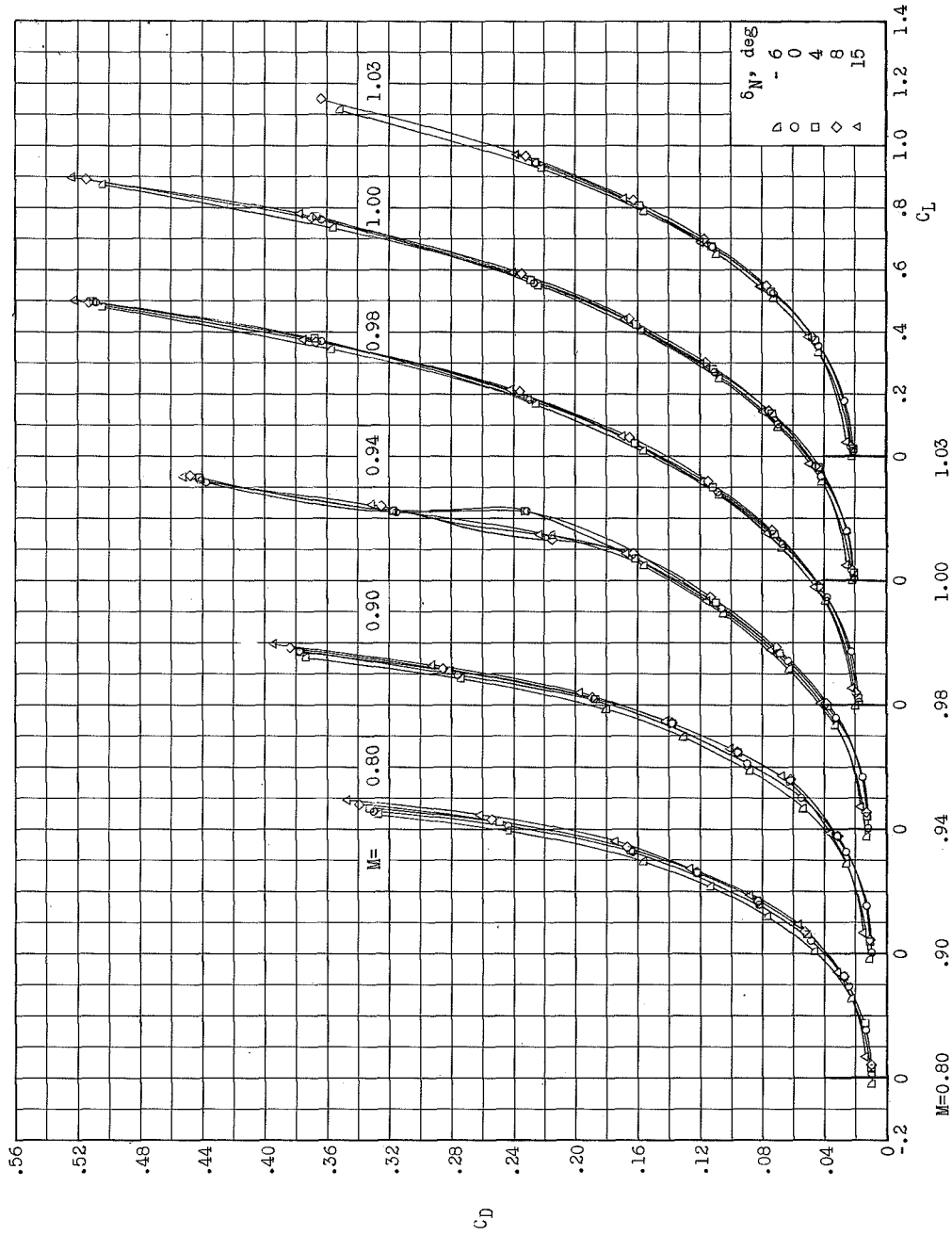
(b) $C_D$ against $C_L$.
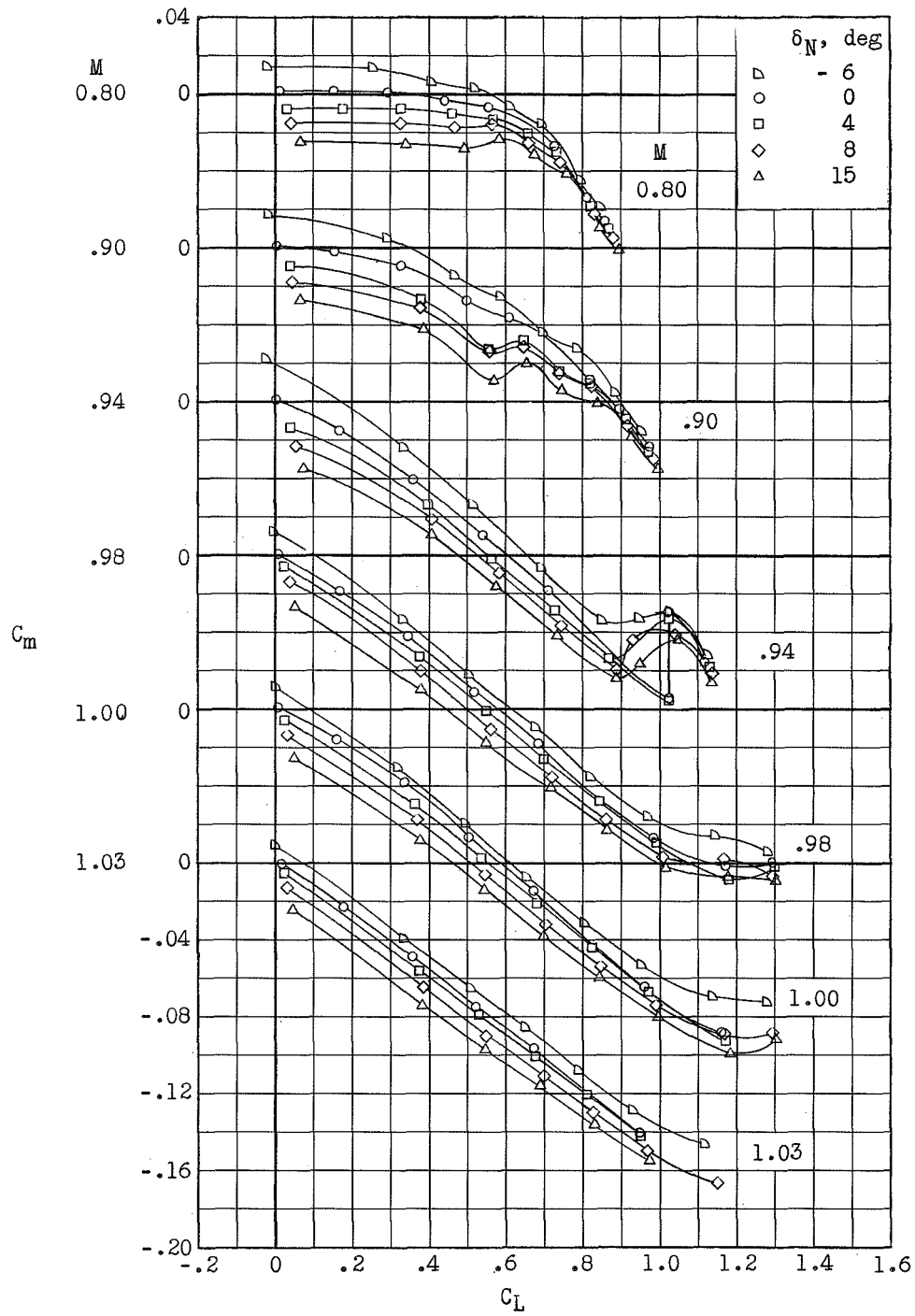
Figure 4.- Continued.

(c)  $C_m$  against  $C_L$.
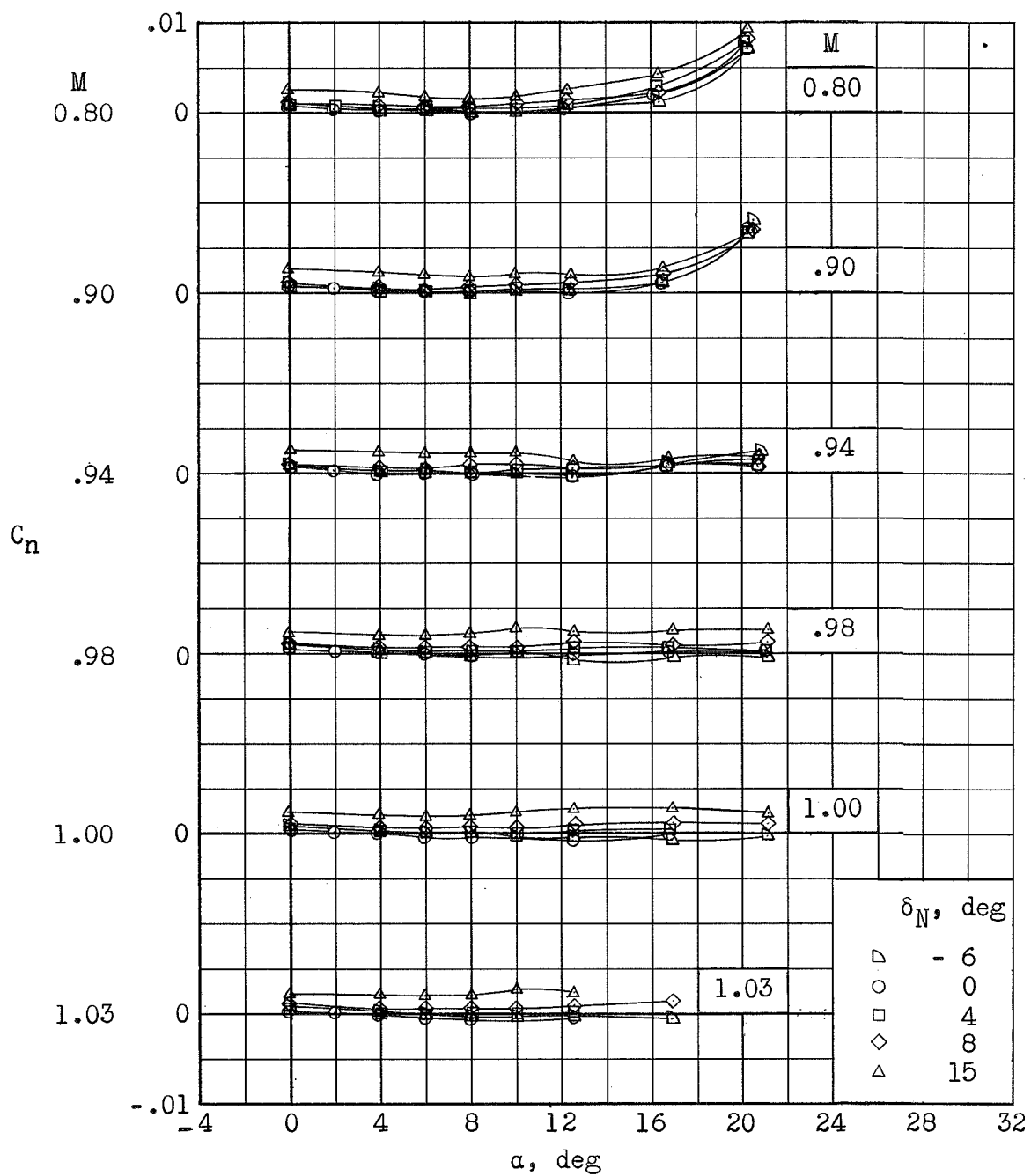
Figure 4.- Continued.

(d)  $C_n$  against  $\alpha$.

Figure 4.- Continued.
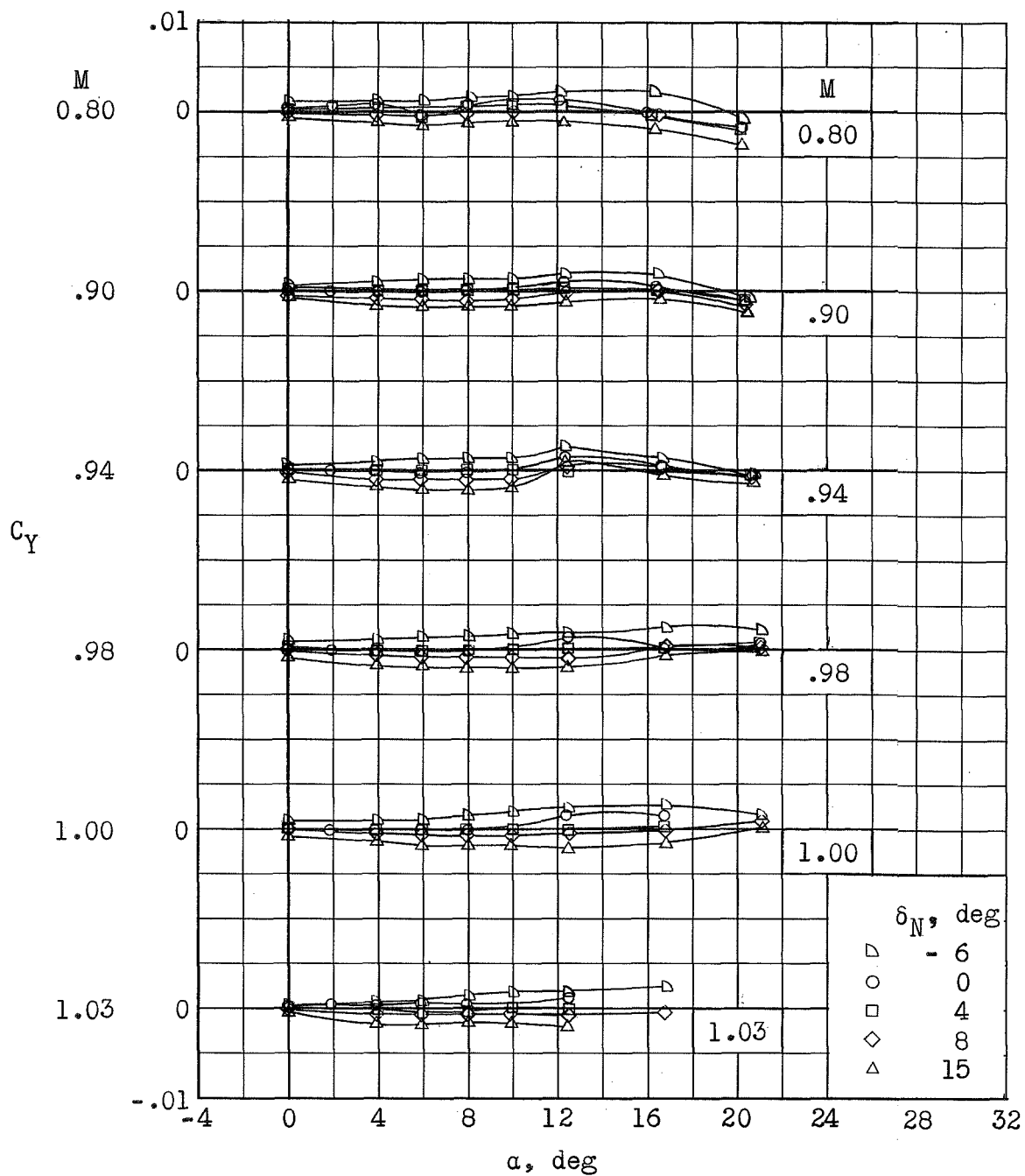
(e) $C_Y$ against $\alpha$.

Figure 4.- Concluded.
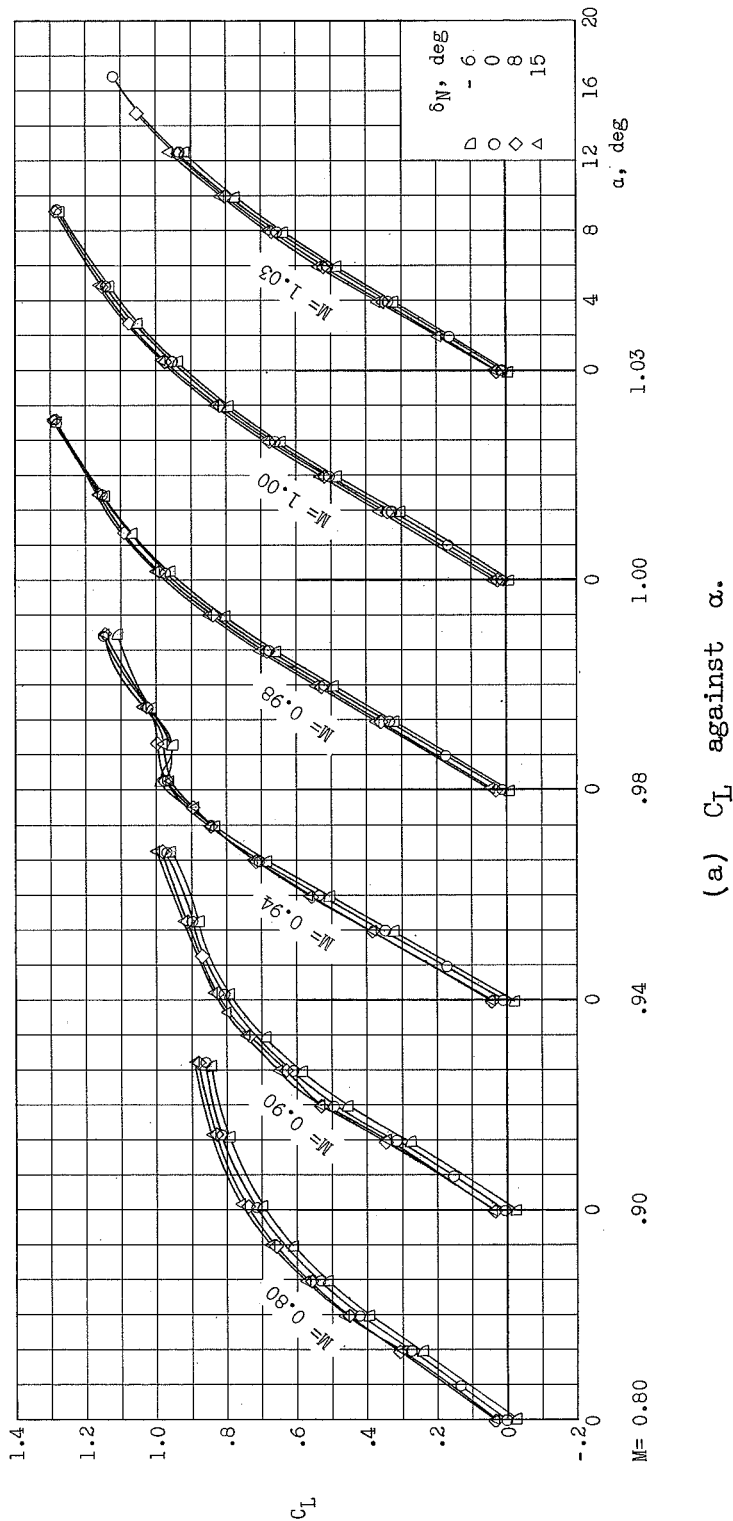
(a) $C_L$ against $\alpha$.

Figure 5.- Variation with angle of attack or lift coefficient of the force and moment character-
istics of the wing-body combination equipped with a slab-sided balanced aileron at several
control-deflection angles for constant Mach numbers.
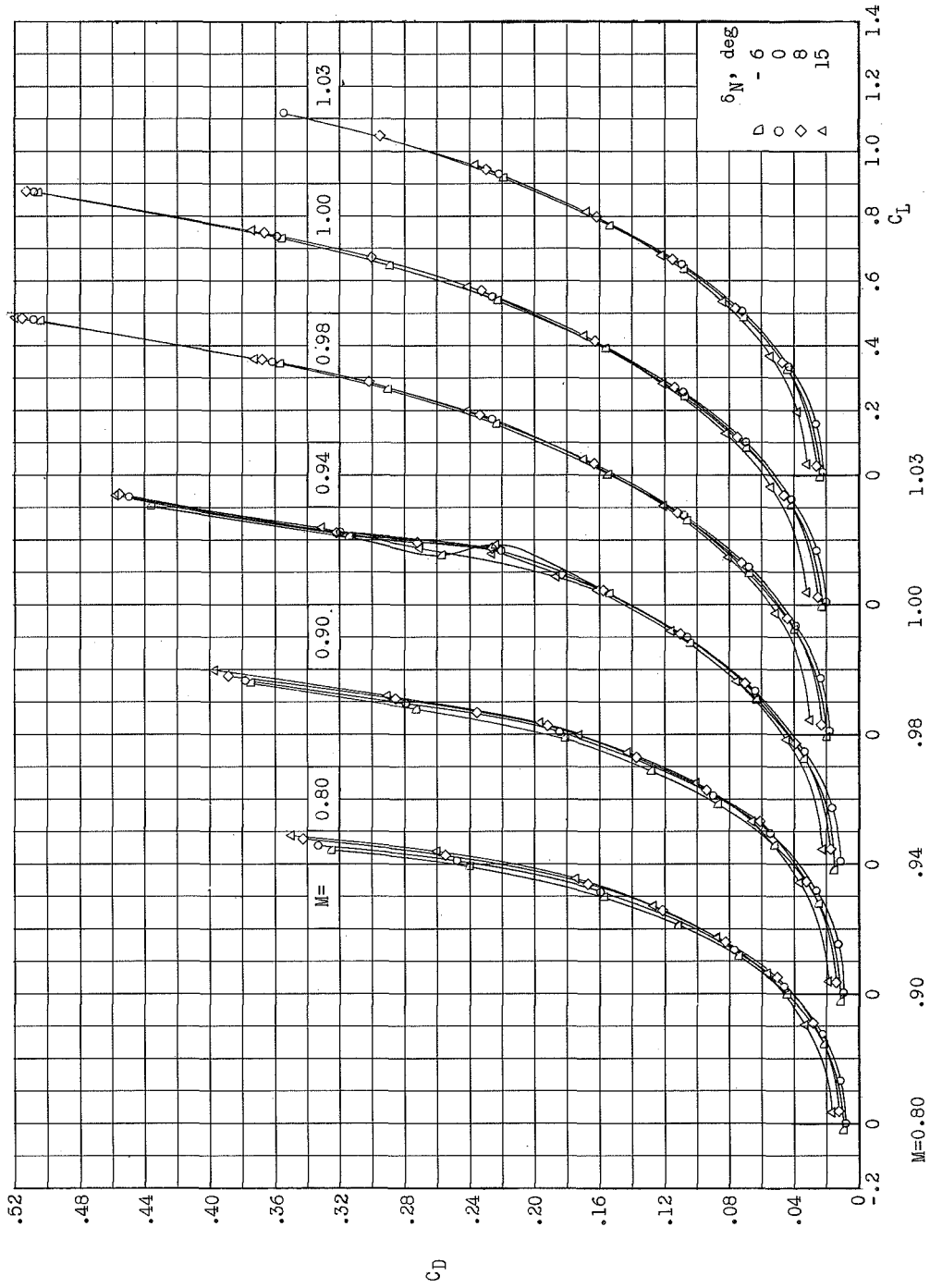
(b) $C_D$ against $C_L$.
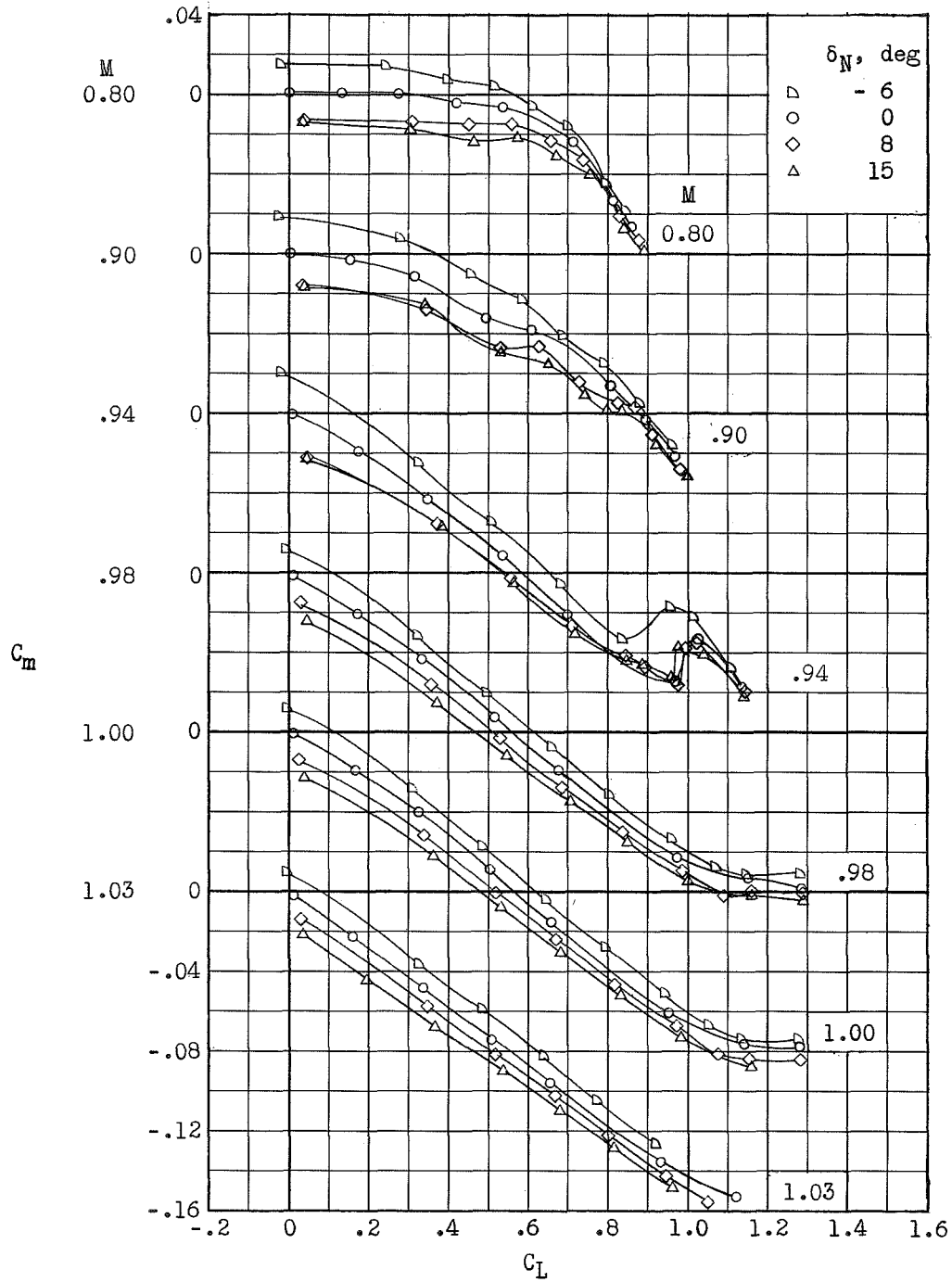
Figure 5.- Continued.

(c)  $C_m$  against  $C_L$.
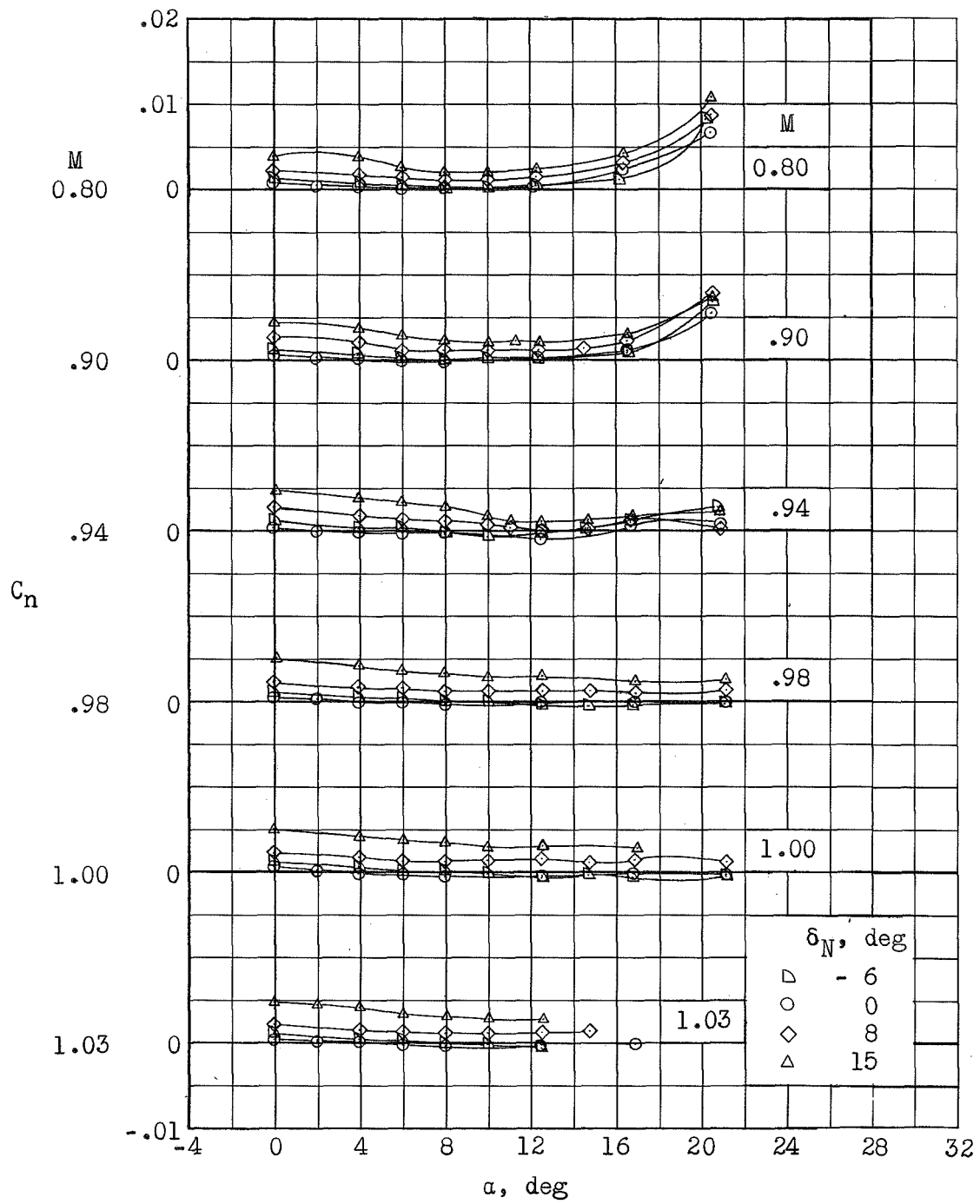
Figure 5.- Continued.

(d)  $C_n$  against  $\alpha$.

Figure 5.- Continued.
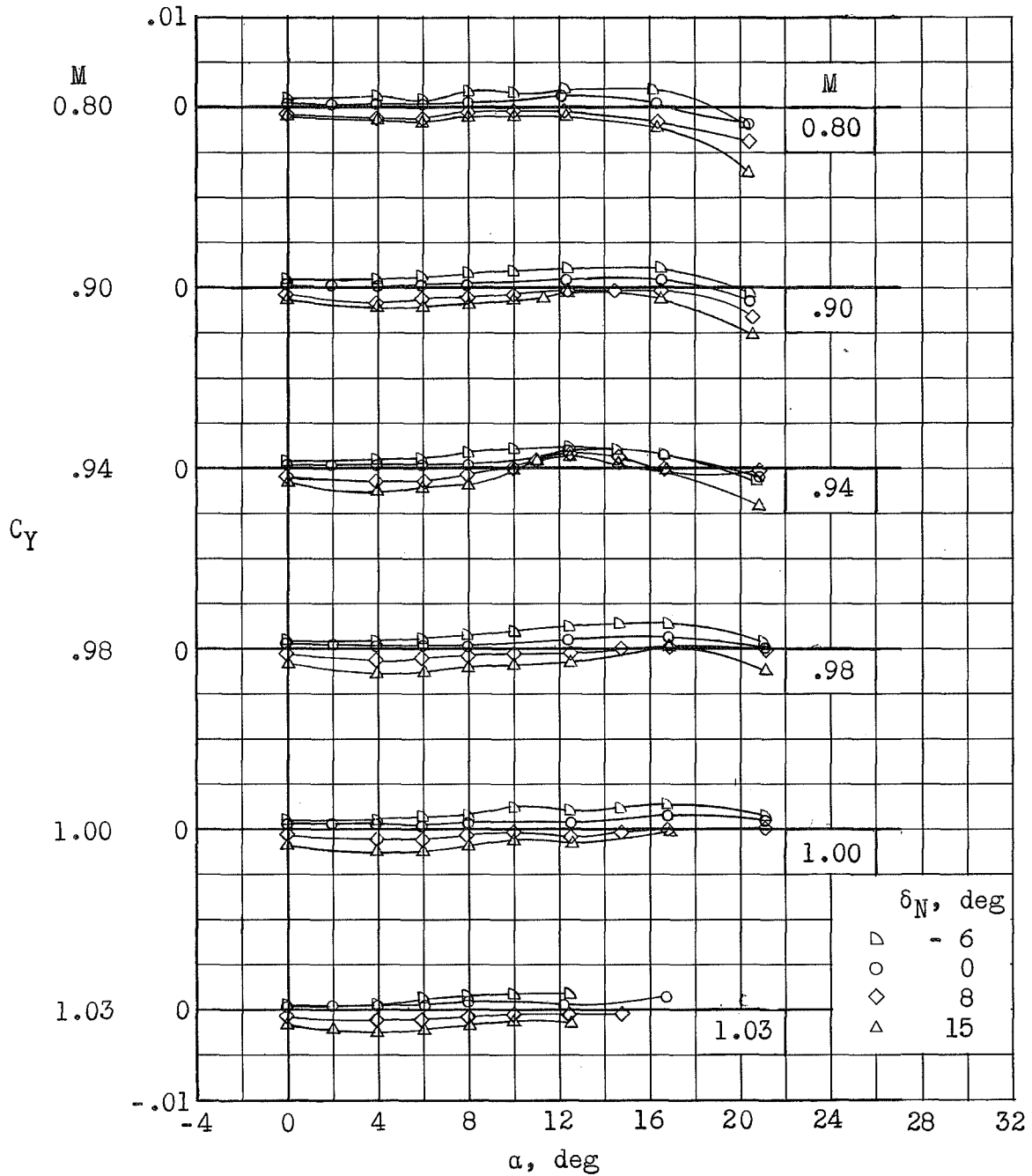
(e) $C_Y$ against $\alpha$.

Figure 5.- Concluded.
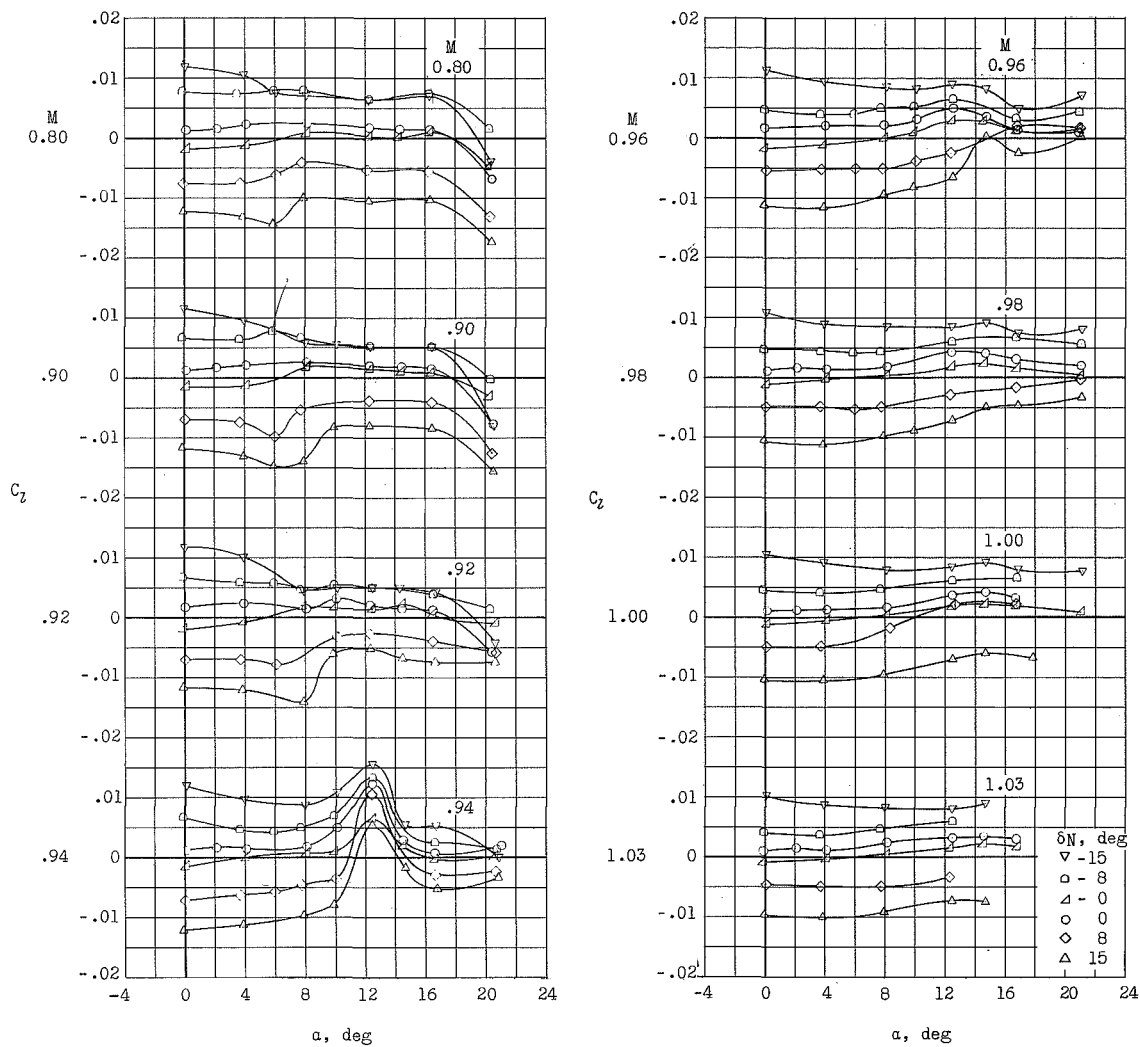
(a)  t = 0.

Figure 6.- Variation with angle of attack of the rolling-moment char-
acteristics of the three aileron configurations at various Mach num-
bers for several nominal angles of deflection.
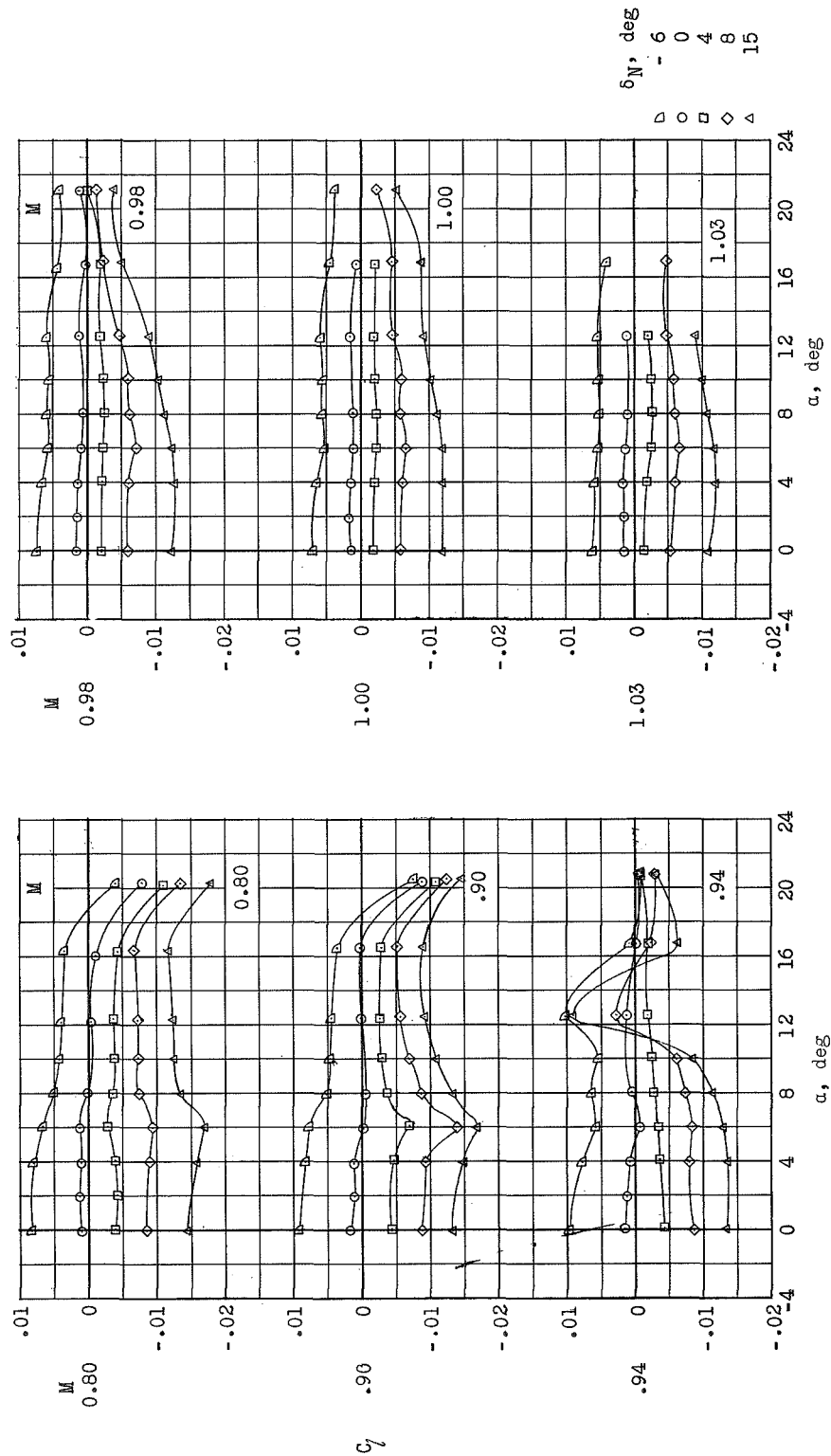
(b)  t = 1.0.

Figure 6.- Continued.
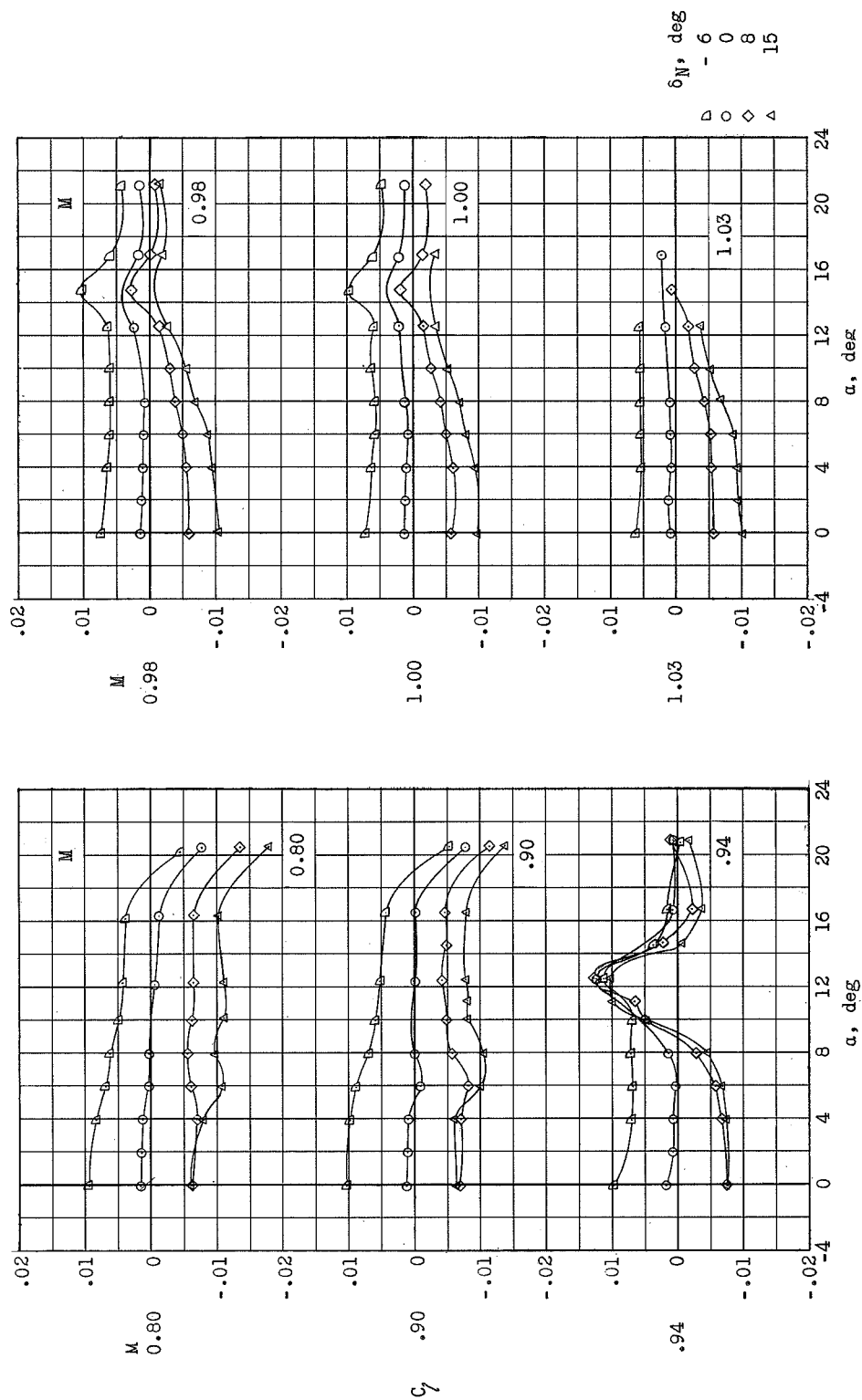
(c)  t = 1.0, balanced.

Figure 6.- Concluded.
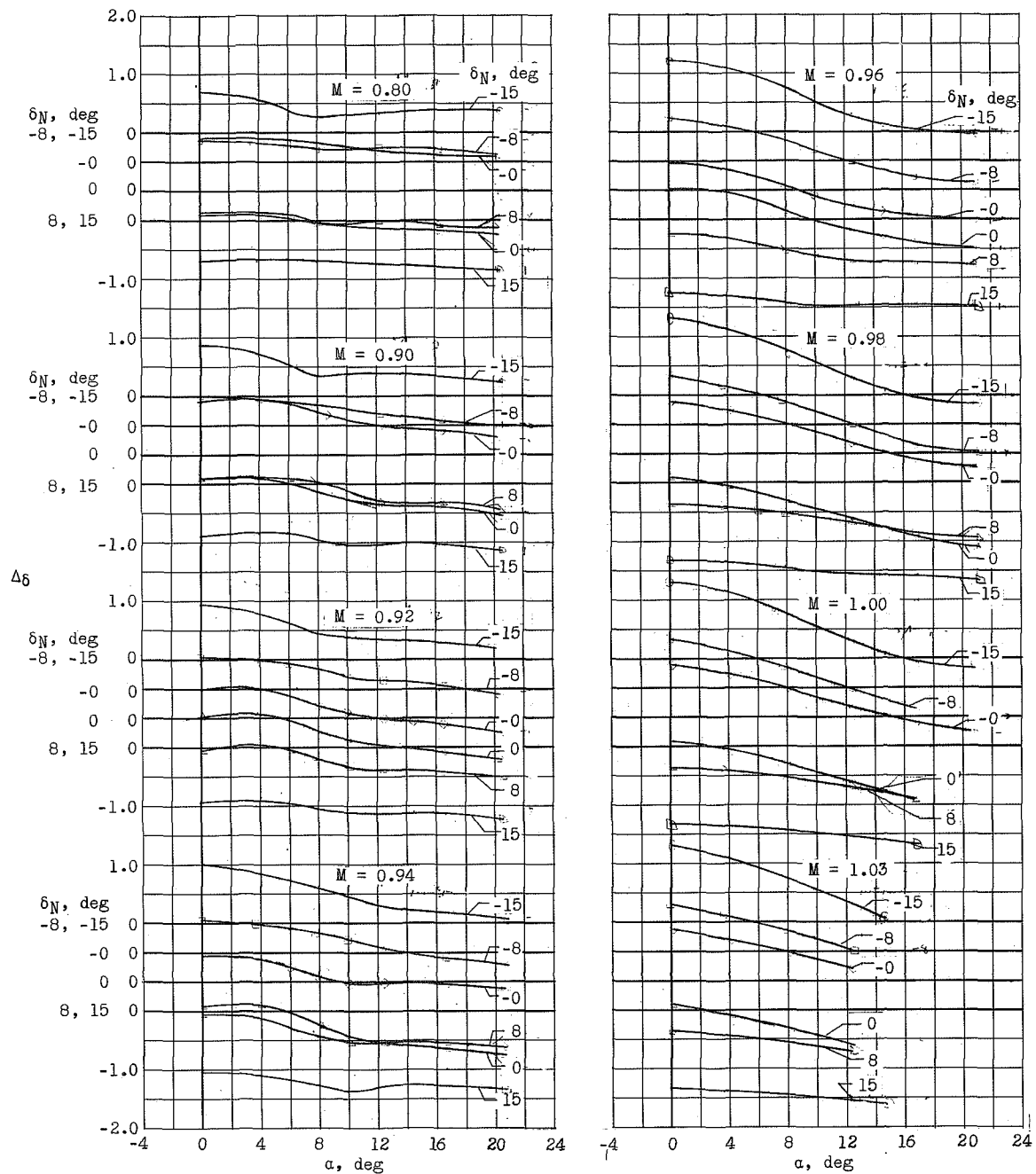
(a)  t = 0.

Figure 7.- Variation with angle of attack of the deviation of the
    actual control-deflection angle from the nominal control settings
    for each Mach number.
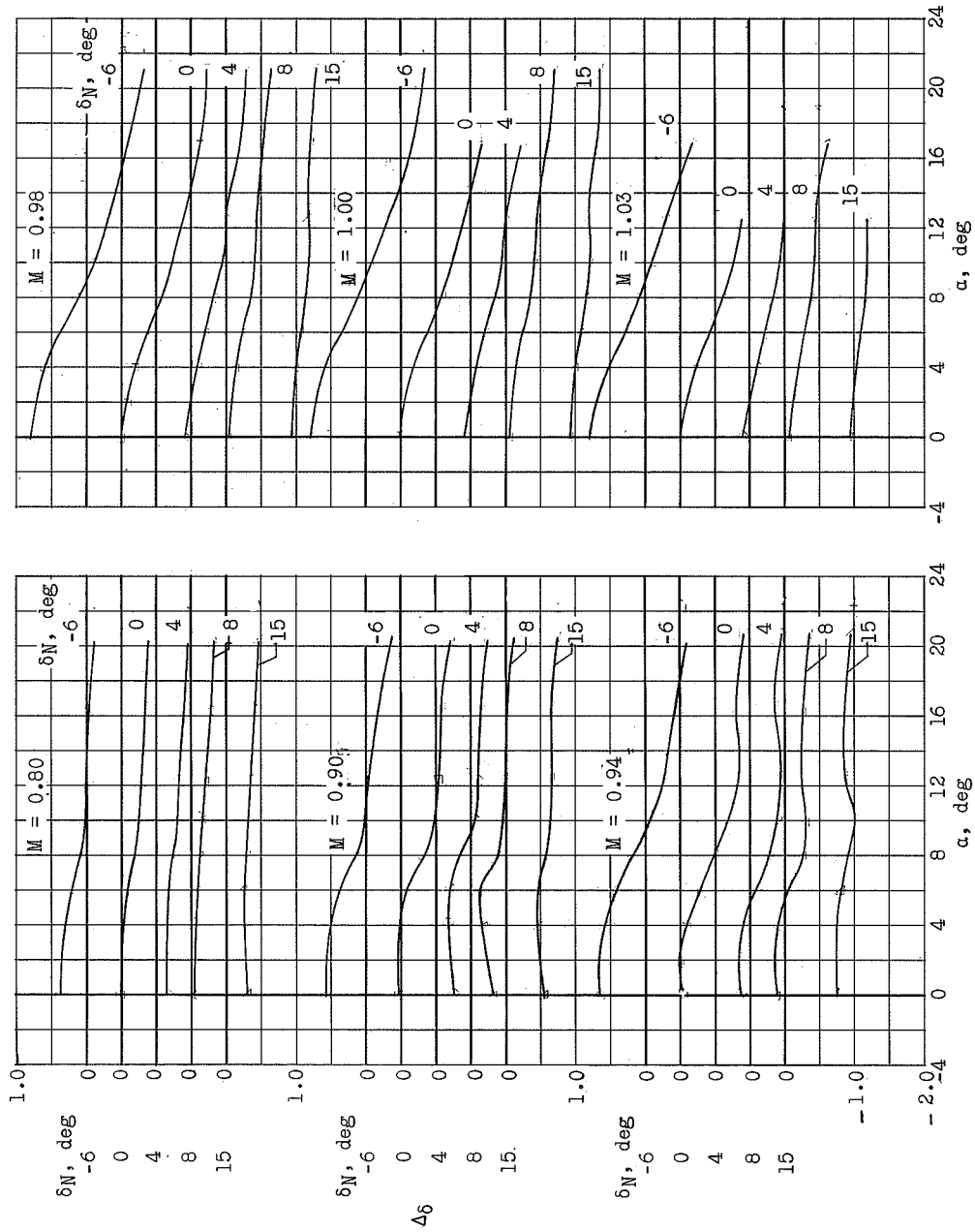
(b)  t = 1.0.

Figure 7.- Continued.
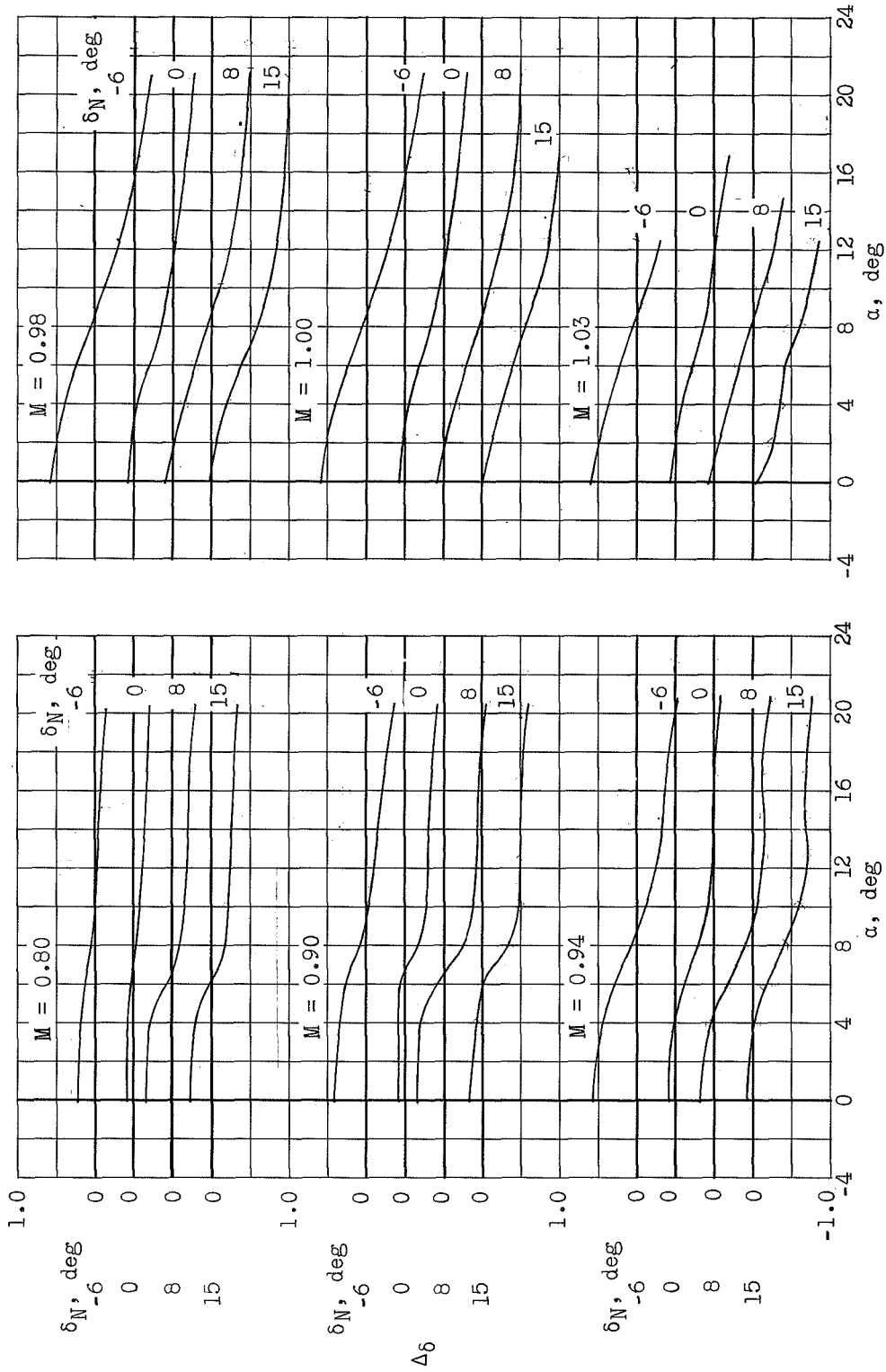
(c)  t = 1.0, balanced.

Figure 7.- Concluded.
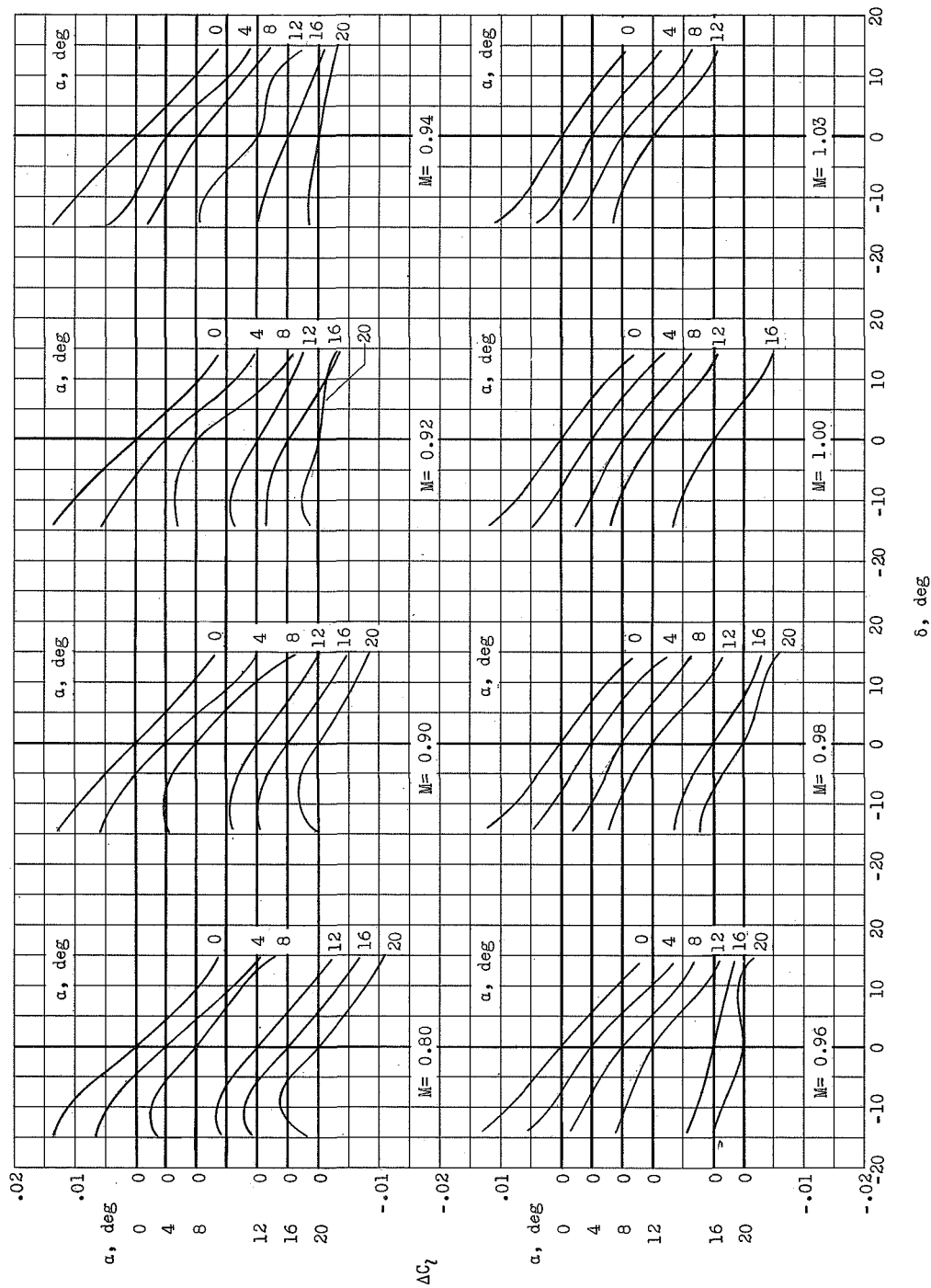
(a) t = 0.

Figure 8.- Variation with control-deflection angle of the incremental rolling-moment coefficients of the three aileron configurations at various Mach numbers for constant angles of attack up to 20°.
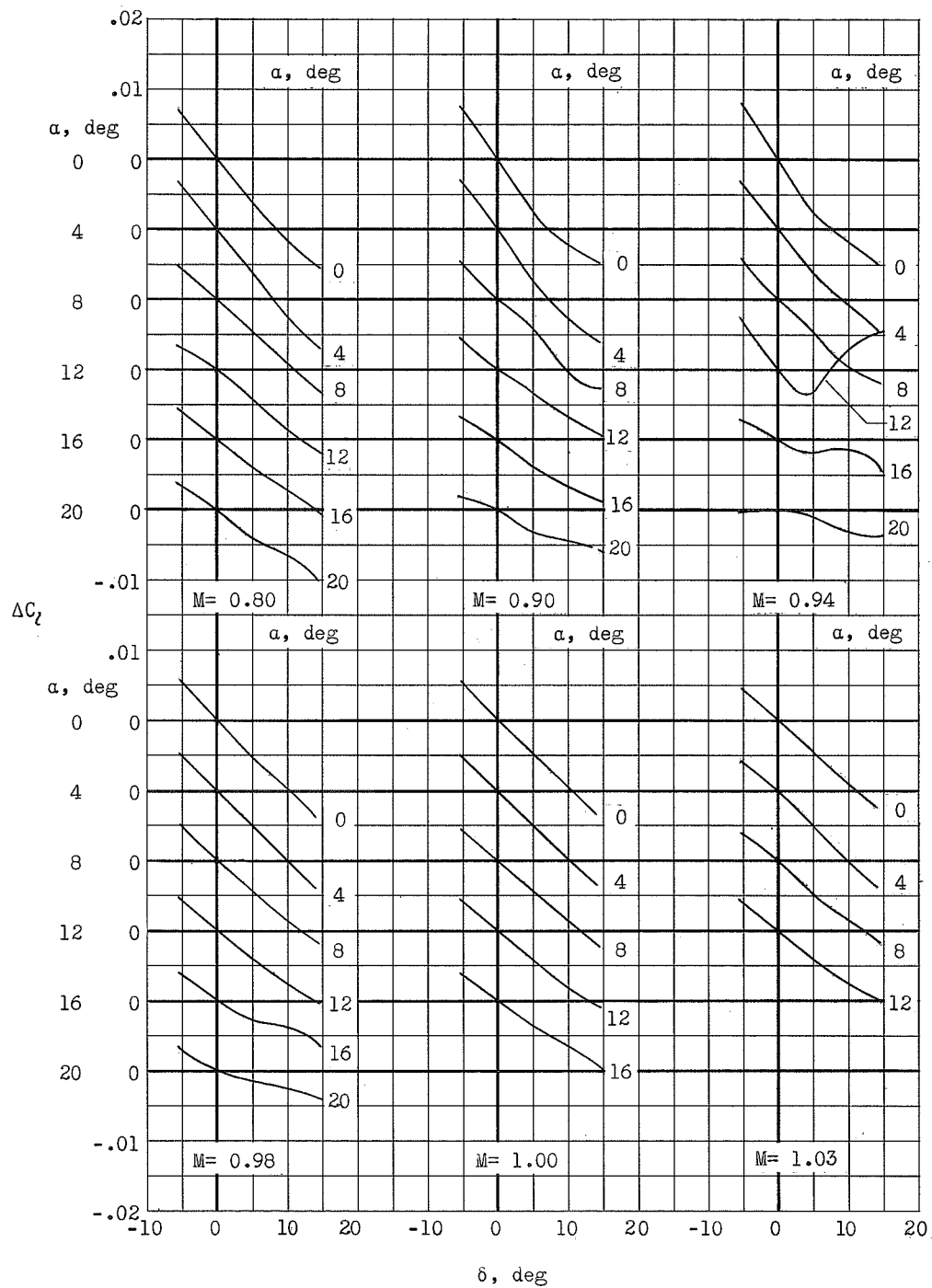
(b)  t = 1.0.

Figure 8.- Continued.
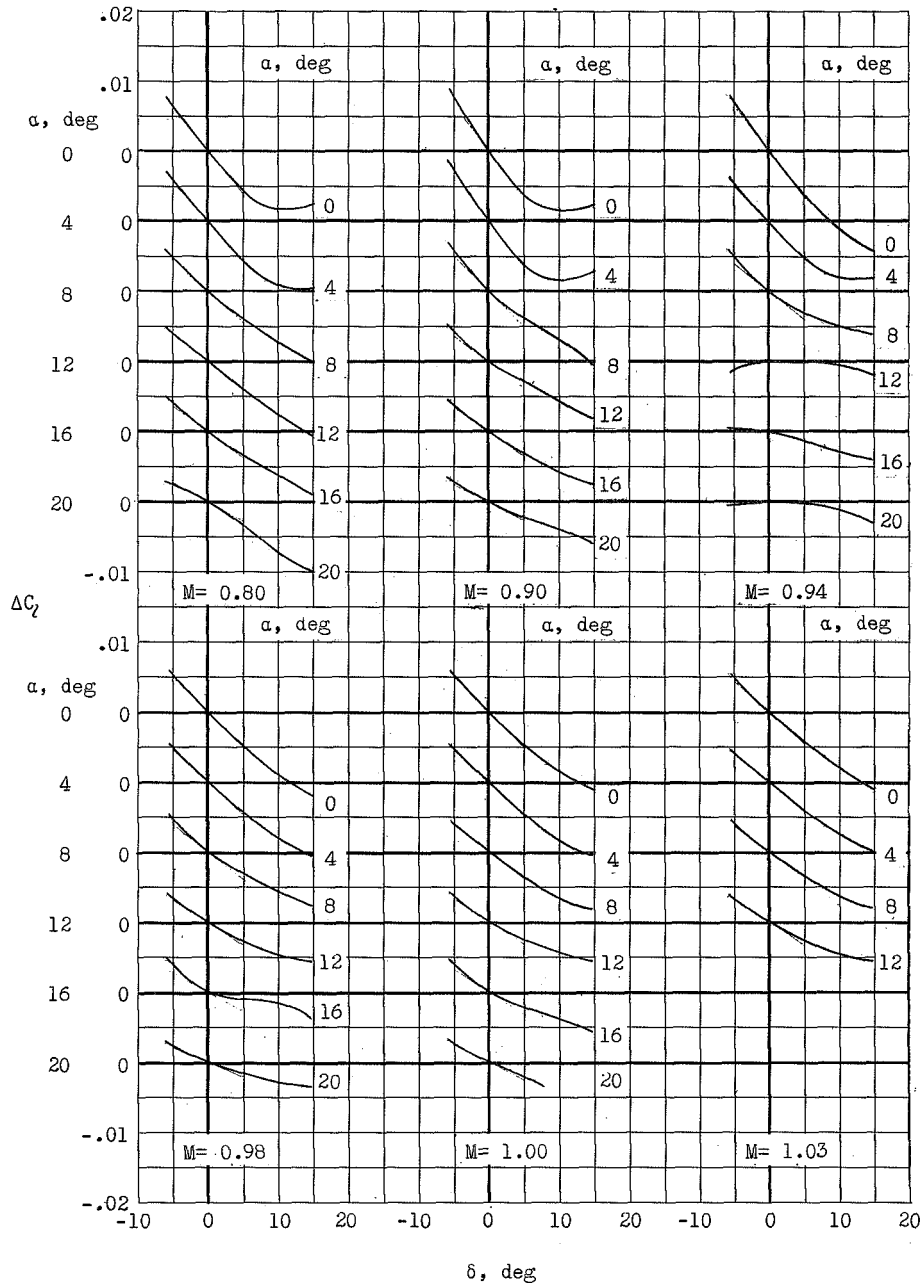
(c)   t = 1.0, balanced.

Figure 8.- Concluded.
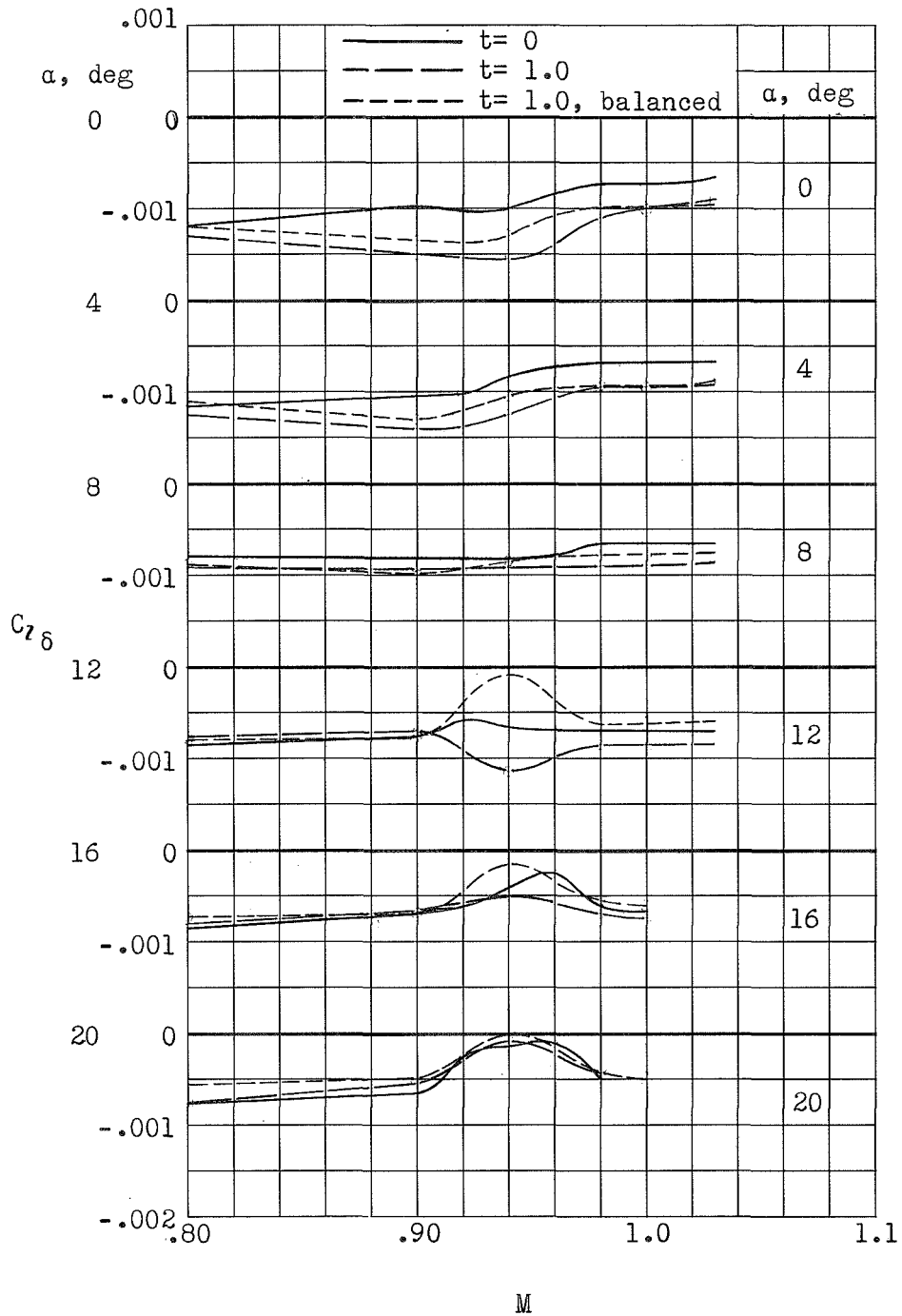
Figure 9.- Variation with Mach number of the aileron rolling-moment
    effectiveness parameter for the three aileron configurations at
    constant angles of attack up to 20°.
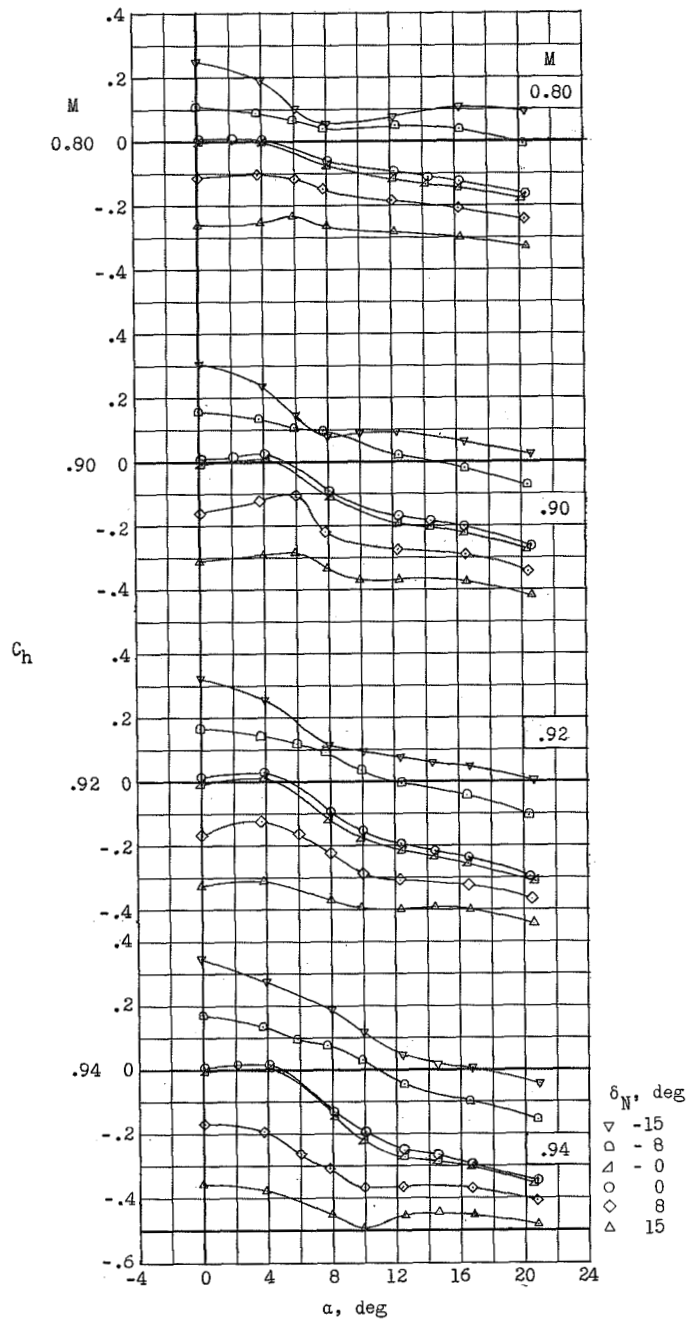
(a)  t = 0.

Figure 10.- Variation with angle of attack of the hinge-moment char-
acteristics of the three aileron configurations for several nominal
control-deflection angles and Mach numbers.
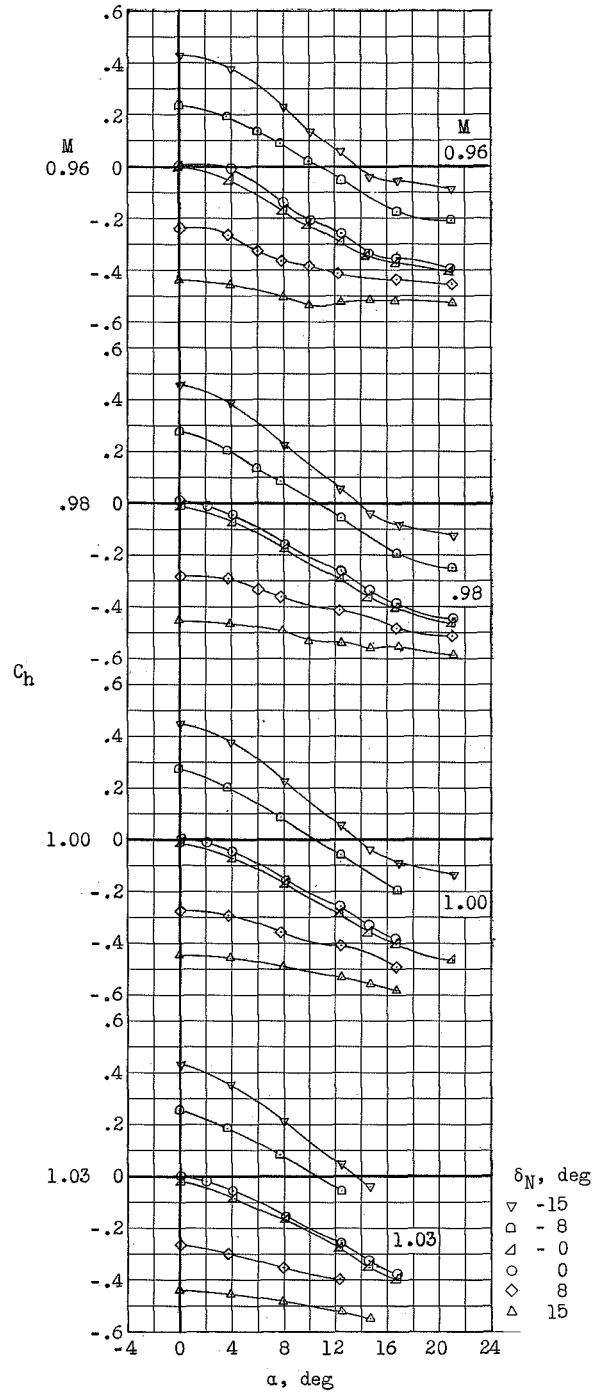
(a) Concluded.

Figure 10.- Continued.
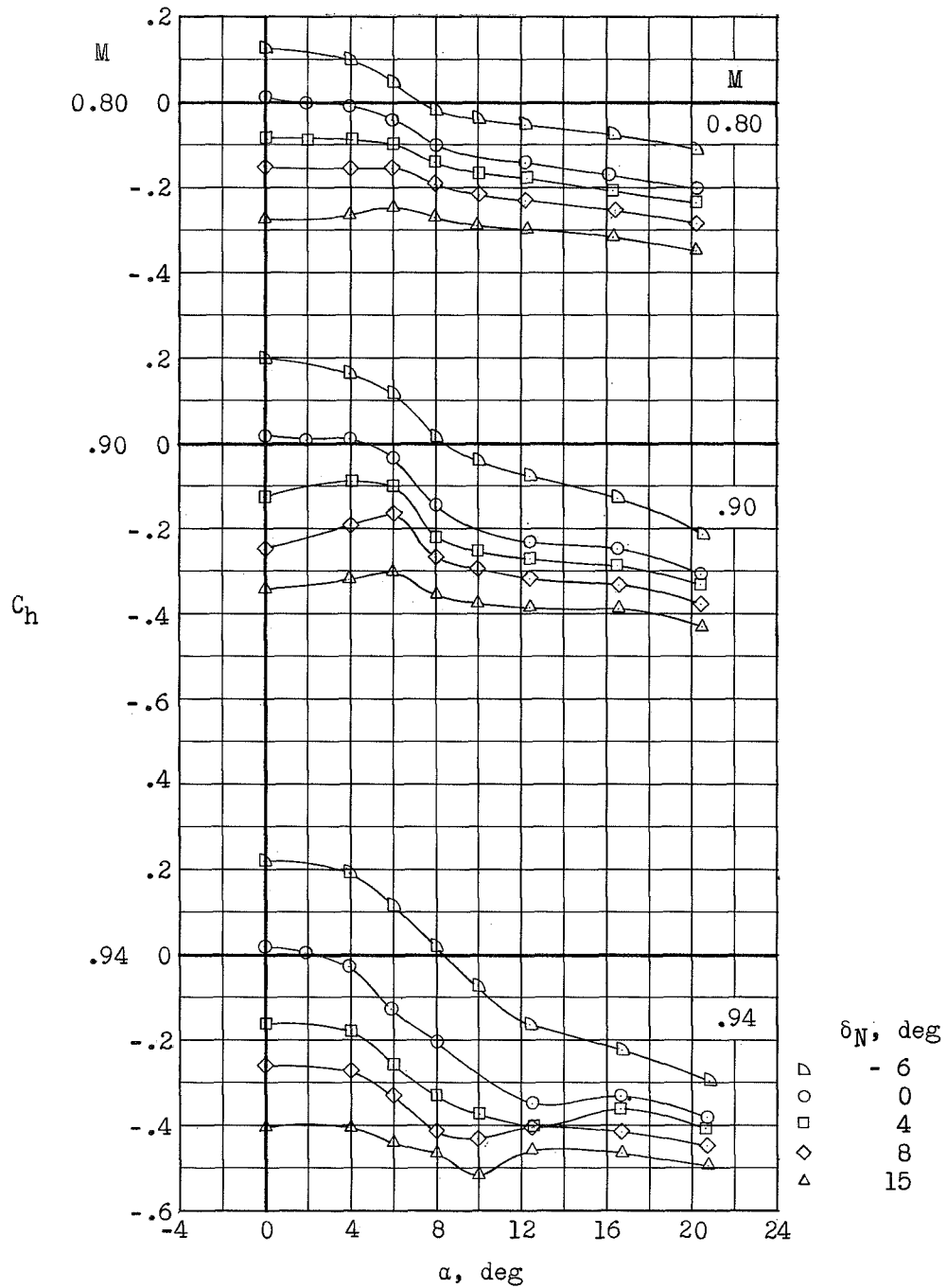
(b)   t = 1.0.

Figure 10.- Continued.
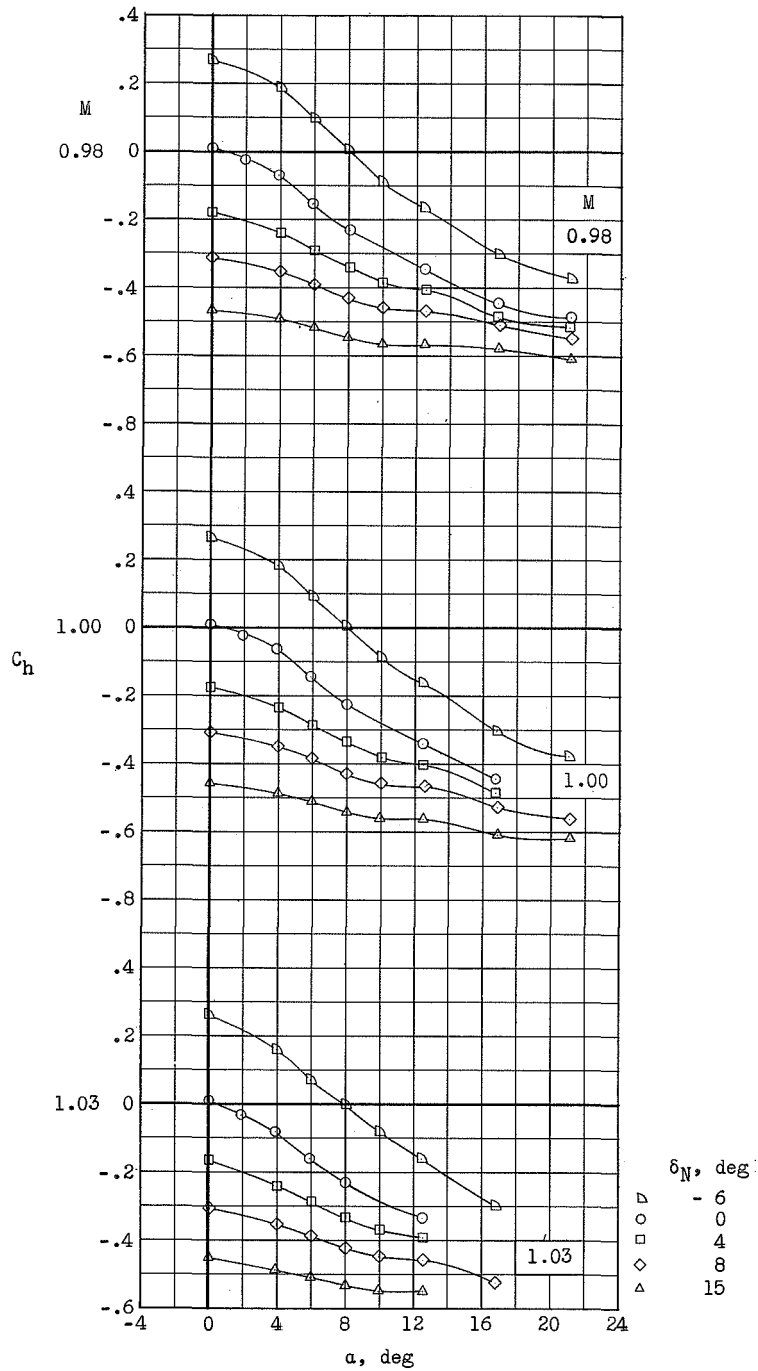
(b) Concluded.

Figure 10.- Continued.
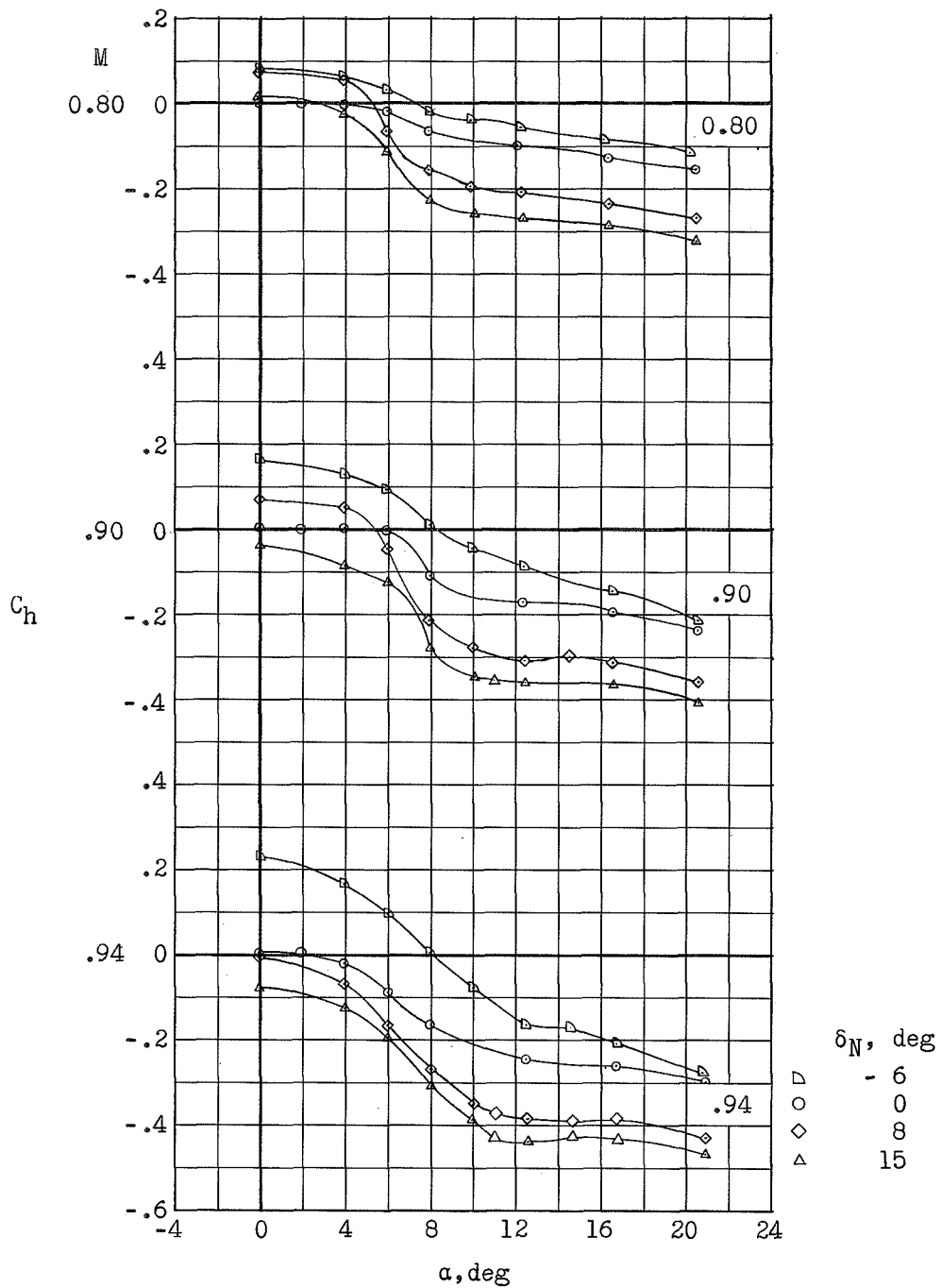
(c)  t = 1.0, balanced.

Figure 10.- Continued.
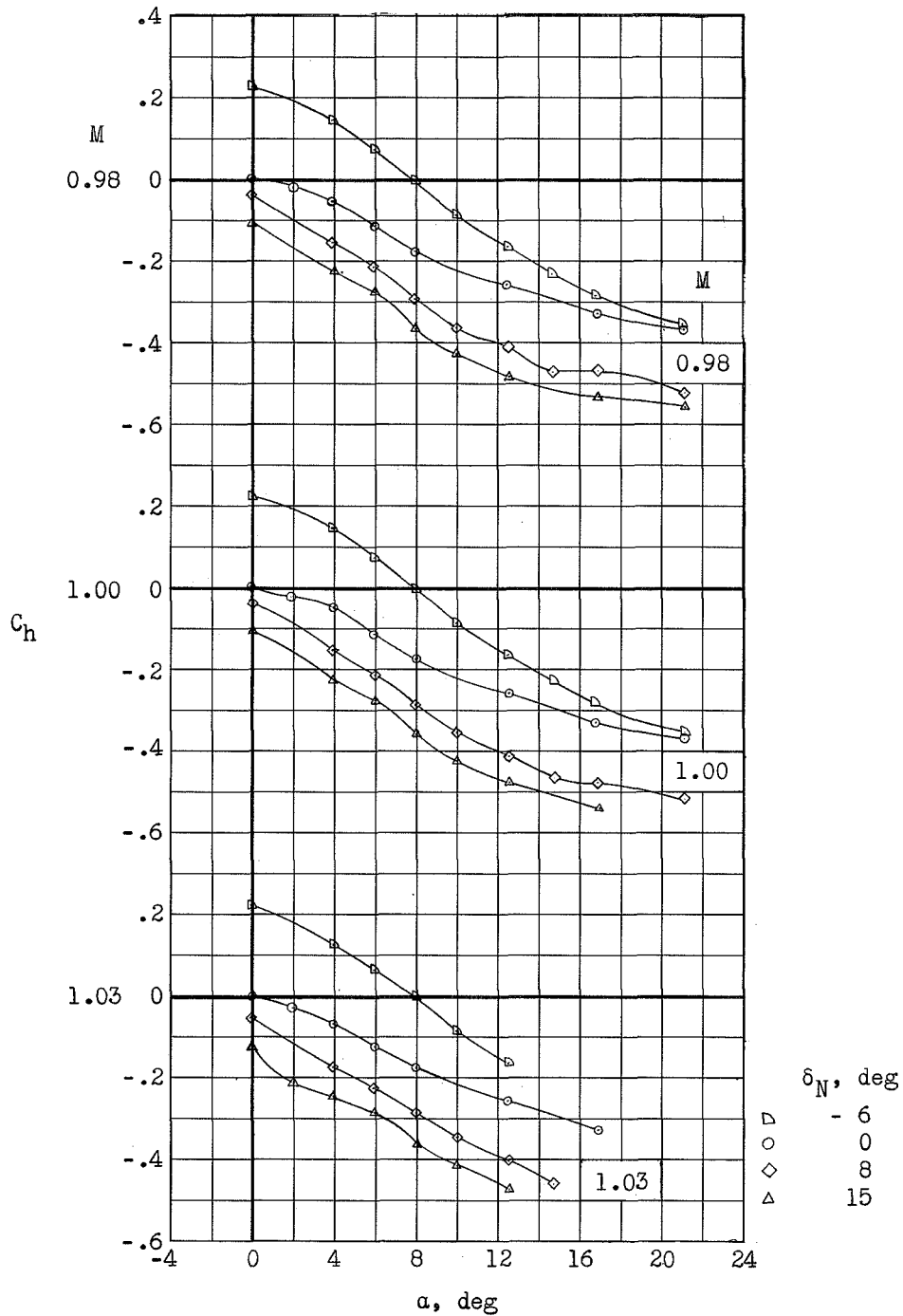
(c) Concluded.

Figure 10.- Concluded.
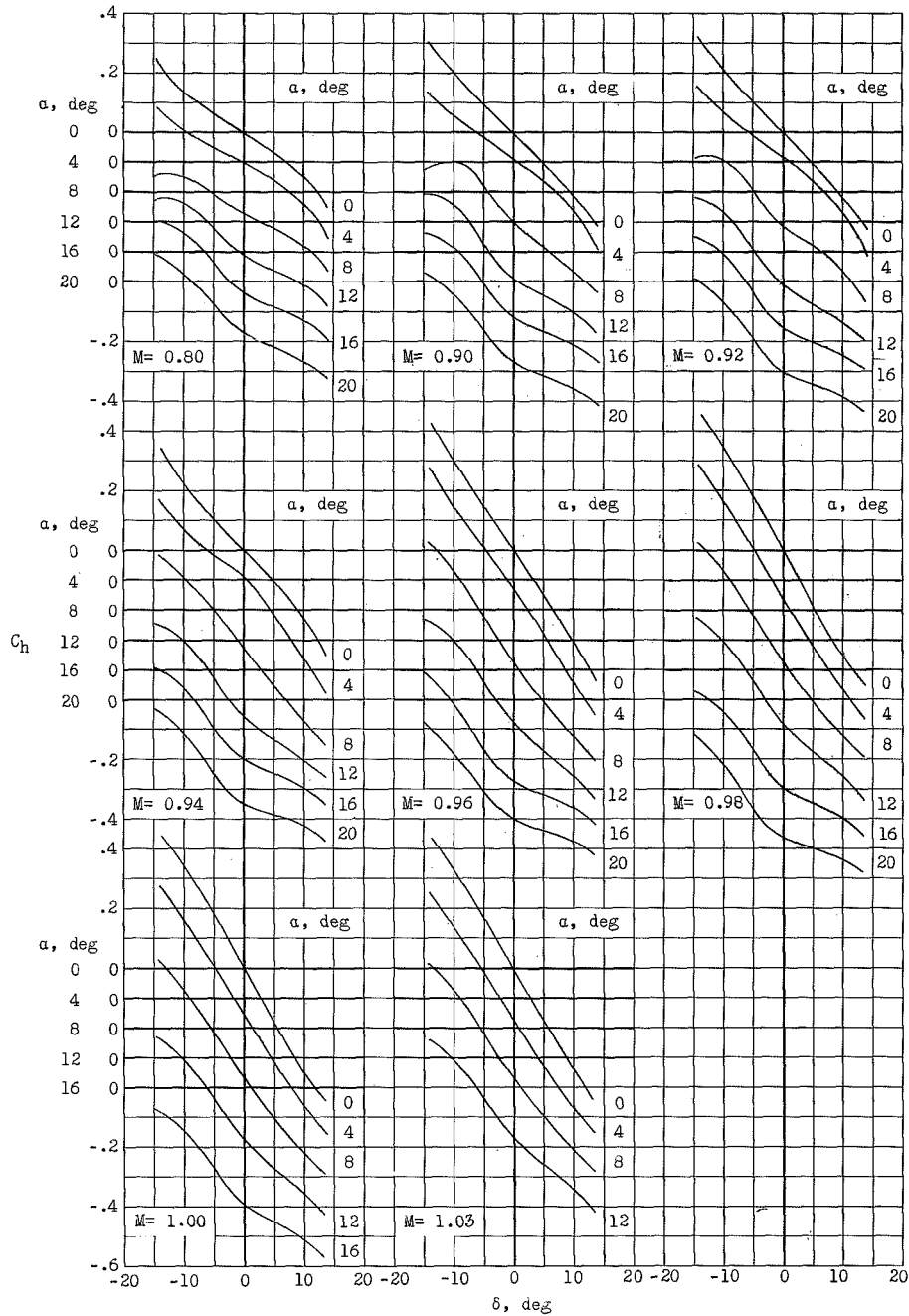
(a)  t = 0.

Figure 11.- Variation with control-deflection angle of the aileron
    hinge-moment coefficient for the three configurations at various
    Mach numbers.
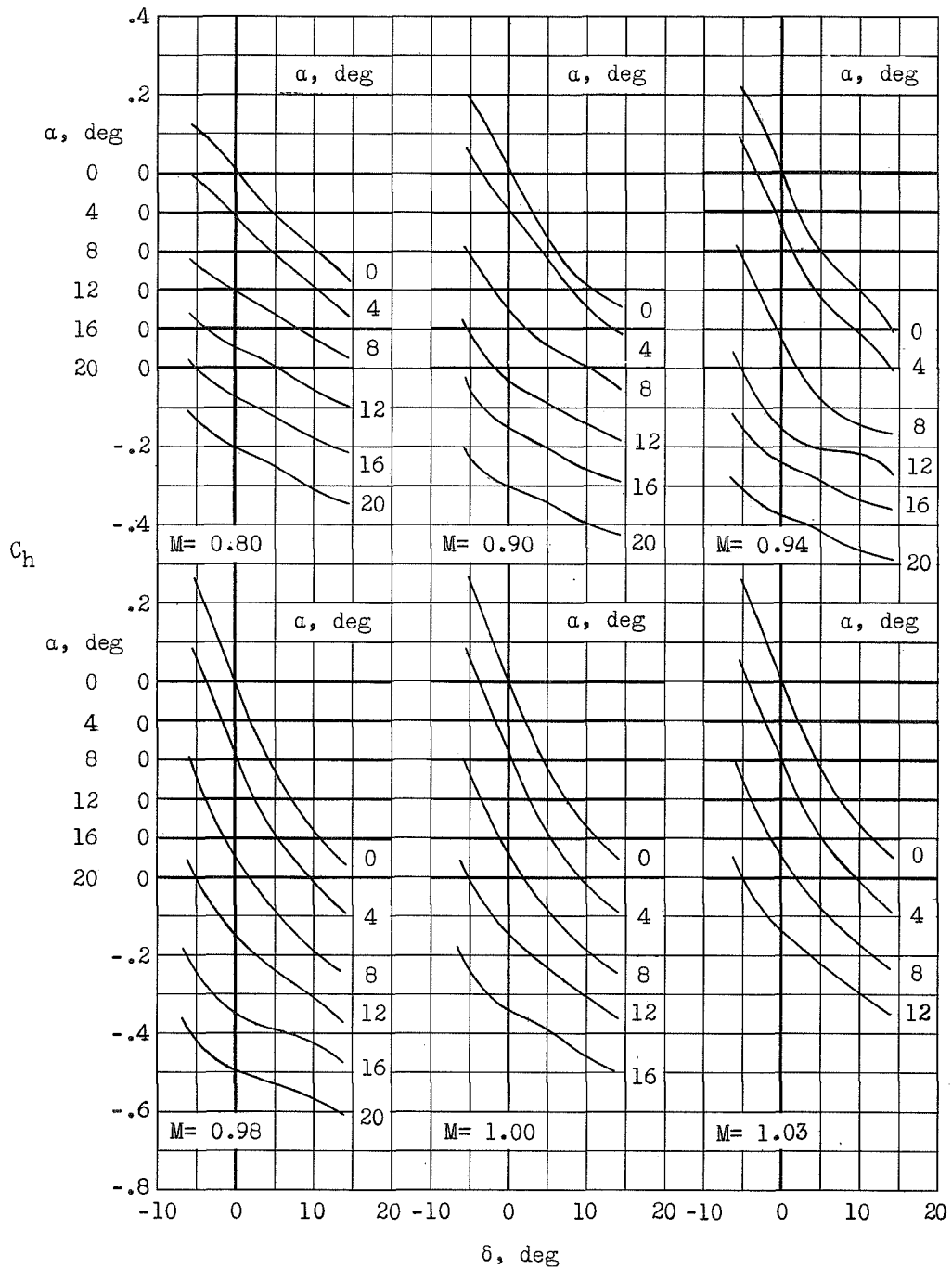
(b)  t = 1.0.

Figure 11.- Continued.
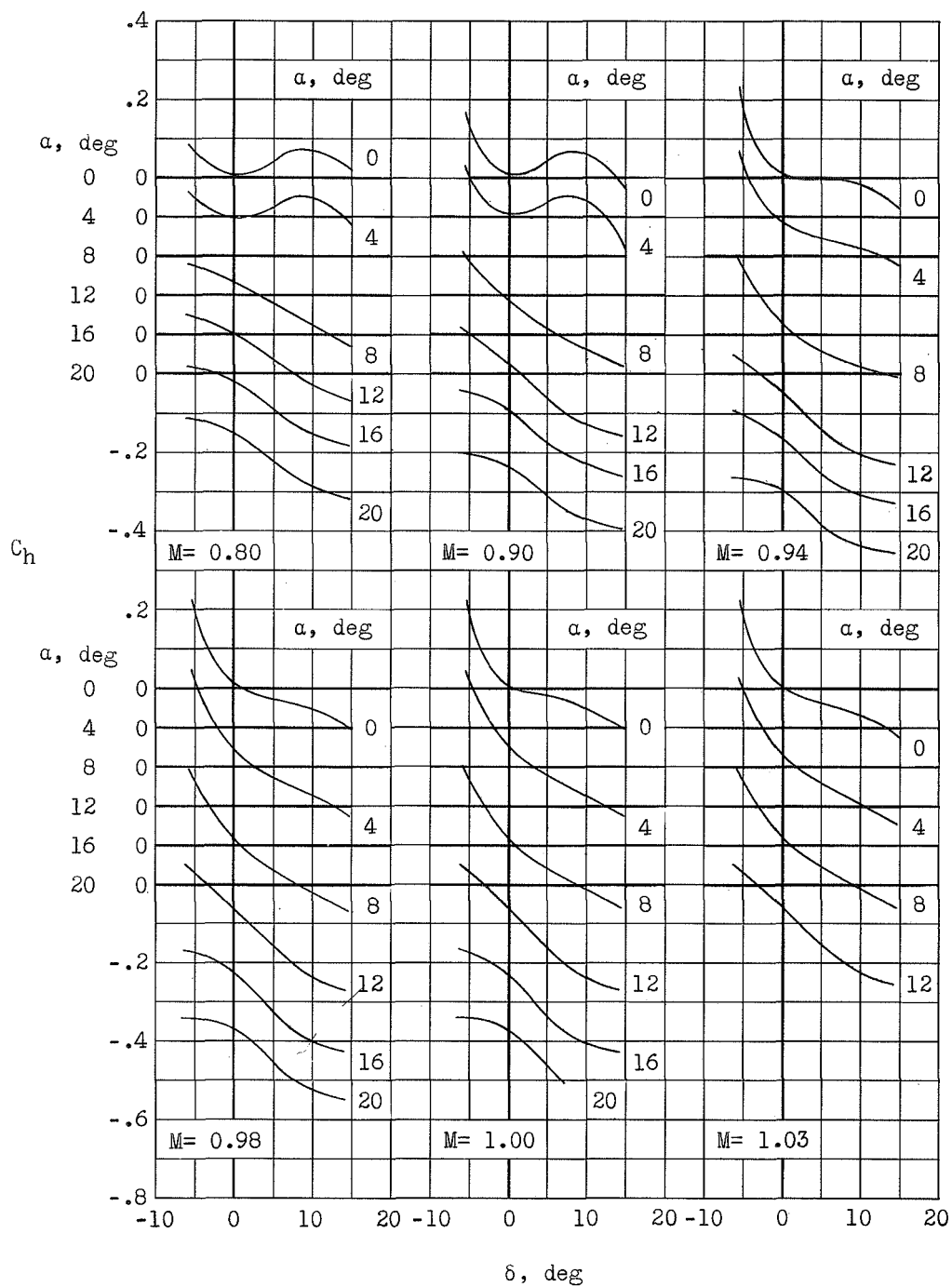
(c)  t = 1.0, balanced.

Figure 11.- Concluded.
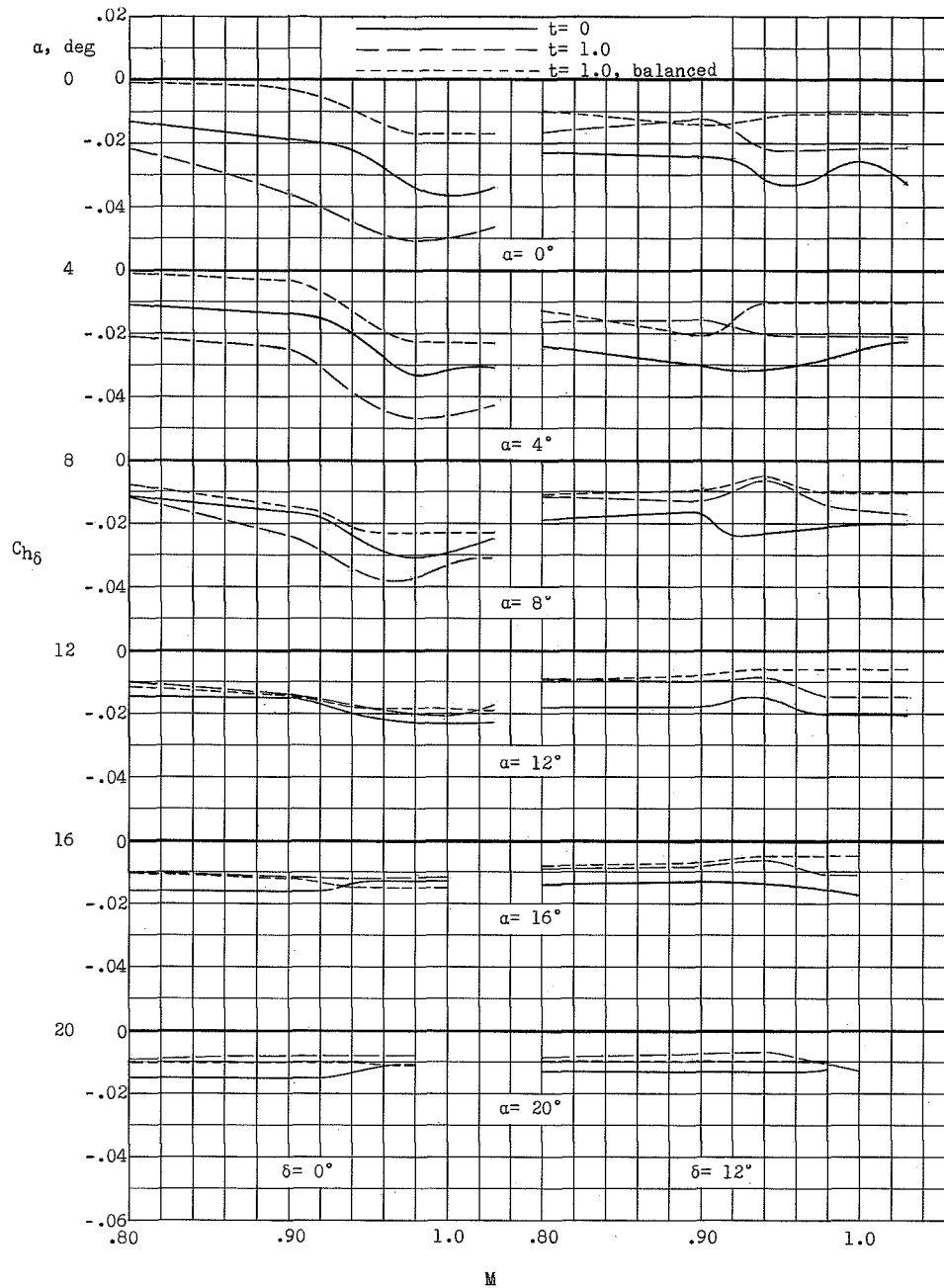
(a)  $C_{h_\delta}$  against  M.

Figure 12.- Variation with Mach number of  $C_{h_\delta}$  at  $\delta = 0^O$  and  $12^O$

and  $C_{h_\alpha}$  at  $\alpha = 0^O$  with  $\delta = 0^O$  for the three configurations.
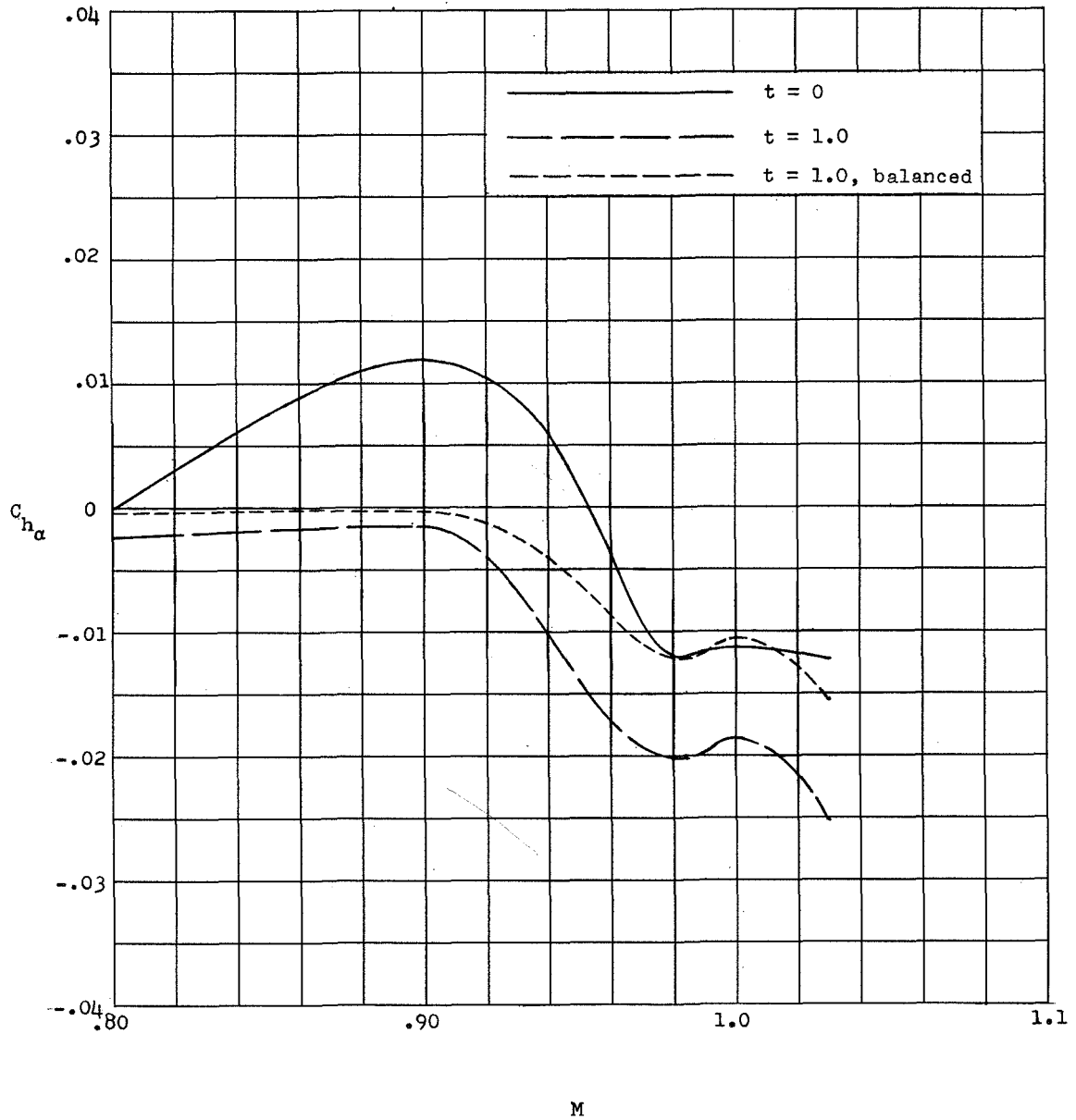
(b) $C_{h_\alpha}$ against M.

Figure 12.- Concluded.
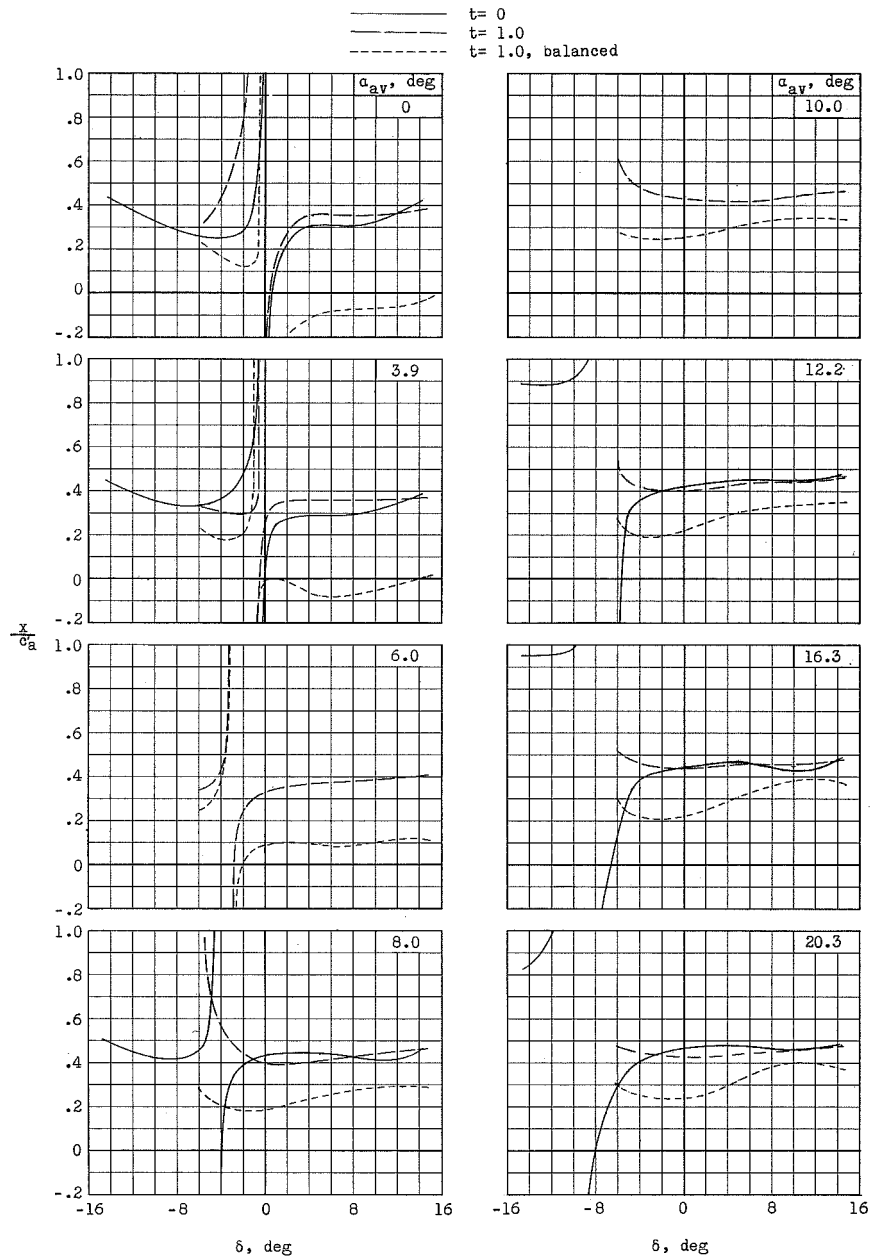
(a)  M = 0.80.

Figure 13.- Effect of aileron deflection on the chordwise location of
the center of pressure for the three aileron configurations at
various angles of attack and Mach numbers.
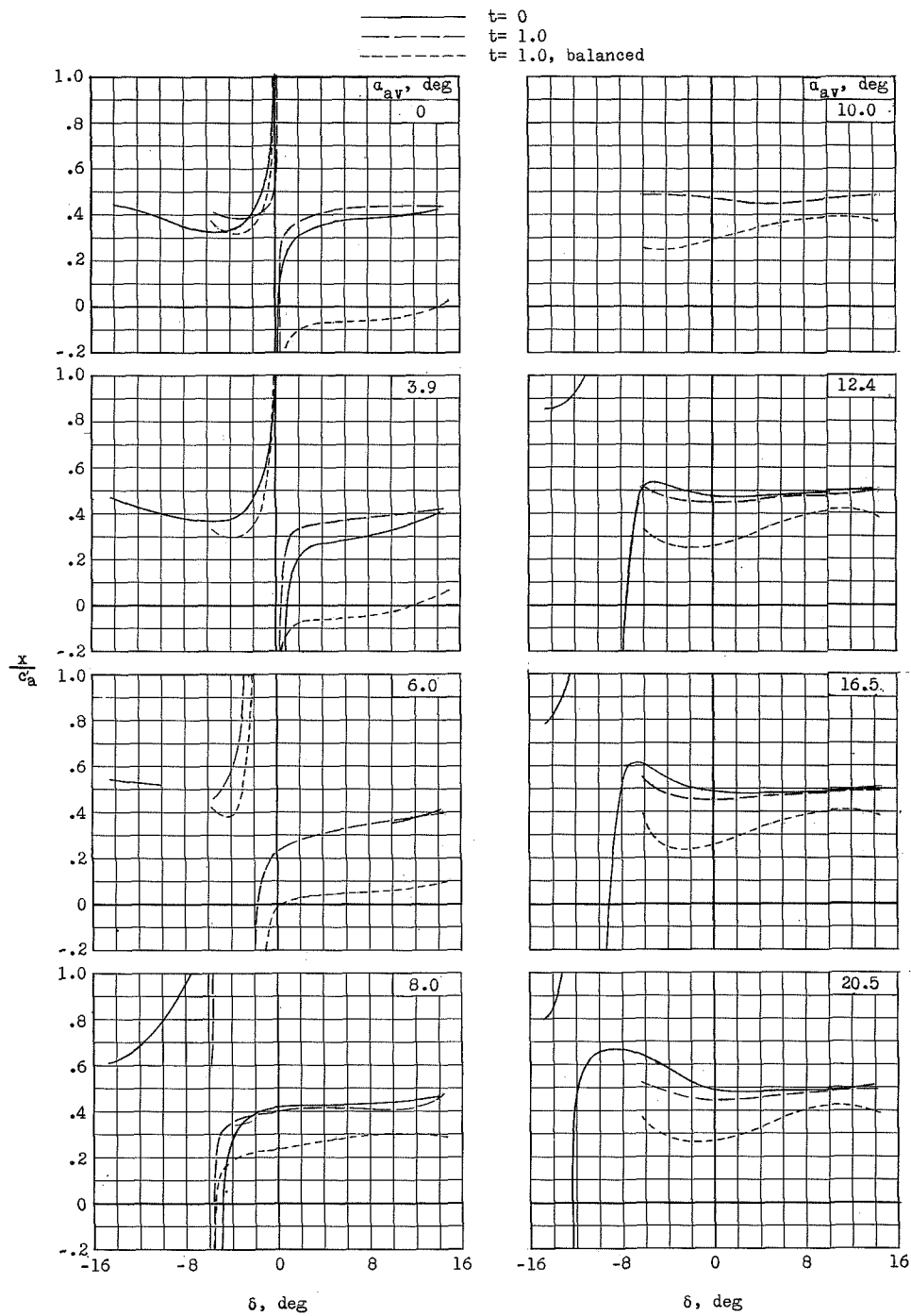
(b)   M = 0.90.

Figure 13.- Continued.
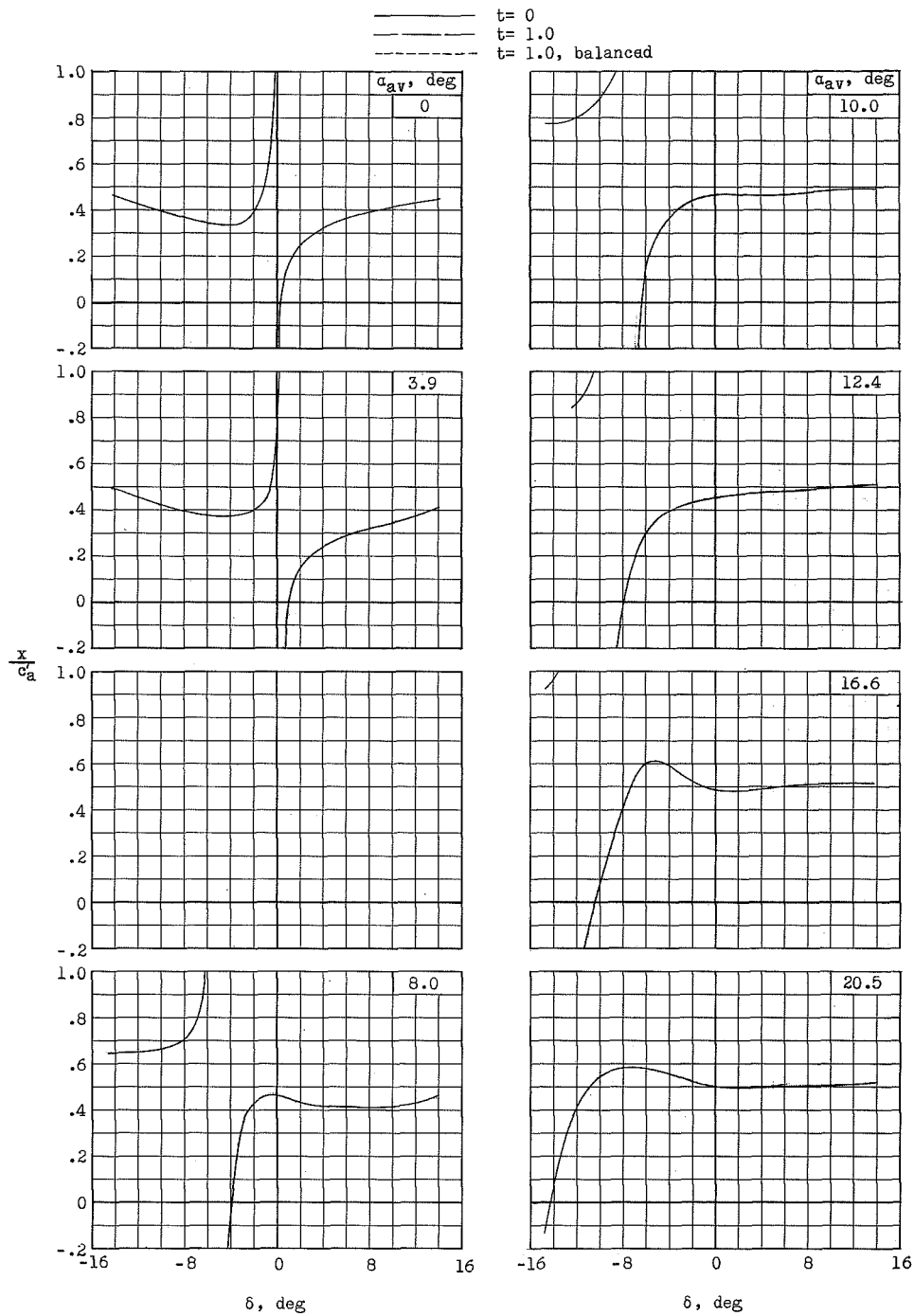
(c)   M = 0.92.

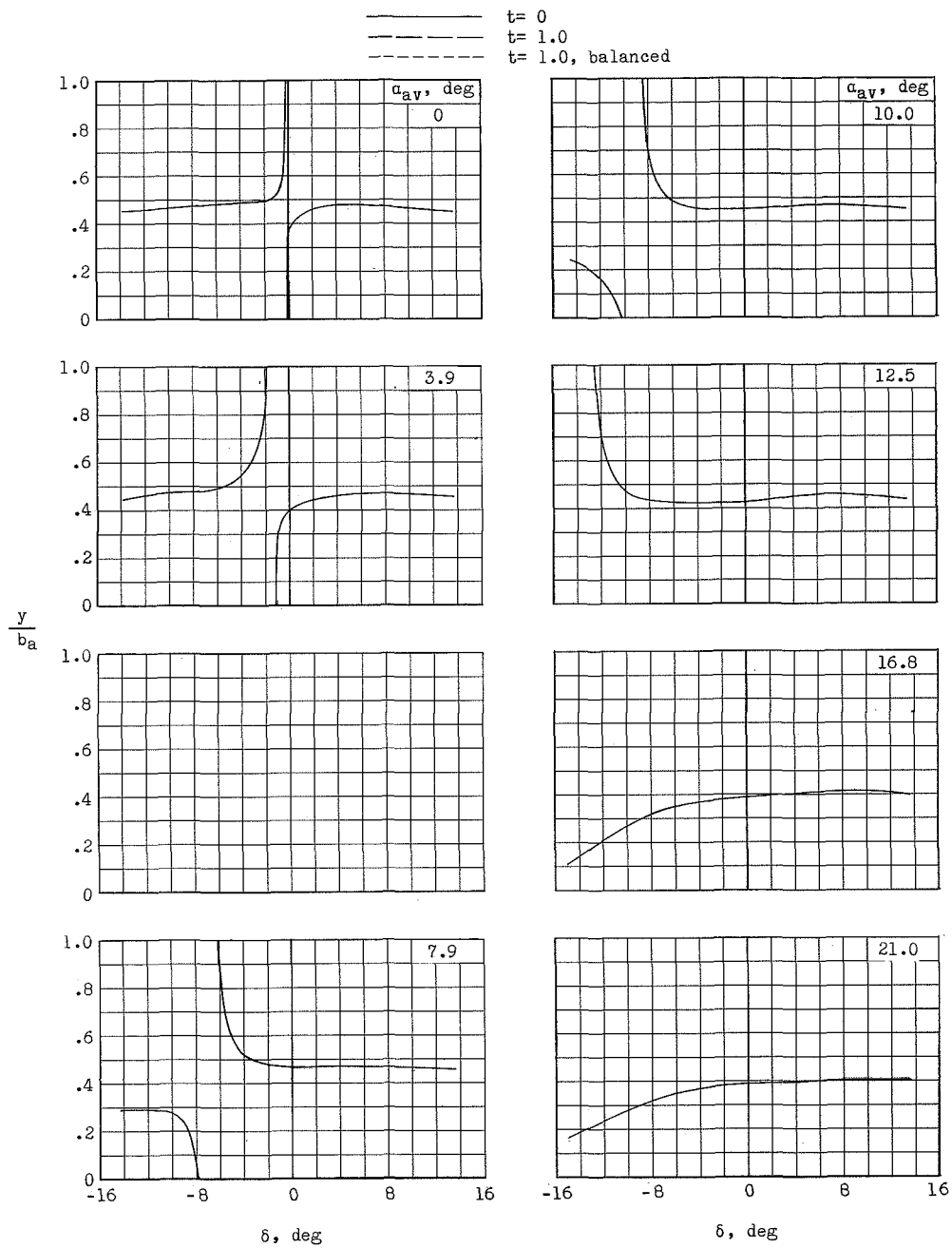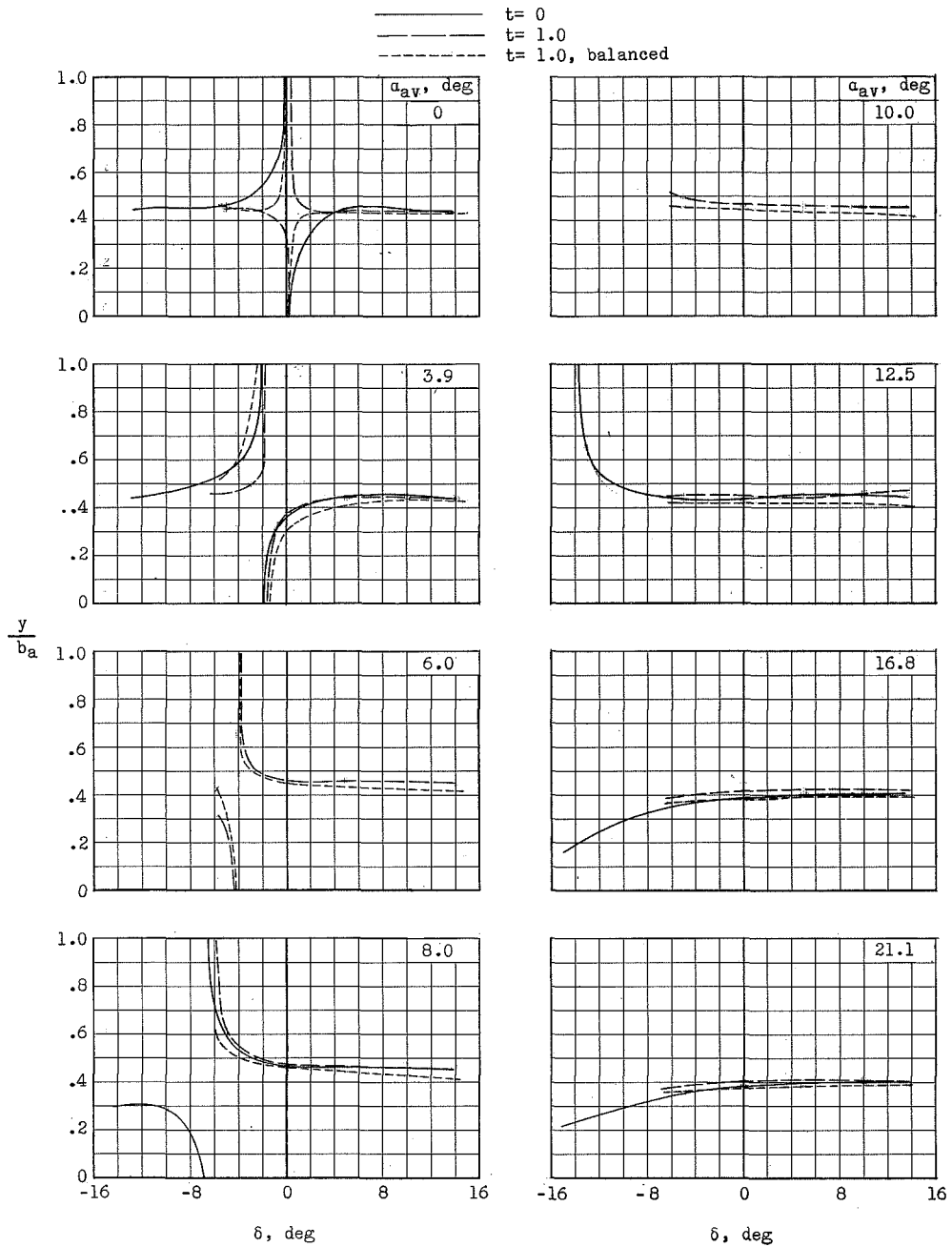Figure 13.- Continued.
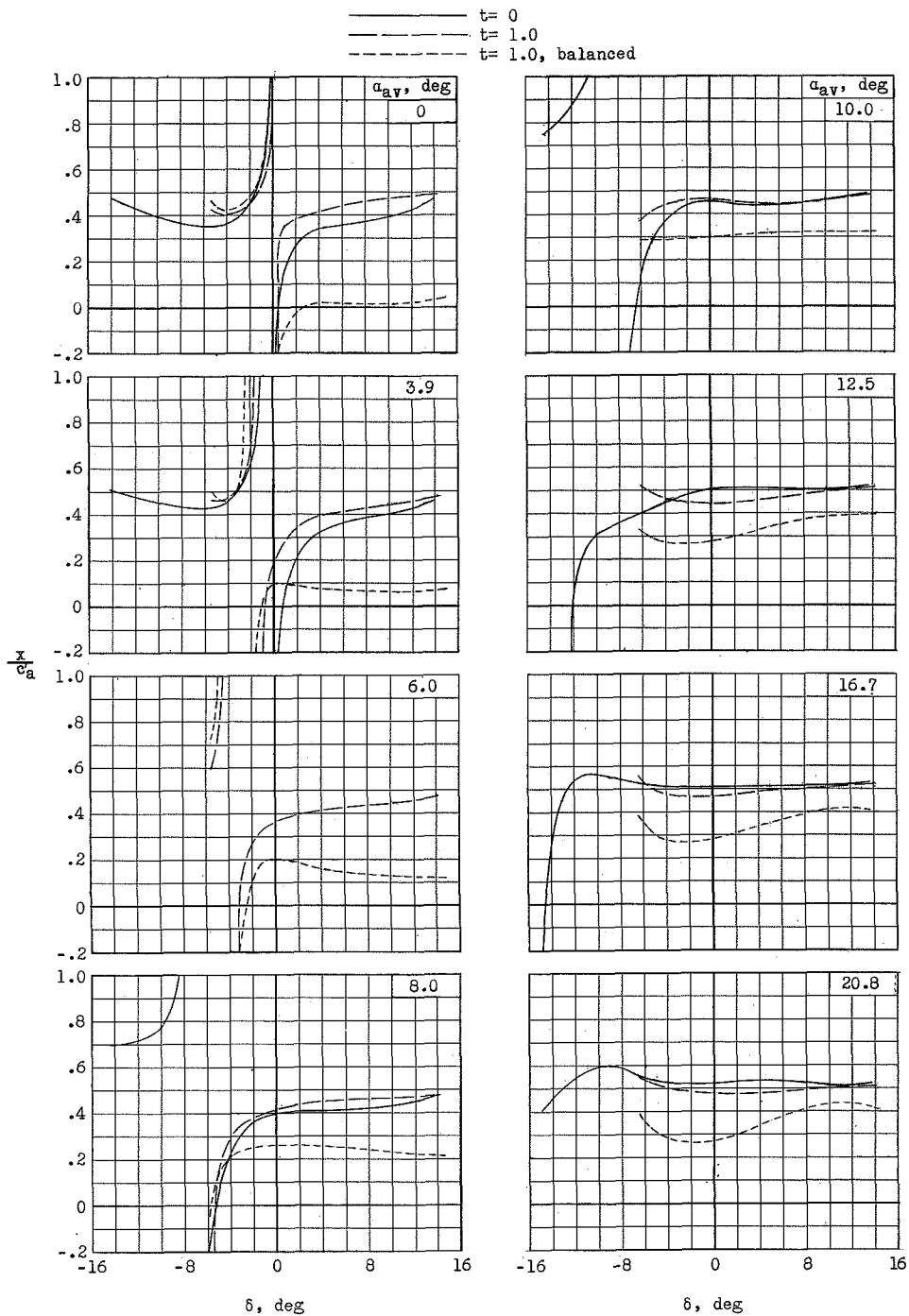
(d)  M = 0.94.

Figure 13.- Continued.
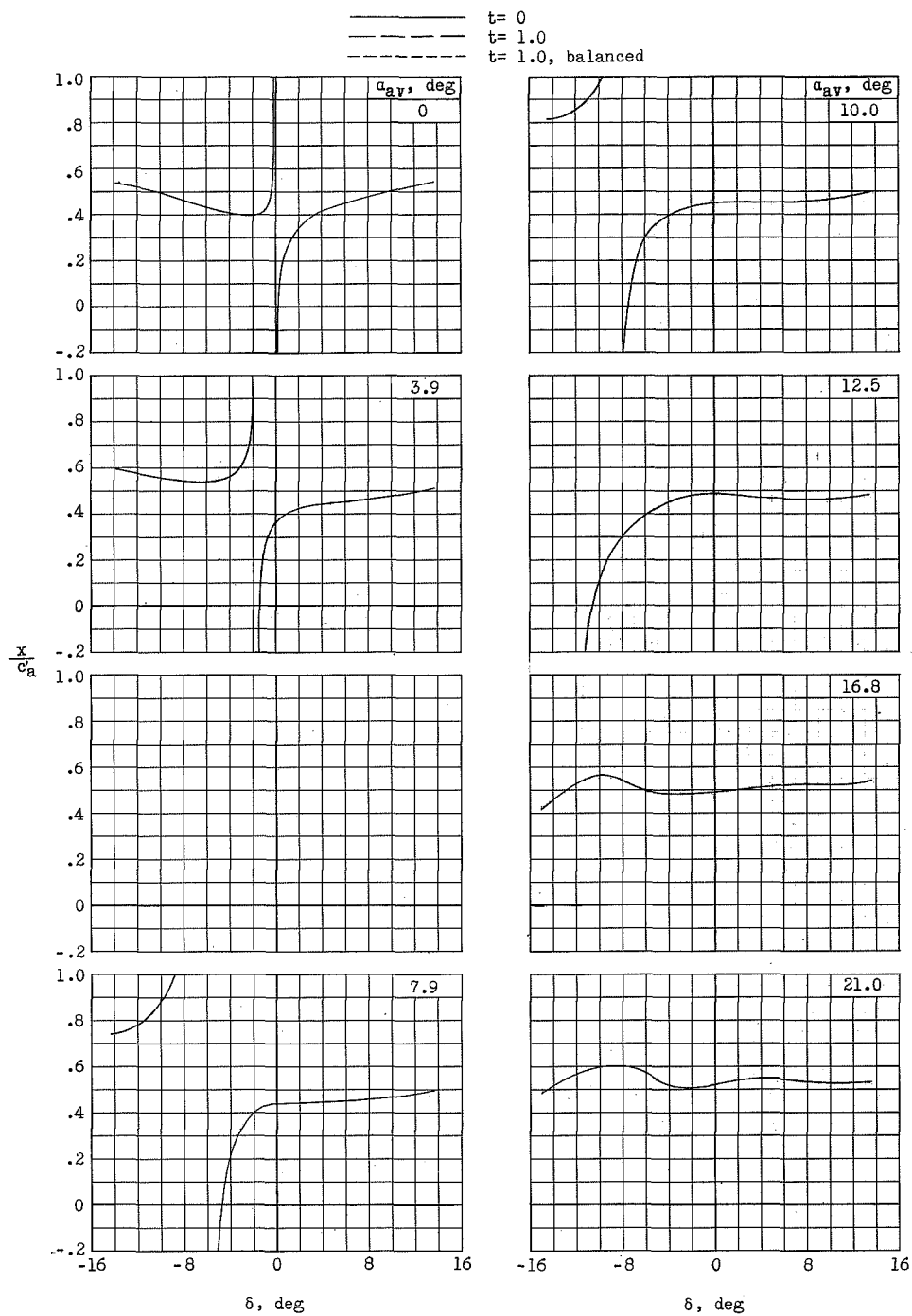
(e)   M = 0.96.

Figure 13.- Continued.
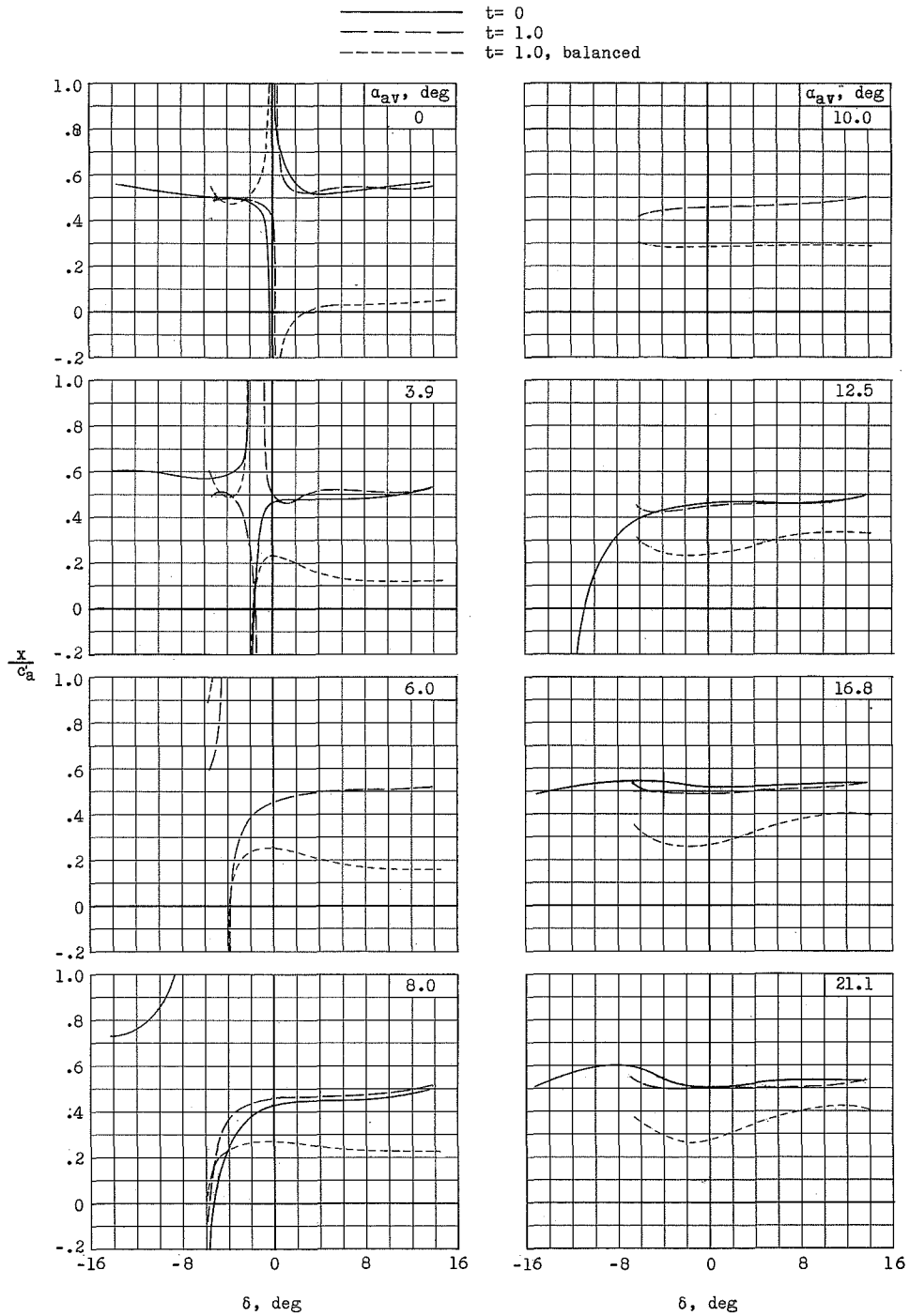
(f)  M = 0.98.

Figure 13.- Continued.
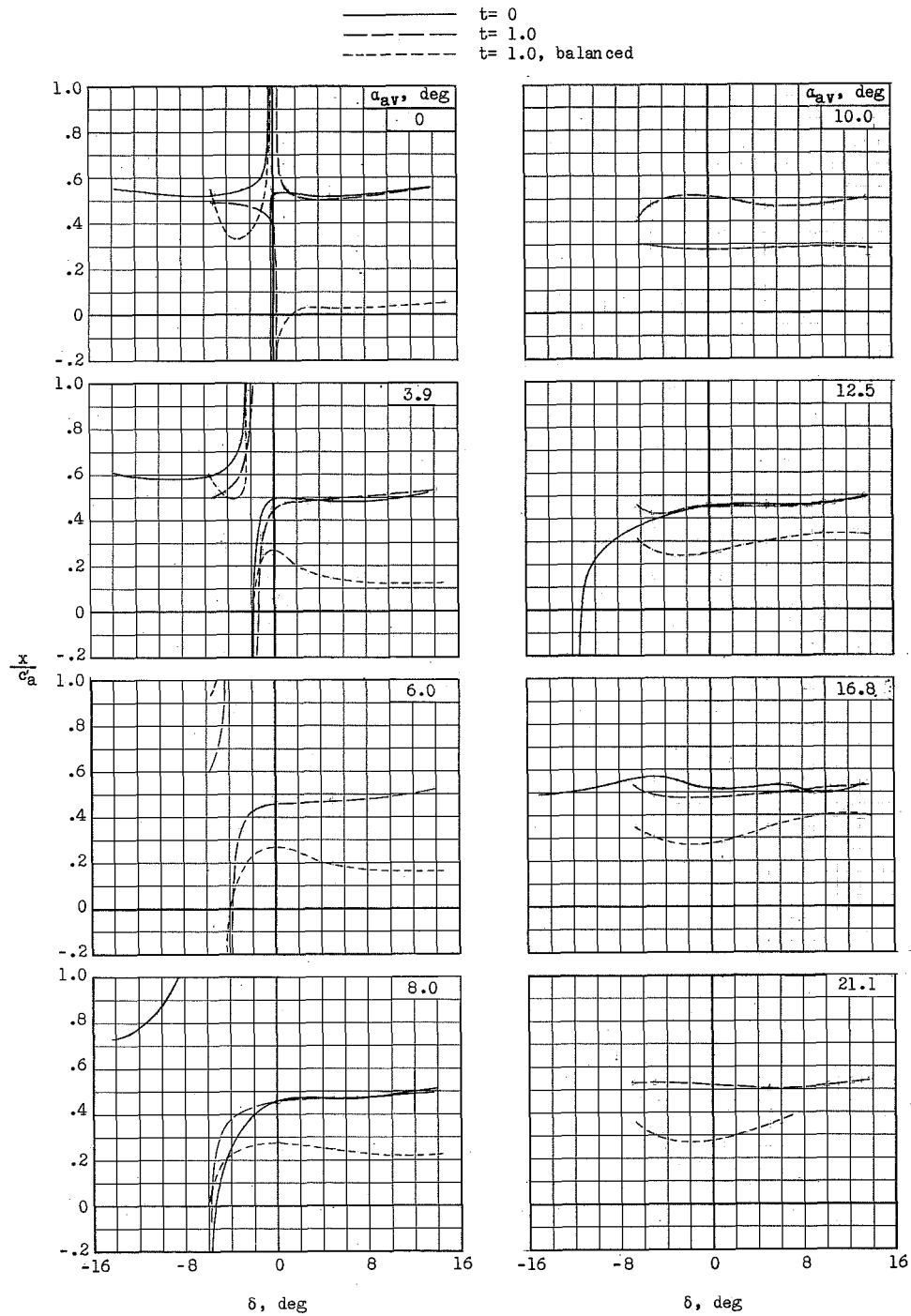
(g)  M = 1.00.

Figure 13.- Continued.
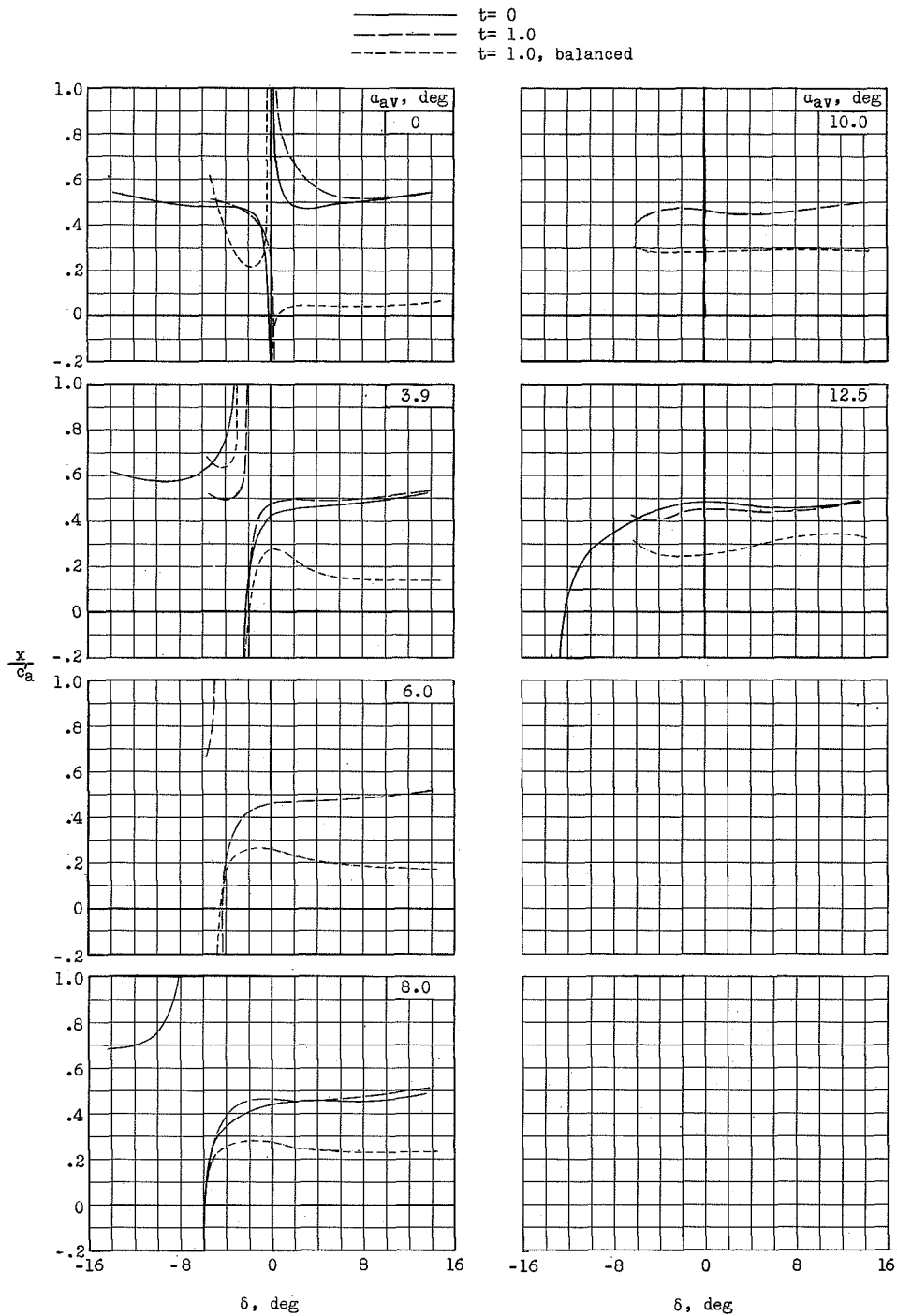
(h)   M = 1.03.

Figure 13.- Concluded.
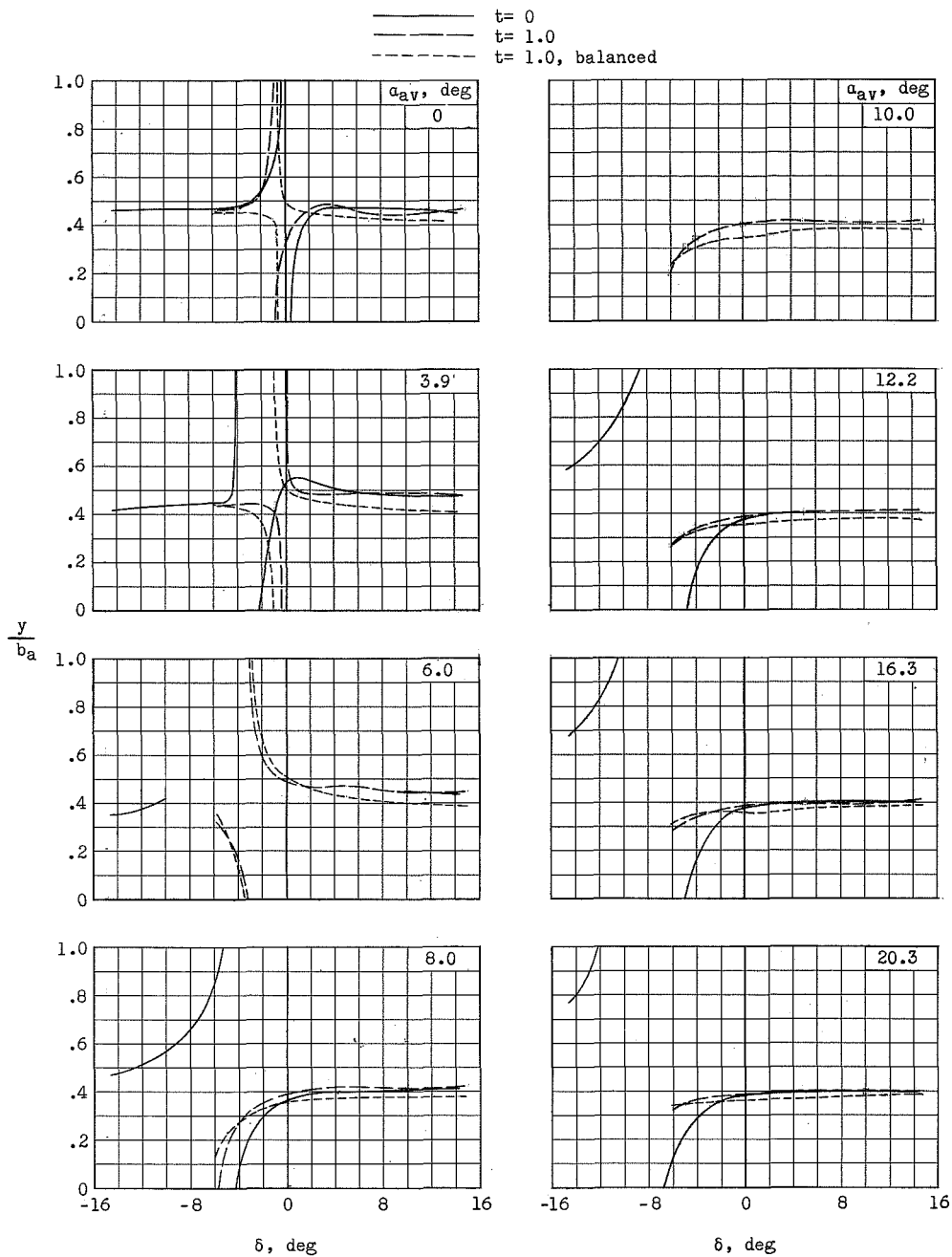
(a)  M = 0.80.

Figure 14.- Effect of aileron deflection on the spanwise location of
the center of pressure for the three aileron configurations at vari-
ous angles of attack and Mach numbers.
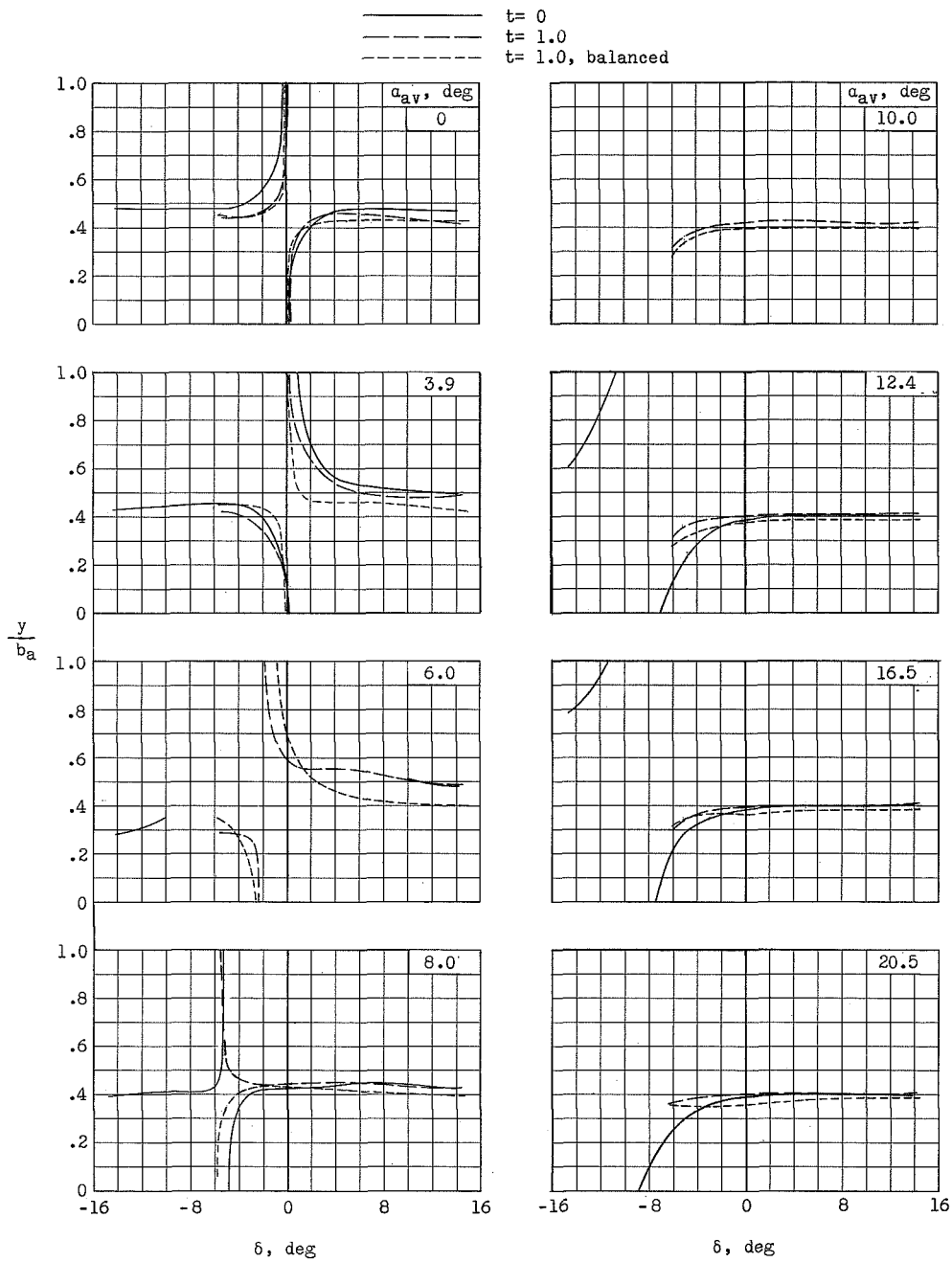
(b)  M = 0.90.

Figure 14.- Continued.
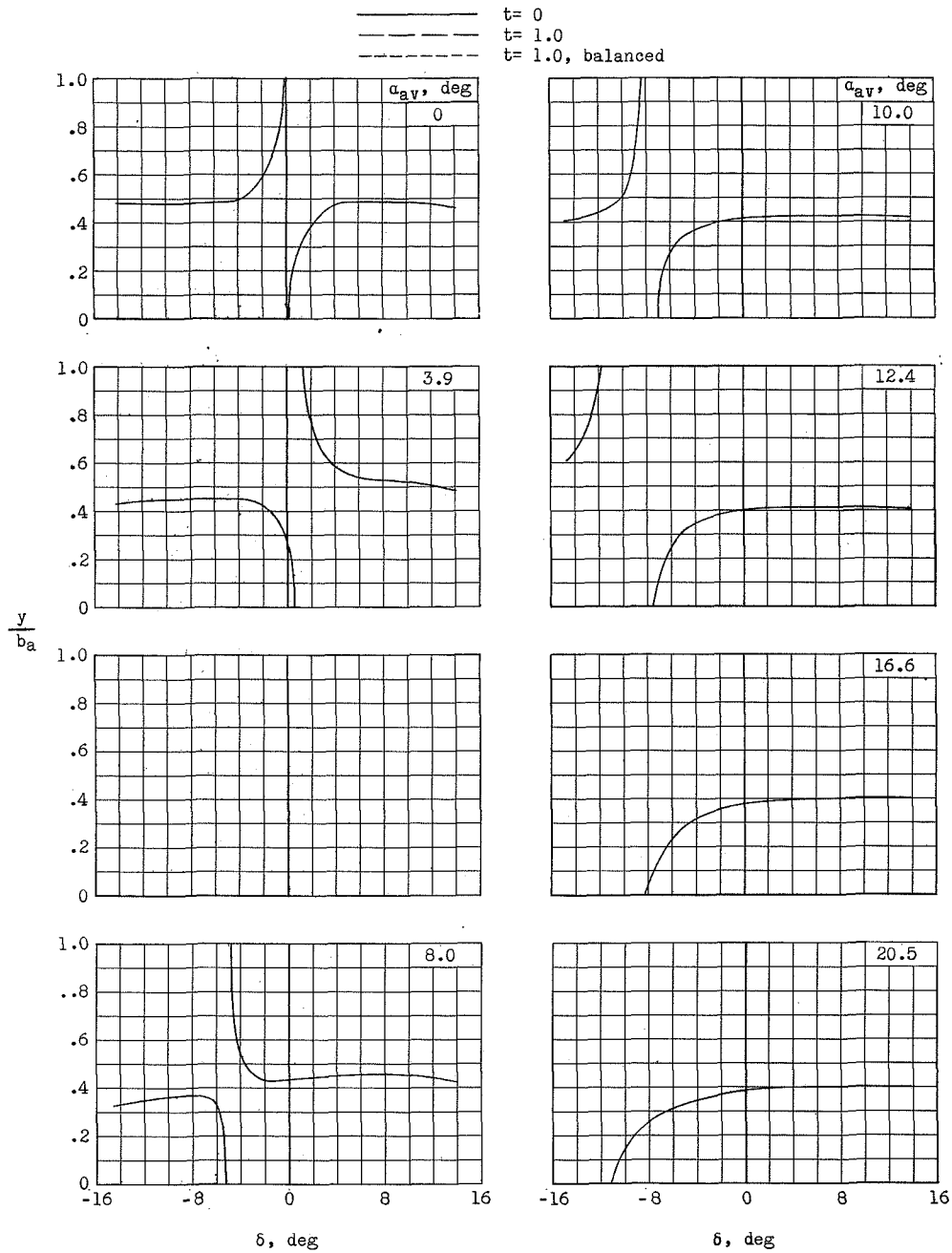
(c)  M = 0.92.

Figure 14.- Continued.
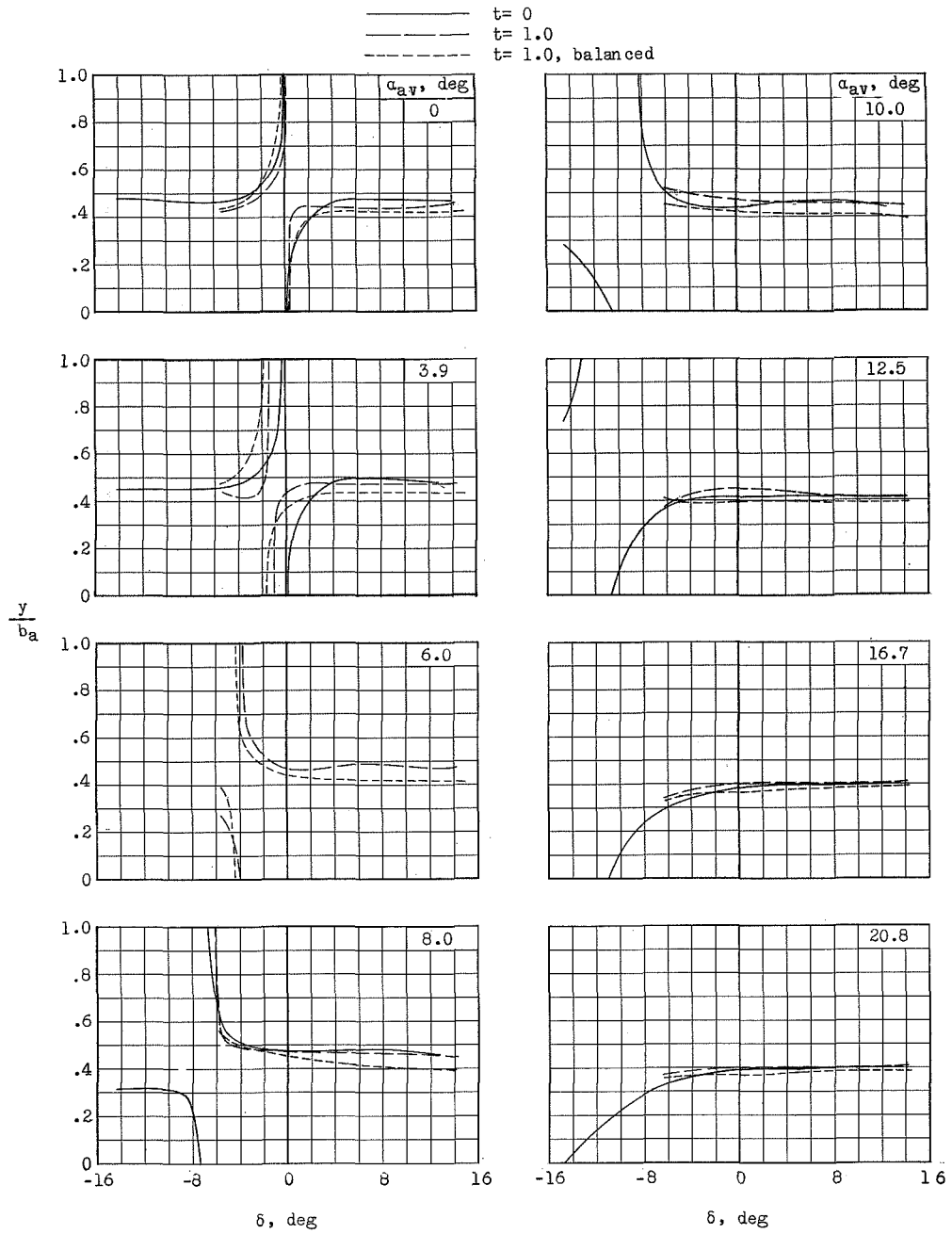
(d)   M = 0.94.

Figure 14.- Continued.

(e)   M = 0.96.

Figure 14.- Continued.
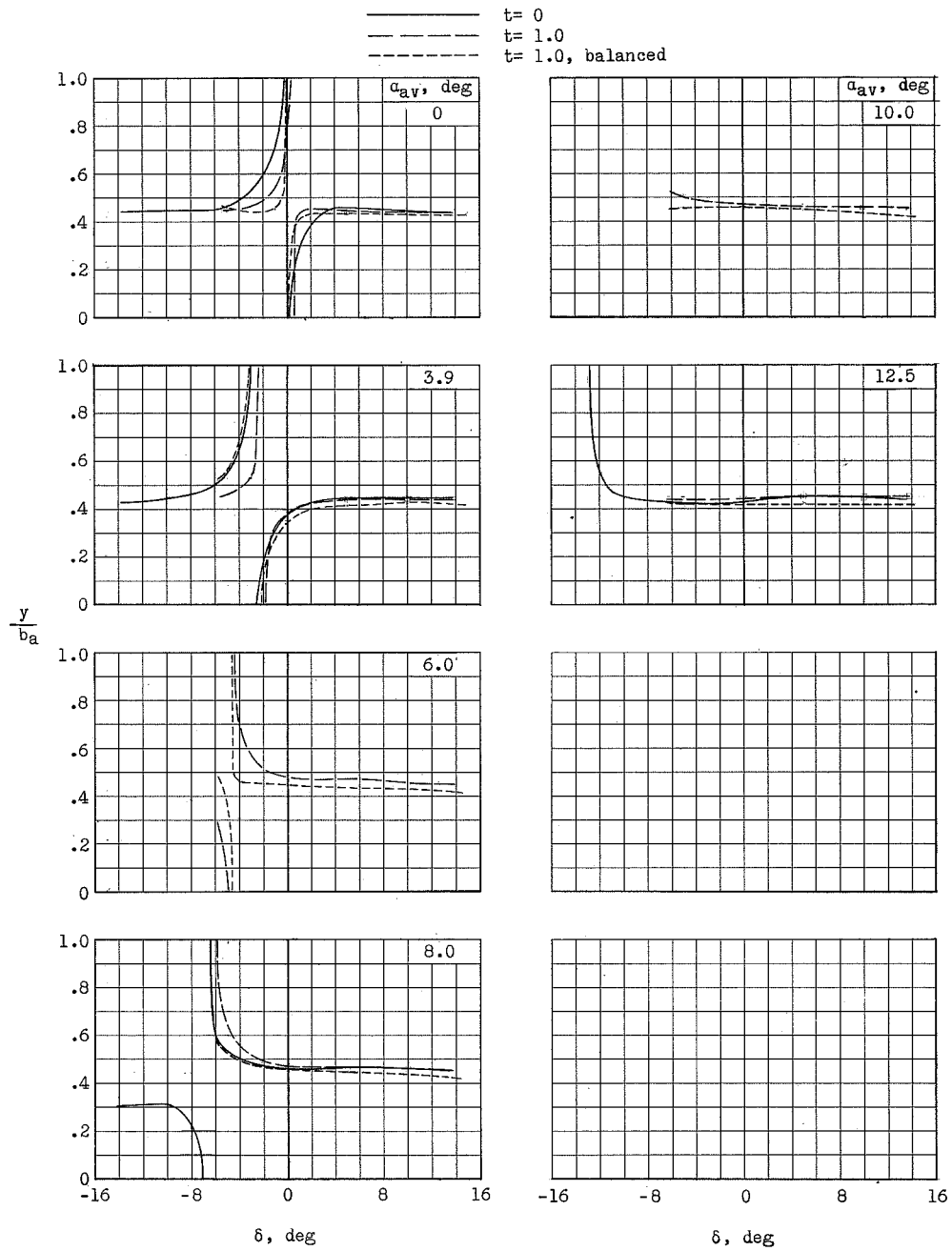
(f)  M = 0.98.

Figure 14.- Continued.
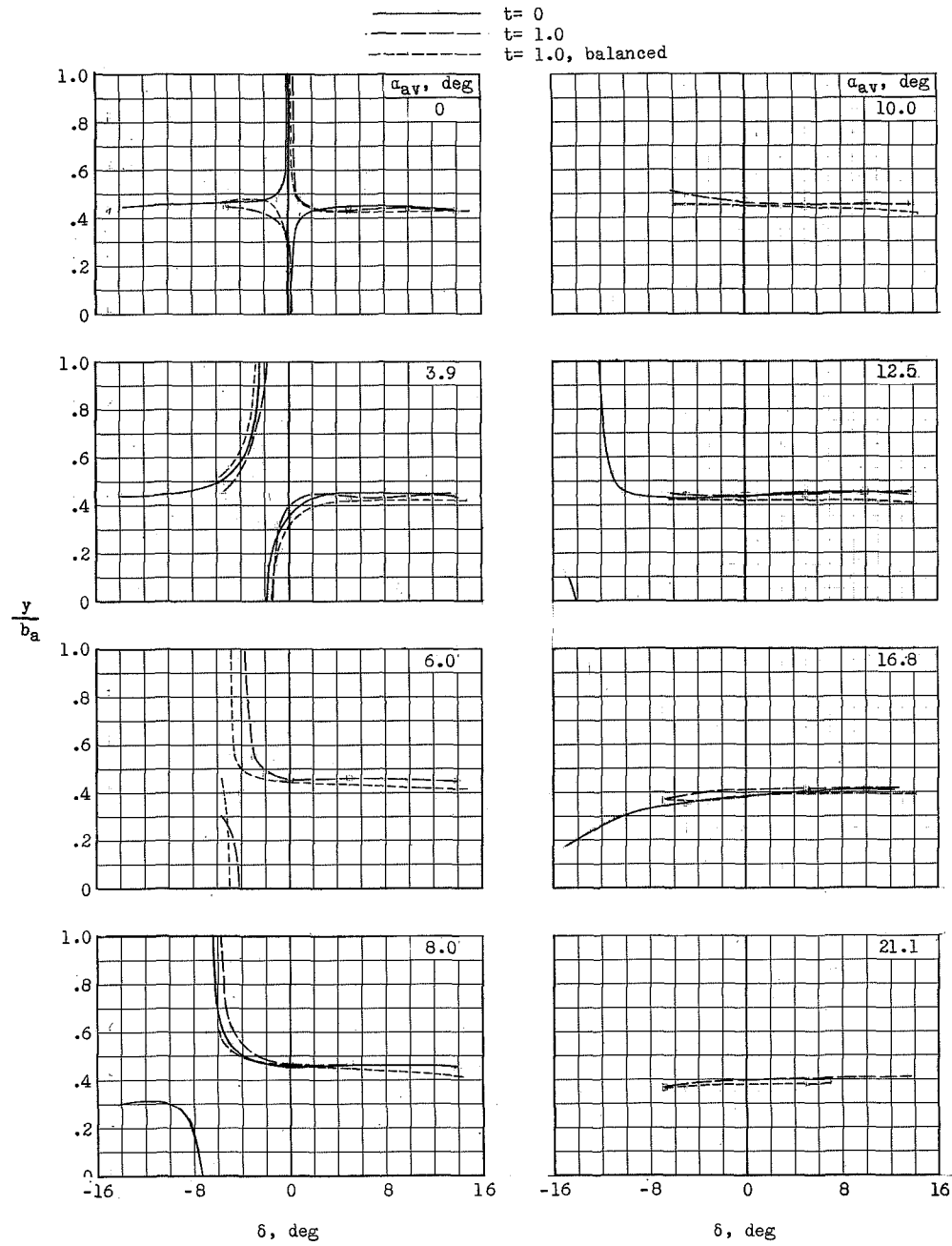
(g)   M = 1.00.

Figure 14.- Continued.

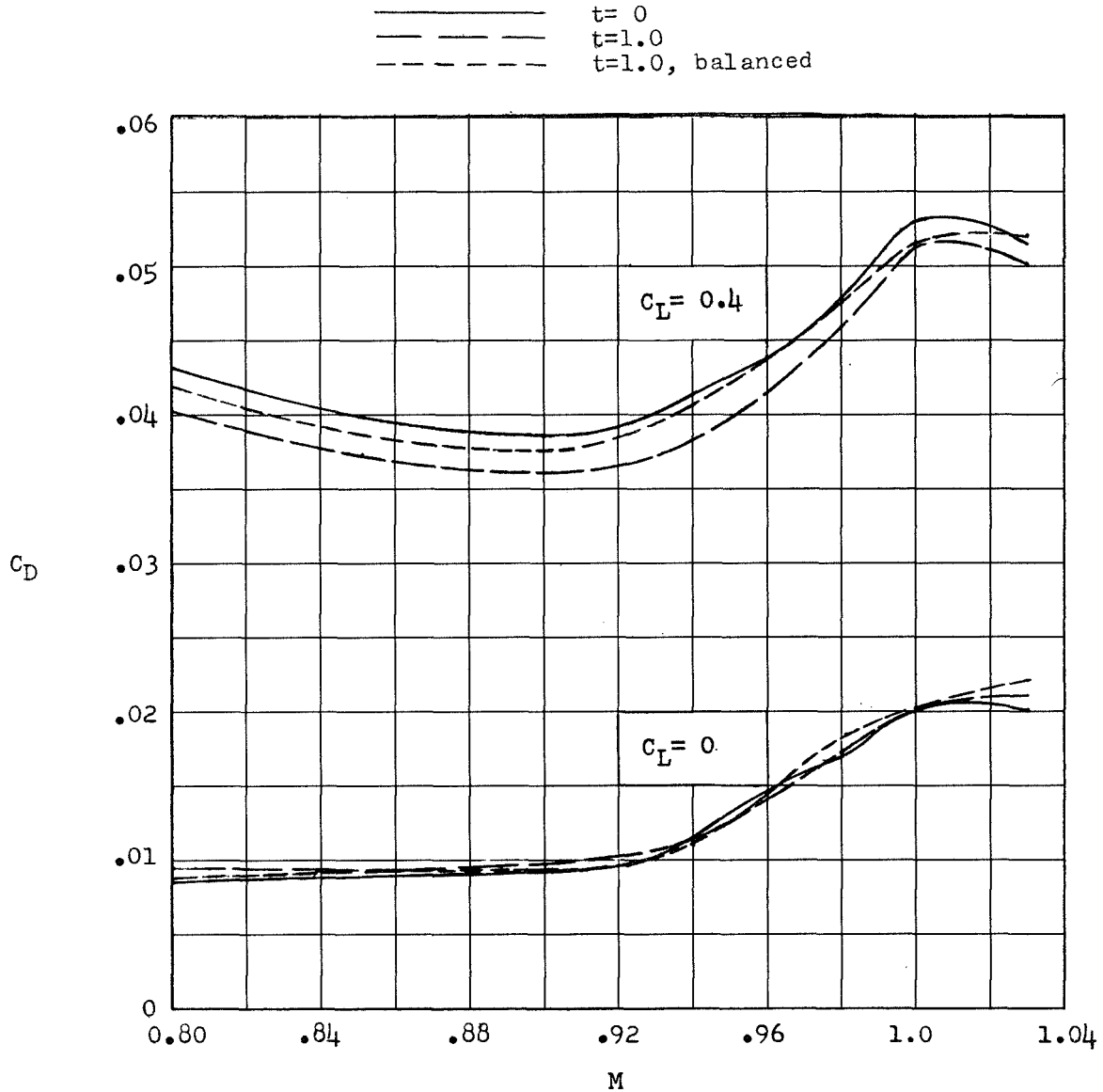(h)   M = 1.03.

Figure 14.- Concluded.

Figure 15.- Variation with Mach number of the drag coefficient for the three aileron configurations at constant lift coefficients of 0 and 0.4.  $\delta = 0^{\circ}$.